

# LEARNING LOW-RANK LATENT MESOSCALE STRUCTURES IN NETWORKS

HANBAEK LYU<sup>†</sup>, YACOB H. KUREH<sup>\*</sup>, JOSHUA VENDROW<sup>\*</sup>, AND MASON A. PORTER<sup>\*,\*\*</sup>

**ABSTRACT.** It is common to use networks to encode the architecture of interactions between entities in complex systems in applications in the physical, biological, social, and information sciences. To study the large-scale behavior of complex systems, it is useful to study mesoscale structures in networks as building blocks that influence such behavior [25, 35]. We present a new approach for describing low-rank mesoscale structure in networks, and we illustrate our approach using several synthetic network models and empirical friendship, collaboration, and protein–protein interaction (PPI) networks. We find that these networks possess a relatively small number of ‘latent motifs’ that together can successfully approximate most subgraphs of a network at a fixed mesoscale. We use an algorithm that we call ‘network dictionary learning’ (NDL) [45], which combines a network-sampling method [40] and nonnegative matrix factorization [6, 45], to learn the latent motifs of a given network. The ability to encode a network using a set of latent motifs has a wide variety of applications to network-analysis tasks, such as comparison, denoising, and edge inference. Additionally, using our new network denoising and reconstruction (NDR) algorithm, we demonstrate how to denoise a corrupted network by using only the latent motifs that one learns directly from the corrupted networks.

It is often insightful to examine structures in networks [36] at intermediate scales (i.e., at ‘mesoscales’) that lie between the microscale of nodes and edges but below macroscale distributions of local network properties. Researchers have considered subgraph patterns (i.e., the connection patterns of subsets of nodes) as building blocks of network structure at various mesoscales [48]. In particular, it is common to identify  $k$ -node (where  $k$  is typically between 3 and 5) subgraph patterns in a network that are unexpectedly common in comparison to some random-graph null model as ‘motifs’ of that network [7]. In the past two decades, the study of motifs has been an important approach for analyzing various networked systems in many areas, including biology [8, 19, 9, 29, 11], sociology [27, 15], and economics [18, 37]. However, to the best of our knowledge, researchers have not examined how to use such motifs (or related mesoscale structures), after their discovery, as building blocks to reconstruct a network. In this paper, we provide this missing computational framework to bridge inferred subgraph-based mesoscale structures and the global structure of networks. To do this, we propose (1) a ‘network dictionary learning’ (NDL) algorithm that learns ‘latent motifs’ from samples of certain random  $k$ -node subgraphs and (2) a complementary algorithm for ‘network denoising and reconstruction’ (NDR) that constructs a best ‘mesoscale linear approximation’ of a given network using the learned latent motifs. We also provide a rigorous theoretical analysis of the proposed algorithms. This analysis includes a novel result in which we prove that one can accurately reconstruct an entire

---

<sup>†</sup> DEPARTMENT OF MATHEMATICS, UNIVERSITY OF WISCONSIN-MADISON, WI 53706, USA

<sup>\*</sup> DEPARTMENT OF MATHEMATICS, UNIVERSITY OF CALIFORNIA, LOS ANGELES, CA 90095, USA

<sup>\*\*</sup> SANTA FE INSTITUTE, SANTE FE, NM 87501, USA

*E-mail addresses:* hlyu@math.wisc.edu, {ykureh, jvendrow, mason}@math.ucla.edu.

Our code for the main algorithms and simulations is available at [https://github.com/HanbaekLyu/NDL\\_paper](https://github.com/HanbaekLyu/NDL_paper). At <https://github.com/jvendrow/Network-Dictionary-Learning>, we provide a user-friendly version as a PYTHON package NDLEARN.

network if one has a dictionary of latent motifs that can accurately approximate mesoscale structures of the network. We compare the present work to related prior work [45] in the Methods section and in our Supplementary Information (SI).

Using our approach, we find that various real-world networks (such as Facebook friendship networks, Coronavirus and *Homo sapiens* protein–protein interaction (PPI) networks, and an arXiv collaboration network) have low-rank subgraph patterns, in the sense that one can successfully approximate their  $k$ -node subgraph patterns by a weighted sum of a small number of latent motifs. The latent motifs of these networks thereby reveal their low-rank mesoscale structures. Our claim of the low-rank nature of a network’s mesoscale structure concerns the space of certain subgraph patterns, rather than the embedding of an entire network into a low-dimensional Euclidean space (as considered in spectral-embedding and graph-embedding methods [28, 32]). It is impossible to obtain such a low-dimensional graph embedding for networks with small mean degrees and large clustering coefficients [46]. Additionally, as we demonstrate in this paper, the ability to encode a network using a set of latent motifs has a wide variety of applications in network analysis. Such applications include network comparison, denoising, and edge inference.

**$k$ -path motif sampling.** Computing all  $k$ -node subgraphs of a network is computationally expensive and is the main computational bottleneck of traditional motif analysis [7]. Our approach, which bypasses this issue, is to learn latent motifs by drawing random samples of a particular class of  $k$ -node connected subgraphs. We consider random  $k$ -node subgraphs that we obtain by uniformly randomly sampling a ‘ $k$ -path’ from a network and including all edges between the sampled nodes of the network. A  $k$ -path is a subgraph that consists of  $k$  distinct nodes, with the  $i$ th node adjacent to the  $(i + 1)$ th node for all  $i \in \{1, \dots, k - 1\}$ . Sampling a  $k$ -path first serves two purposes: (1) It ensures that the sampled  $k$ -node induced subgraph is connected with the minimum number of imposed edges; and (2) it induces a natural node ordering of the  $k$ -node induced subgraph. (Such an ordering is important for computations that involve subgraphs.) By using the ‘ $k$ -walk’ motif-sampling algorithm in [40] in conjunction with rejection sampling, we can sample a large number of  $k$ -paths and obtain their associated induced subgraphs.

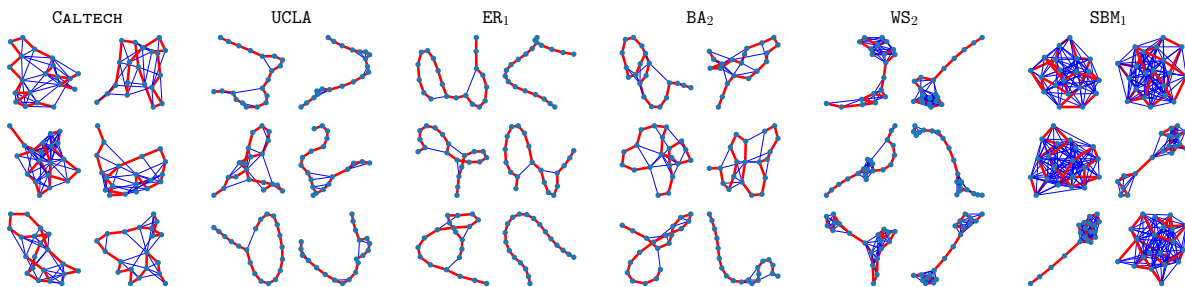


FIGURE 1. Six subgraphs that are induced by uniformly sampled  $k$ -paths with  $k = 20$  (red edges) from CALTECH and UCLA Facebook networks, an Erdős–Rényi (ER) random graph ( $ER_1$ ), a Barabási–Albert (BA) random graph ( $BA_2$ ), a Watts–Strogatz (WS) small-world network ( $WS_2$ ), and a stochastic-block-model (SBM) network ( $SBM_1$ ). See the Methods section for more details about these networks.

The  $k$ -node subgraph that is induced by such a uniformly random  $k$ -path is guaranteed to be connected and can exhibit diverse connection patterns (see Figure 1), depending on the architecture of the original network. These  $k$ -node subgraphs are the mesoscale structures that we consider in the present paper. We study the connection patterns of such a random  $k$ -node subgraph by decomposing it as a weighted sum of more elementary subgraph patterns (possibly with continuous-valued edge weights), which we call *latent motifs*. To study mesoscale structures

in networks, we investigate several questions. How many distinct latent motifs does one need to successfully approximate all such  $k$ -node subgraph patterns? What do they look like? How do these latent motifs differ for different networks?

**Dictionary learning and latent motifs.** *Dictionary-learning* algorithms are machine-learning techniques that learn interpretable latent structures of complex data sets. They are employed regularly in the data analysis of text and images [10, 13, 16]. Dictionary-learning algorithms usually consist of two steps. First, one samples a large number of structured subsets of a data set (e.g., square patches of an image or collections of a few sentences of a text); we refer to such a subset as a *mesoscale patch* of a data set. Second, one finds a set of basis elements such that taking a nonnegative linear combination of them can successfully approximate each of the sampled mesoscale patches. Such a set of basis elements is called a *dictionary*, and one can interpret each basis element as a latent structure of the data set.

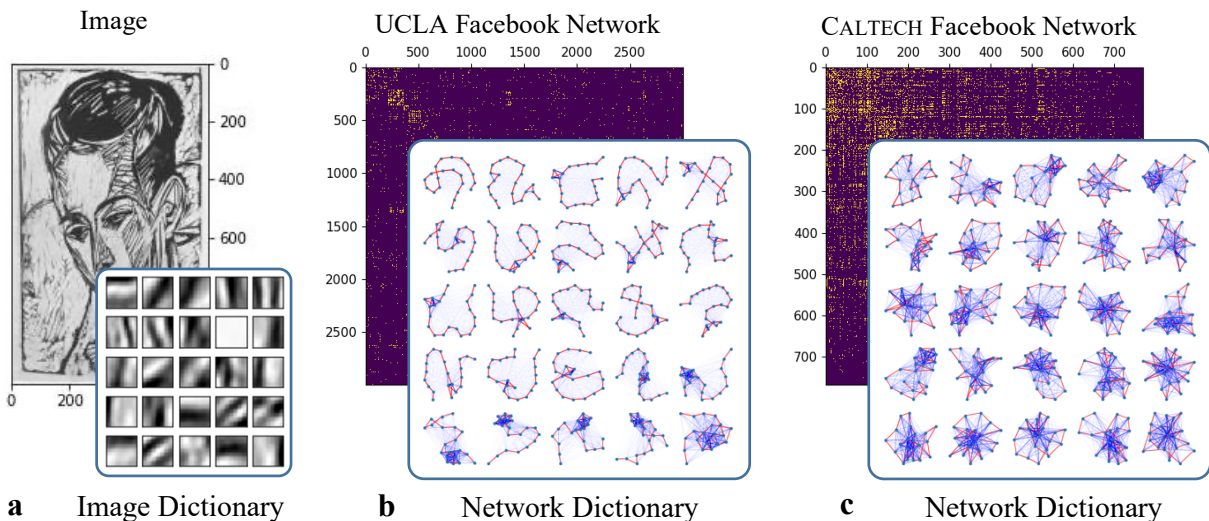


FIGURE 2. Illustration of mesoscale structures that we learn from (a) images and (b,c) networks. In each experiment in this figure, we form a matrix  $X$  of size  $d \times n$  by sampling  $n$  mesoscale patches of size  $d = 21 \times 21$  from the corresponding object. For the image in panel a, the columns of  $X$  are square patches of  $21 \times 21$  pixels. In panels b and c, we show both networks and adjacency matrices. We take the columns of  $X$  to be the  $k \times k$  adjacency matrices of the connected subgraphs that are induced by a path of  $k = 21$  nodes, where a path of  $k$  nodes consists of  $k$  distinct nodes  $x_1, \dots, x_k$  such that  $x_i$  and  $x_{i+1}$  are adjacent for all  $i \in \{1, \dots, k-1\}$ . Using nonnegative matrix factorization (NMF), we compute an approximate factorization  $X \approx WH$  into nonnegative matrices  $W$  and  $H$ , where  $W$  is called a dictionary and has  $r = 25$  columns. Because of this factorization, we can approximate any sampled mesoscale patches (i.e., the columns of  $X$ ) of an object by a nonnegative linear combination of the columns of  $W$ , which we interpret as latent shapes for the images and latent motifs (i.e., subgraphs) for the networks, respectively. The columns of  $H$  give the coefficients in these linear combinations. The network dictionaries of latent motifs that we learn from the (b) UCLA and (c) CALTECH Facebook networks have distinctive social structures. In the heatmap of the UCLA network, we show only the first 3000 nodes (according to the node labeling in the data set). The image in panel a is from the collection **DIE GRAPHIK ERNST LUDWIG KIRCHNERS BIS 1924, VON GUSTAV SCHIEFLER BAND I BIS 1916** (Accession Number 2007.141.9, Ernst Ludwig Kirchner, 1926). We use the image with permission from the National Gallery of Art in Washington, DC, USA.]

As an example, consider the artwork image in Figure 2a. We first uniformly randomly sample 10,000 square patches of  $21 \times 21$  pixels and vectorize them to get a  $21^2 \times 10,000$  matrix  $X$ . The choice of vectorization  $\mathbb{R}^{k \times k} \rightarrow \mathbb{R}^{k^2}$  is arbitrary; we use the column-wise vectorization

in Algorithm A4 in the Supplementary Information (SI). We then use a nonnegative matrix factorization (NMF) [6] algorithm to find an approximate factorization  $X \approx WH$ , where  $W$  and  $H$  are nonnegative matrices of sizes  $21^2 \times 25$  and  $25 \times 10,000$ , respectively. Reshaping the columns of  $W$  into  $21 \times 21$  square images yields an image dictionary that describes ‘latent shapes’ in the image.

Our *network dictionary learning* (NDL) algorithm for computing a ‘network dictionary’ that consists of latent motifs is based on a similar idea. As mesoscale patches of a network, we use the  $k \times k$  binary (i.e., unweighted) matrices that encode connectivity patterns between the nodes that form a uniformly random  $k$ -path. After obtaining sufficiently many mesoscale patches of a network (e.g., by using a motif-sampling algorithm [40] with rejection sampling), we apply a dictionary-learning algorithm (e.g., NMF [6]) to obtain latent motifs of the network. A latent motif is a  $k$ -node weighted network with nodes  $\{1, \dots, k\}$  and edges that have weights between 0 and 1. We use the term ‘on-chain edges’ for the edges of a latent motif between nodes  $i$  and  $i + 1$  for  $i \in \{1, \dots, k - 1\}$ ; we use the term ‘off-chain edges’ for all other edges. We give more background about our NDL algorithm in the Methods section and provide a complete implementation of our approach in Algorithm NDL of the SI. We give theoretical guarantees for Algorithm NDL in Theorems 7.4 and 7.7 in the SI.

In Figure 2, we compare 25 latent motifs with  $k = 21$  nodes of Facebook friendship networks (which were collected on one day in fall 2005) from UCLA (‘UCLA’) and Caltech (‘CALTECH’) [22, 26]. Each node in one of these networks is a Facebook account of an individual, and each edge encodes a Facebook friendship between two individuals. The latent motifs reveal striking differences between these networks in the connection patterns in the subgraphs that are induced by  $k$ -paths with  $k = 21$ . For example, the latent motifs in UCLA’s dictionary (see Figure 2b) have sparse off-chain connections with a few clusters, whereas CALTECH’s dictionary (see Figure 2c) has relatively dense off-chain connections. Most of CALTECH’s latent motifs have ‘hub’ nodes (which are adjacent to many other nodes in the latent motif) or communities with six or more nodes. (See Figure 3 for community-size statistics.) An important property of  $k$ -node latent motifs is that any network structure (e.g., hub nodes, communities, and so on) in the latent motifs must also exist in actual  $k$ -node subgraphs. Indeed, we observe hubs and communities in the subgraph samples from CALTECH in Figure 1. By contrast, most of UCLA’s latent motifs do not have such structures, as is also the case for the subgraph samples from UCLA in Figure 1.

**Example networks.** We demonstrate our approach using 16 example networks; 8 of them are real-world networks and 8 of them synthetic networks. The 8 real-world networks are CORONAVIRUS PPI (for which we use the shorthand CORONAVIRUS) [41, 47, 42] and HOMO SAPIENS PPI (for which we use the shorthand H. SAPIENS) [41, 32]; Facebook networks from CALTECH, UCLA, HARVARD, and MIT [22, 26]; SNAP FACEBOOK (for which we use the shorthand SNAP FB) [23, 32]; and ARXIV ASTRO-PH (for which we use the shorthand ARXIV) [44, 32]. The first network is a protein–protein interaction (PPI) network of proteins that are related to the coronaviruses that cause Coronavirus disease 2019 (COVID-19), Severe Acute Respiratory Syndrome (SARS), and Middle Eastern Respiratory Syndrome (MERS) [47]. The second network is a PPI network of proteins that are related to *Homo sapiens* [41]. The third network is a 2012 Facebook network that was collected from participants in a survey [23]. The fourth network is a collaboration network based on coauthorship of preprints that were posted in the astrophysics category of the arXiv preprint server. The last four real-world networks are 2005 Facebook networks from four universities from the FACEBOOK100 data set [26]. In each Facebook network, nodes represent accounts and edges encode Facebook ‘friendships’ between these accounts.

For the eight synthetic networks, we generate two instantiations each of Erdős–Rényi (ER)  $G(N, p)$  networks [1], Watts–Strogatz (WS) networks [4], Barabási–Albert (BA) networks [5],

and stochastic-block-model (SBM) networks [3]. These are four types of well-studied random-graph models [36]. Each of the ER networks has 5,000 nodes, and we independently connect each pair of nodes with probabilities of  $p = 0.01$  (in the network that we call  $ER_1$ ) and  $p = 0.02$  (in  $ER_2$ ). For the WS networks, we use rewiring probabilities of  $p = 0.05$  (in  $WS_1$ ) and  $p = 0.1$  (in  $WS_2$ ) starting from a 5,000-node ring network in which each node is adjacent to its 50 nearest neighbors. For the BA networks, we use  $m = 25$  (in  $BA_1$ ) and  $m = 50$  (in  $BA_2$ ), where  $m$  denotes the number of edges of each new node when it connects (via linear preferential attachment) to the existing network, which we grow from an initial network of  $m$  isolated nodes (i.e., none of them are adjacent to any other node) until it has 5,000 nodes. The SBM networks  $SBM_1$  and  $SBM_2$  have three planted 1,000-node communities and two nodes in the  $i_0$ th and the  $j_0$ th communities are connected by an edge independently with probability 0.5 if  $i_0 = j_0$  (i.e., if they are in the same community) and 0.001 for  $SBM_1$  and 0.1 for  $SBM_2$  if  $i_0 \neq j_0$  (i.e., if they are in different communities). See the Methods section for more details.

**Community sizes in subgraph samples and latent motifs.** By comparing the 21-node latent motifs of UCLA and CALTECH (we extract  $r = 25$  of each) in Figure 2, we observe that most latent motifs of CALTECH have larger communities than those of UCLA. To what extent does the community structure of the latent motifs carries over to the subgraph samples in these networks? Latent motifs are  $k$ -node networks with nonnegative edge weights, so we can examine this question quantitatively by performing community detection using a standard approach on these  $k$ -node networks. We will use the locally greedy Louvain method for modularity maximization [14]. For most of our example networks, we observe that the community-size statistics of the learned latent motifs are close approximations of the corresponding statistics for the subgraph samples of the networks. In Figure 3, we compare box plots of community sizes of 10,000-node subgraphs that are induced by uniformly randomly sampled  $k$ -paths to the corresponding box plots from community detection of  $r = 25$  latent motifs of various networks. In our calculations, the subgraphs and latent motifs from the networks UCLA and CALTECH have the same median community sizes. Moreover, the box plots for subgraphs and latent motifs in Figure 3 are in good agreement for most of our example networks.

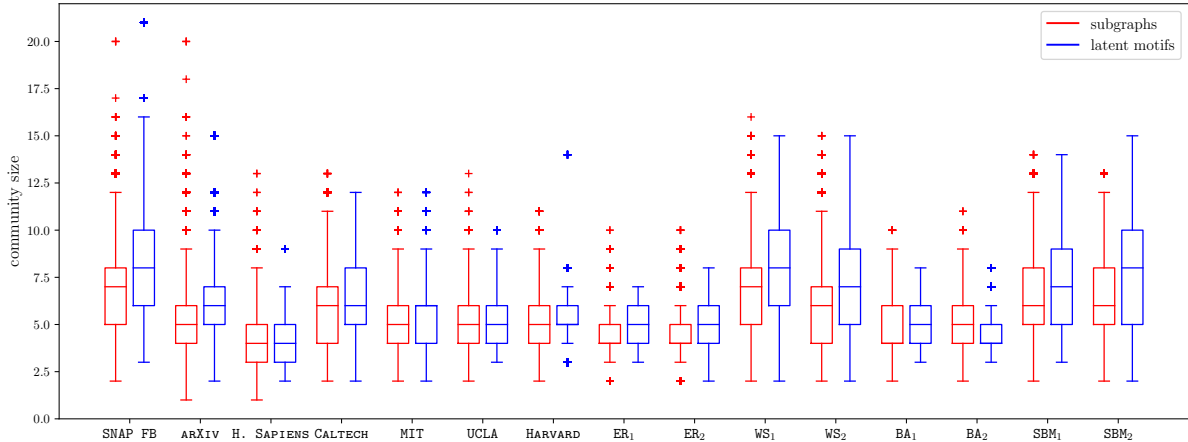


FIGURE 3. A comparison of box plots of community sizes for 10,000 randomly sampled subgraphs that are induced by uniformly random paths with  $k = 21$  nodes (in red) to corresponding box plots from  $r = 25$  latent motifs of  $k = 21$  nodes for various real-world and synthetic networks. We obtain communities of the subgraphs and latent motifs by using the Louvain modularity-maximization algorithm [14].

**Latent motifs of networks at various mesoscales.** Because  $k$ -node latent motifs encode basic connectivity patterns of  $k$  nodes that are at most  $k - 1$  edges apart, one can interpret  $k$  as a scale parameter. With each latent motif, we associate a scalar ‘dominance score’, which measures its total contribution in our reconstruction of the sampled  $k$ -node subgraphs. (See Section D.2 of our SI for details.) In Figure 4, we show the two most-dominant latent motifs (i.e., the two with the largest dominance scores) that we learn from each of 15 example networks (i.e., for all of them except CORONAVIRUS PPI) at various scales (specifically, for  $k = 6$ ,  $k = 11$ ,  $k = 21$ , and  $k = 51$ ) when we use a dictionary with  $r = 25$  latent motifs.

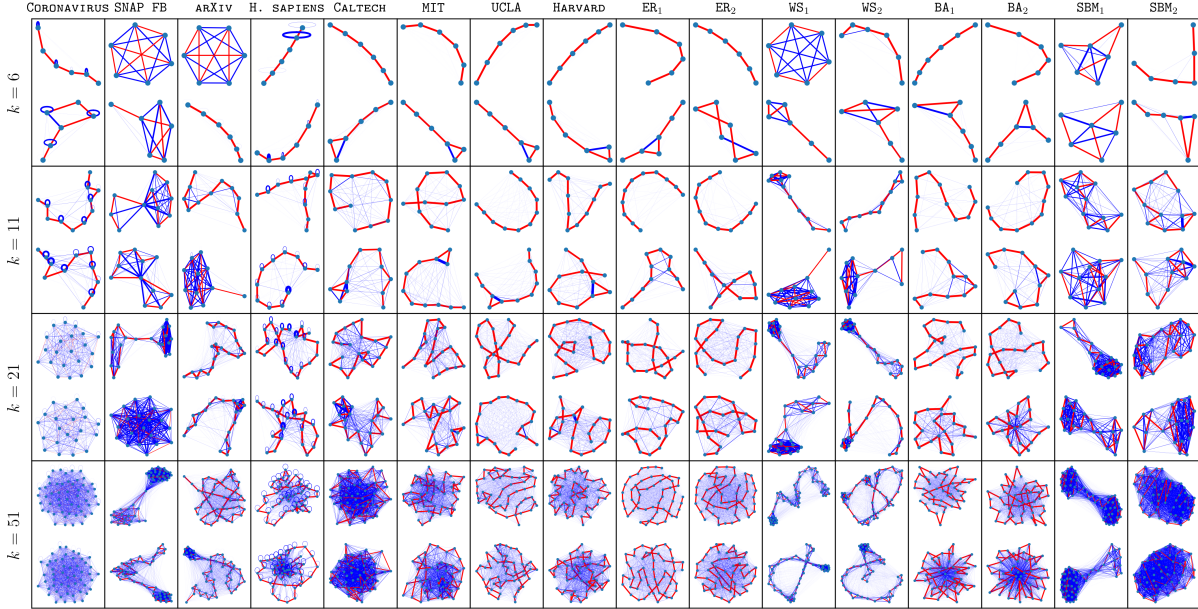


FIGURE 4. Latent motifs that we learn from 16 networks (eight real-world networks and eight synthetic networks, which include two distinct instantiations of each of four random-graph models) at four different scales (specifically, for  $k = 6$ ,  $k = 11$ ,  $k = 21$ , and  $k = 51$ ), have distinct mesoscale structures in the networks. Using NDL, we learn network dictionaries of  $r = 25$  latent motifs with  $k$  nodes for each of the 16 networks. For each network at each scale, we show the (top) first and (bottom) second most-dominant latent motif from each dictionary. See Section D.2 of our SI for details about how we measure latent-motif dominance.

As we increase the scale parameter  $k$  for each network, various mesoscale structures emerge in the latent motifs in Figure 4. For instance, **SNAP FB**, **ARXIV**, and **WS<sub>1</sub>** all have fully connected top (i.e., most dominant) latent motifs at scale  $k = 6$  but their second latent motifs are distinct. In **SNAP FB**, **CALTECH**, and **MIT** at scales  $k \in \{6, 11, 21\}$  and for the **BA** networks at scales  $k \in \{11, 21, 51\}$ , the two most dominant latent motifs in Figure 4 have nodes that are adjacent to many other nodes in the latent motif. Hubs (i.e., nodes that are adjacent to many other nodes) are characteristic of both **BA** networks (which have heavy-tailed degree distributions) [5] and most social networks (which typically have heavy-tailed degree distributions) [36]. We also observe hubs in the network dictionaries of the latent motifs of the Facebook networks **UCLA** and **HARVARD**. (See Figure 14 in our SI.)

In Figure 3, we saw that community sizes in latent motifs reflect community sizes of actual subgraphs in a network. Importantly, the type of community structure that we examine is very different from typical network community structure. For example, consider the **WS** networks. The top latent motif of the network **WS<sub>1</sub>** at scale  $k = 6$  is fully connected, but the top latent

motif of  $WS_2$  is not fully connected because of its larger rewiring probability. At larger scales (i.e., for larger  $k$ ), both WS networks have latent motifs with multiple communities. The WS networks have locally densely connected nodes on a ring of nodes and random ‘shortcut’ edges that can connect distant nodes of the ring. Therefore, when one samples a  $k$ -path uniformly at random, it is very likely to use at least one shortcut edge. When a  $k$ -path uses a shortcut edge, we expect the resulting sampled induced subgraph to have two distinct densely connected communities. This local ‘community structure’ in the WS networks is rather different from standard types of community structure [17, 31]. While we do observe such community structures on subgraphs that are induced by  $k$ -paths as in Figure 1, it does not imply that the entire node set of the WS networks is partitioned into a few communities. We can also see the difference between our mesoscale structures and community structure by examining the latent motifs of the SBM networks at different scales in Figure 4. The SBM networks have three (equal-sized) communities by construction, but its latent motifs at none of the scales have three communities; uniformly sampled  $k$ -paths do not always intersect with all three communities. For example, the six 20-paths from  $SBM_1$  in Figure 1 intersect with only one or two of the network’s planted communities.

**Network denoising and reconstruction using latent motifs.** Suppose that we are given a network  $G$  and a dictionary  $W$  of latent motifs at scale  $k$ , where we may or may not learn  $W$  from  $G$ . Consider the following two scenarios. In one scenario, we suppose that we know  $G$  exactly, and we ask how to measure the ‘effectiveness’ of  $W$  at approximating mesoscale patches of  $G$  at scale  $k$ . In the other scenario, we suppose that  $G$  is a noisy version of some true network  $G_{\text{true}}$  and that  $W$  is ‘faithful’ in the sense that it can well-approximate mesoscale patches of  $G_{\text{true}}$  at scale  $k$ . (See (6) in the SI for a precise formulation of this idea.) We then ask how to infer the true network  $G_{\text{true}}$  from  $G$  and  $W$ .

To examine the above questions, we develop an algorithm that we call *network denoising and reconstruction* (NDR) (see Algorithm NDR) that takes a network  $G$  and network dictionary  $W$  as input and outputs a weighted network  $G_{\text{recons}}$  that has the same node set as  $G$ . Until it converges, the NDR algorithm repeatedly samples mesoscale patches of  $G$  at scale  $k$  and obtains a nonnegative linear approximation of those patches using the latent motifs in  $W$ . Because each edge  $e$  of  $G$  can appear in multiple mesoscale patches of  $G$ , this procedure can yield multiple reconstructed weights for  $e$ . To obtain the final weight of  $e$  in  $G_{\text{recons}}$ , we calculate their mean (see Algorithm NDR). The reconstructed network  $G_{\text{recons}}$  is a version of the original network  $G$  from the ‘lens’ of the latent motifs in the dictionary  $W$ . The latent motifs thereby dictate the types of subgraph structures of  $G$  that are captured in  $G_{\text{recons}}$ . This network-reconstruction process is inspired by patch-based image reconstruction [10, 51]. We illustrate both patch-based image reconstruction and our NDR algorithm in the Methods section.

**Network reconstruction using latent motifs.** To measure the effectiveness of  $W$  for an unweighted network  $G$  (i.e., edges are either present or absent and there are no multi-edges), one can threshold the weighted edges of  $G_{\text{recons}}$  at some fixed value  $\theta \in [0, 1]$  to obtain an undirected reconstructed network  $G_{\text{recons}}(\theta)$  with binary edge weights (of either 0 or 1), which one can then compare directly with the original unweighted network  $G$ . We regard  $W$  as effective at describing  $G$  at scale  $k$  if  $G_{\text{recons}}(\theta)$  is close to  $G$  for some  $\theta$ . (We will quantify our notion of ‘closeness’ in the next paragraph.) We interpret the edge weights in  $G_{\text{recons}}$  as measures of confidence of the corresponding edges in  $G$  with respect to  $W$ . For example, if an edge  $e$  has the smallest weight in  $G_{\text{recons}}$ , we regard it as the most ‘outlying’ with respect to the latent motifs in  $W$ . See Theorems 7.10 and 7.14 in the SI for theoretical guarantees and error bounds for NDR.

In Figure 5, we show the results of several network-reconstruction experiments using several real-world networks and synthetic networks. We perform these experiments for various values of

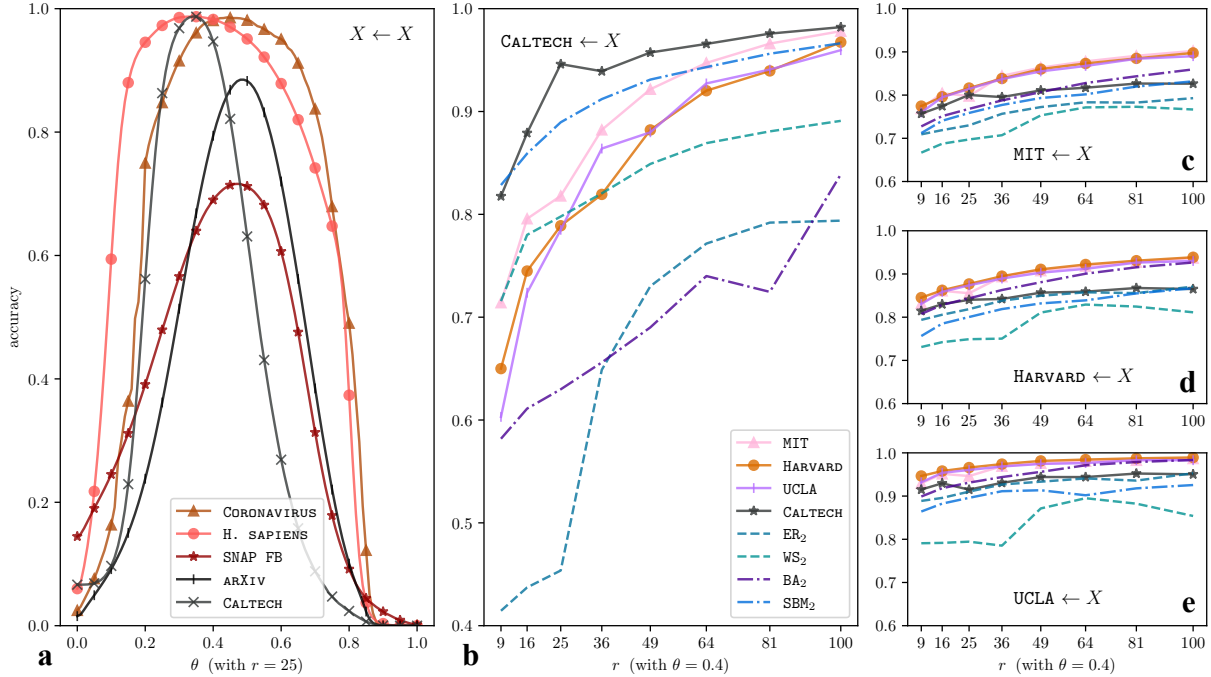


FIGURE 5. Self-reconstruction and cross-reconstruction accuracy of several real-world and synthetic networks versus the edge threshold  $\theta$  and the number  $r$  of latent motifs in a network dictionary. The label  $X \leftarrow Y$  indicates that we reconstruct network  $X$  using a network dictionary that we learn from network  $Y$ . The reconstruction process produces a weighted network that we turn into an unweighted network by thresholding the edge weights at a threshold value  $\theta$ ; we keep only edges whose weights are strictly larger than  $\theta$ . We measure reconstruction accuracy by calculating the Jaccard index of an original network’s edge set and an associated reconstructed network’s edge set. In panel **a**, we plot accuracies versus  $\theta$  (with the number of latent motifs fixed at  $r = 25$ ), where  $X$  is one of five real-world networks (two PPI networks, two Facebook networks, and one collaboration network). In panels **b–e**, we reconstruct each of the four Facebook networks using network dictionaries with  $r \in \{9, 16, 25, 36, 64, 81, 100\}$  latent motifs that we learn from one of eight networks (with the threshold value fixed at  $\theta = 0.4$ ).

the edge threshold  $\theta \in [0, 1]$  and  $r \in \{9, 16, 25, 36, 49, 81, 100\}$  latent motifs in a single dictionary. Each network dictionary in Figure 5 has  $k = 21$  nodes, for which the dimension of the space of all possible mesoscale patches (i.e., the adjacency matrices of the induced subgraphs) is  $\binom{21}{2} - 20 = 190$ . An important observation is that one can reconstruct a given network using an arbitrary network dictionary, which one can even learn from a different network. Such a ‘cross-reconstruction’ allows us to quantitatively compare the learned mesoscale structures of different networks. We label each subplot of Figure 5 with  $Y \leftarrow X$  to indicate that we are reconstructing network  $Y$  using a network dictionary that we learn from network  $X$ . (The reconstruction also uses the original network  $Y$ .) We turn the weighted reconstructed networks into unweighted networks by thresholding their edges using a threshold  $\theta$ . We measure the reconstruction accuracy by calculating the Jaccard index between the original network’s edge set and the reconstructed network’s edge set. That is, to measure the similarity of two edge sets, we calculate the number of edges in the intersection of these sets divided by the number of edges in the union of these sets. This gives a ‘global’ measure of reconstruction accuracy in the sense that if this measure is 1, then the reconstructed network is precisely the same as the original one. We obtain the same qualitative results as in Figure 5 if we instead measure similarity using the Rand index [2]).



In Figure 5a, we plot the accuracy for ‘self-reconstruction’  $X \leftarrow X$  versus the threshold  $\theta$  (with  $r = 25$ ), where  $X$  is one of the real-world networks CORONAVIRUS, H. SAPIENS, SNAP FB, CALTECH, and ARXIV. The accuracies for CORONAVIRUS, H. SAPIENS, and CALTECH peak above 95% when  $\theta \approx 0.4$ ; the accuracies for ARXIV and SNAP FB peak above 88% and 70%, respectively, for  $\theta \approx 0.6$ . We choose  $\theta = 0.4$  for the cross-reconstruction experiments for the Facebook networks CALTECH, HARVARD, MIT, and UCLA in Figures 5b,c. These four Facebook networks have self-reconstruction accuracies above 80% for  $r = 25$  motifs with a threshold of  $\theta = 0.4$ . The total number of dimensions when using mesoscale patches at scale  $k = 21$  is 190, so this result suggests that all eight of these real-world networks have low-rank mesoscale structures at scale  $k = 21$ .

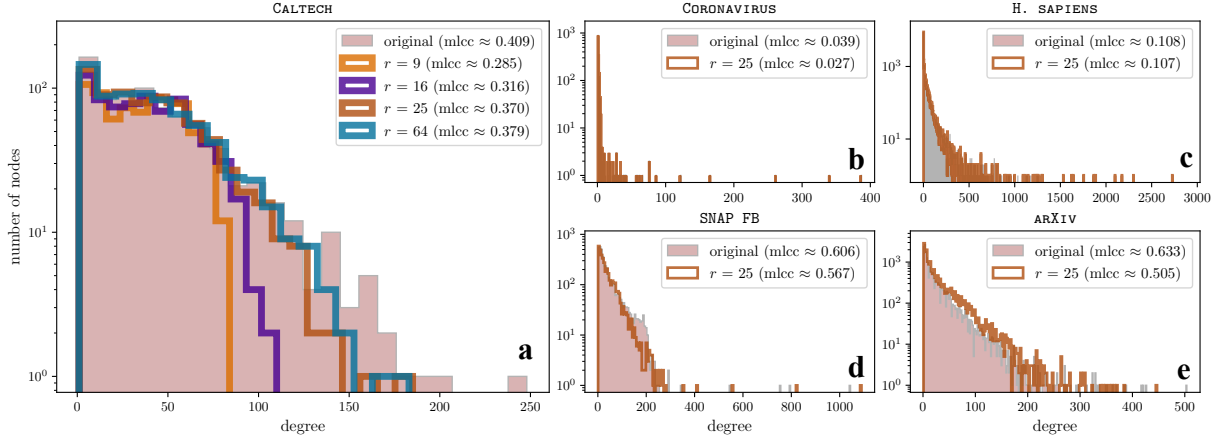


FIGURE 6. A comparison of the degree distributions (which we show as histograms) and the mean local clustering coefficients (which we write in the legends as ‘mlcc’) of the original network and the reconstructed networks using  $r$  latent motifs at scale  $k = 21$  for the five networks in Figure 5a. In panel a, we use the four unweighted reconstructed networks for CALTECH with  $r \in \{9, 16, 25, 64\}$  latent motifs that we used to compute the self-reconstruction accuracy in 5b. As we increase  $r$ , we observe that the mean local clustering coefficient increases towards its value in the original network and that the degree distributions of the reconstructed networks converge to that of the original network. (By increasing  $r$ , we are able to include nodes with progressively larger degrees in the latent motifs.) In panels b–e, we show the mean local clustering coefficients and degree distributions of the unweighted reconstructed networks for CORONAVIRUS, H. SAPIENS, SNAP FB, and ARXIV with  $r = 25$  latent motifs that we used to compute the self-reconstruction accuracy in Figures 5b–e.

We gain further insights into our self-reconstruction experiments by comparing the degree distributions and the mean local clustering coefficients of the original and the unweighted reconstructed networks with threshold  $\theta = 0.4$  (see Figure 6). The mean local clustering coefficients of all reconstructed networks are close to those of the corresponding original networks. In Figure 6a, we show that the degree distributions of the reconstructed networks for CALTECH with  $r \in \{9, 16, 25, 64\}$  latent motifs converge toward that of the original network as we increase  $r$ . Reconstructing CALTECH with larger values of  $r$  appears to gain accuracy by including nodes with a larger degree than is possible for smaller values of  $r$ . In other words, ‘low-rank’ reconstructions (i.e., those with small values of  $r$ ) of CALTECH seem to recover only a small number of the edges of each node, even though it is able to achieve a large reconstruction accuracy (e.g., over 81% for  $r = 9$ ).

We consider cross-reconstruction accuracies  $Y \leftarrow X$  in Figures 5b,c, where  $Y$  is one of the Facebook networks CALTECH, HARVARD, MIT, and UCLA and  $X$  (with  $X \neq Y$ ) is one of the these

four networks or one of the four synthetic networks  $ER_2$ ,  $WS_2$ ,  $BA_2$ , and  $SBM_2$ . From the cross-reconstruction accuracies and examining the network structures of the the latent motifs (see Section B.4 of the SI) in Figures 2 and 4 (also see Figures 14, 16, and 17 in the SI), we draw the following conclusions at scale  $k = 21$ . First, the mesoscale structure of **CALTECH** is distinct from those of **HARVARD**, **UCLA**, and **MIT**. This is consistent with prior studies of these networks (see, e.g., [26, 30]). Second, **CALTECH**'s mesoscale structure at scale  $k = 21$  has a higher dimension than those of the other three universities' Facebook networks. Third, **CALTECH** has a lot more communities with at least 10 nodes than the other three universities' Facebook networks (also see Figure 3). Fourth, the BA network  $BA_2$  captures the mesoscale structures of **MIT**, **HARVARD**, and **UCLA** at scale  $k = 21$  better than the synthetic networks that we generate from the ER, WS, and SBM models; However,  $SBM_2$  captures the mesoscale structure of **CALTECH** better than all other networks in Figure 5b except for **CALTECH** itself for  $r \in \{9, 15, 25, 49\}$ . See Section F.5 of the SI for further discussion.

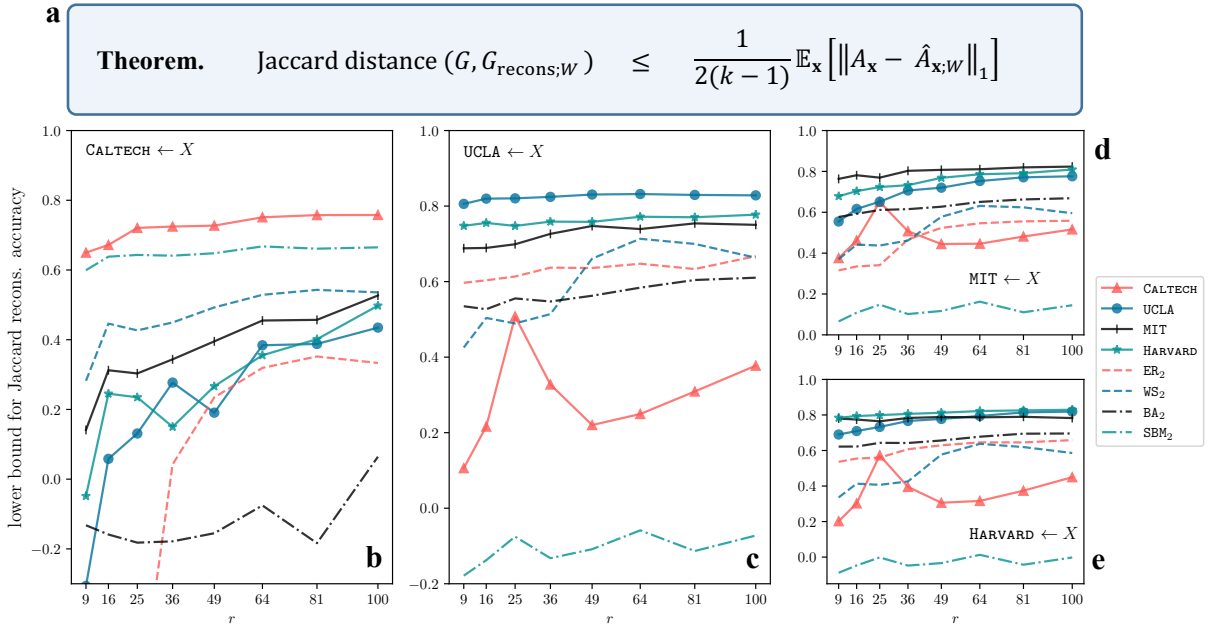


FIGURE 7. We prove that a Jaccard reconstruction error of weighted reconstructed networks (i.e., without thresholding edge weights as in Figure 5) is upper-bounded by the mean approximation error of  $k$ -node subgraphs by  $k$ -path latent motifs divided by  $2(k-1)$ . We state this result concisely as the inequality in panel a. Given a network  $G$  and a network dictionary  $W$  of  $k$ -path latent motifs, let  $G_{\text{recons};W}$  denote the weighted reconstructed network that we obtain using our NDR algorithm (see Algorithm NDR in our SI). We define the Jaccard distance in (30) in the SI. On the right-hand side of the inequality,  $\mathbf{x}$  is a uniformly random  $k$ -path in  $G$ , the matrix  $A_{\mathbf{x}}$  is the  $k \times k$  adjacency matrix of the subgraph that is induced by the node set of  $\mathbf{x}$ , and  $\hat{A}_{\mathbf{x};W}$  is the best nonnegative linear approximation of  $A_{\mathbf{x}}$  that we obtain using the latent motifs in  $W$ . (See Section 7.3 and Theorem 7.4 in our SI for precise statements of relevant definitions and the mathematical result.) Using a crude network dictionary that consists of a single  $k$ -path, this upper bound is the mean number of off-chain edges in mesoscale patches of a network divided by  $k-1$ . For an ER network with expected edge density  $p$ , this quantity equals  $kp/2$ . Subtracting both sides of the inequality in panel a from 1 yields a lower bound for the Jaccard reconstruction accuracy. We plot this lower bound in panels b–e for the same parameters as in Figures 5b–e (i.e.,  $k = 21$  and  $r \in \{6, 16, 25, 36, 49, 64, 81, 100\}$ ).

We also comment briefly about the cross-reconstruction experiments in Figure 5 that use latent motifs that we learn from ER networks. For instance, when reconstructing **MIT**, **HARVARD**,

and UCLA using latent motifs that we learn from  $ER_2$ , we obtain a reconstruction accuracy of at least 72%. This may seem unreasonable at first glance because the latent motifs that we learn from  $ER_2$  should not have any information about the Facebook networks. However, all of these networks are sparse (with edge densities of at most 0.02) and we are sampling subgraphs using  $k$ -paths. The  $k$ -node subgraphs that are induced by uniformly random  $k$ -paths in these sparse networks have only a few off-chain edges (see Figure 1). For example, the  $k$ -node subgraphs that one samples from the sparse ER network  $ER_2$  tend to have  $k$ -node paths and a few extra off-chain edges (see Figure 1). A similarly sparse or sparser network, such as UCLA (whose edge density is about 0.0036) has similar subgraph patterns (even though, unlike the subgraphs of  $ER_2$ , the off-chain edges are not independent). This is the reason that we can reconstruct some networks with high accuracy by using latent motifs that we learn from a completely unrelated network.

Our discussion in the previous paragraph suggests an important question. When reconstructing a sparse network using a network dictionary, how much reconstruction accuracy should we expect as a baseline? More generally, if we have a network dictionary that is effective at approximating the mesoscale patches of a network, how much reconstruction accuracy do we expect? In the present paper, we state and prove a novel theorem that answers this question. Specifically, we prove mathematically that a global Jaccard reconstruction error of a weighted reconstructed network (i.e., without thresholding edge weights as in Figure 5) is upper-bounded by the mean approximation error of the mesoscale patches (i.e.,  $k$ -node subgraphs) of a network by the  $k$ -path latent motifs divided by  $2(k - 1)$ . See Section 7.3 and Theorem 7.4 in our SI for precise statements of the relevant definitions and the mathematical result.

Our NDL algorithm (see Algorithm NDL) finds a network dictionary that approximately minimizes the upper bound in the inequality in Figure 7a. (See Theorem 7.4 in the SI.) Using an arbitrary network dictionary is likely to yield larger values of the upper bound. Therefore, according to the theorem in Figure 7a, it is likely to yield a less accurate weighted reconstructed network. For instance, consider using a network dictionary that consists of a single  $k$ -path, the aforementioned upper bound is the mean number of off-chain edges in mesoscale patches of a network divided by  $k - 1$ . (See the right inequality in Figure 7a.) For any ER network with expected edge density  $p$ , this quantity equals  $kp/2$  in expectation. At scale  $k = 20$  for  $ER_2$ , this value is 0.5. Consequently, we expect a reconstruction accuracy of at least 50% when reconstructing  $ER_2$  using latent motifs (such as the ones for UCLA in Figure 2) that have large on-chain entries and small off-chain entries. Substituting the edge density of UCLA for  $p$ , we expect a reconstruction accuracy of at least 94%. However, according to the first inequality in Figure 7a, the lower bound for the reconstruction accuracy that we obtain using latent motifs of UCLA is about 80%. Therefore, for UCLA, we expect to obtain many more off-chain edges in mesoscale patches than what we expect from an ER network with the same edge density. We plot the lower bound of the reconstruction accuracy in Figures 7b–e for the parameters in Figures 5b–e (i.e.,  $k = 21$  and  $r \in \{6, 16, 25, 36, 49, 64, 81, 100\}$ ). The lower bound for the self-reconstructions is not too far from the actual reconstruction accuracy for unweighted reconstructed networks in Figures 5b–e (it is within 20% for CALTECH and UCLA and within 10% for MIT and HARVARD for all  $r$ ), but there is a much larger accuracy gap for the cross-reconstruction experiments (e.g., there is at least a 50% difference for UCLA←CALTECH). This indicates that, even if one uses latent motifs that are not very efficient at mesoscale approximation, one can obtain unweighted global reconstructions that are significantly more accurate than what is guaranteed by the theoretically proven bounds.

**Network denoising using latent motifs.** In Figure 9, we use our NDL and NDR algorithms to perform two types of network denoising. We can think of these two types of network denoising as distinct binary-classification problems. One of them is network denoising with *subtractive noise*

(which is often called edge ‘prediction’ [49, 12, 21, 39, 43], and the other is network denoising with *additive noise* [38]). In each scenario, we suppose that we are given an observed network  $G = (V, E)$  with a node set  $V$  and an edge set  $E$  and that we are asked to find an unknown network  $G' = (V, E')$  with the same node set  $V$  but a possibly different edge set  $E'$ . We interpret  $G$  as a corrupted version of a ‘true network’  $G'$  that we observe with some uncertainty. We interpret edges and non-edges in  $G$  as ‘false relations’ and ‘false non-relations’, respectively. In the subtractive-noise setting, we assume that  $G$  is a partially observed version of  $G'$  (i.e.,  $E \subsetneq E'$ ), and we seek to classify all non-edges in  $G$  as ‘positives’ (i.e., edges in  $G'$ ) or ‘negatives’ (i.e., non-edges in  $G'$ ). In the additive-noise setting, we suppose that  $G$  is a corrupted version of  $G'$  that includes false edges (i.e.,  $E \supseteq E'$ ), and we seek to classify all edges in  $G$  into ‘positives’ (i.e., edges in  $G'$ ) and ‘negatives’ (i.e., non-edges in  $G'$ ).

In our study of these two binary-classification problems, we use the following five real-world networks: CALTECH, SNAP FB, ARXIV, CORONAVIRUS, and H. SAPIENS. Given a network  $G = (V, E)$ , our experiments proceed as follows. In the subtractive-noise setting, we create a smaller network by removing half of the existing edges, which we choose uniformly at random, such that the remaining network is connected. We refer to this noise type as ‘-ER’. In the additive-noise setting, we create two types of corrupted networks. We create the first type of corrupted network by adding edges between node pairs that we choose independently with a fixed probability so that 50% of the edges in a corrupted network are new. We refer to this noise type as ‘+ER’. We create the second type of corrupted network by adding false edges in a structured way by generating them using the WS model. We select 100 nodes for four of the networks (the exception is that we select 500 for H. SAPIENS) uniformly at random and generate 1,000 new edges (we generate 30,000 new edges for H. SAPIENS) according to the WS model. In this corrupting WS network, each node in a ring of 100 nodes is adjacent to its 20 nearest neighbors and we uniformly randomly choose 30% of the edges to rewire. When rewiring an edge, we choose between its two ends with equal probability of each, and we attach this end to a node in the network that we choose uniformly at random. We add those newly generated edges to the original network. We refer to this noise type as ‘+WS’.

For each corrupted network, we apply NDL to learn a network dictionary. We then use each dictionary to reconstruct the corrupted network. We anticipate that the reconstructed network is similar to its corresponding original (i.e., uncorrupted) network. The reconstruction algorithms output a weighted network  $G_{\text{recons}}$ , where the weight of each edge is our confidence that the edge is a true edge of that network. For denoising subtractive (respectively, additive) noise, we classify each non-edge (respectively, each edge) in a corrupted network as ‘positive’ if its weight in  $G_{\text{recons}}$  is strictly larger than some threshold  $\theta$  and ‘negative’ otherwise. By varying  $\theta$ , we construct a receiver-operating characteristic (ROC) curve that consists of points whose horizontal and vertical coordinates are the false-positive rates and true-positive rates, respectively. For denoising the -ER (respectively, +ER or +WS) noise, one can also infer an optimal value of  $\theta$  for a 50% training set of non-edges (respectively, edges) in  $G$  with known labels and then use this value of  $\theta$  to compute classification measures such as accuracy and precision.

Based on our experiments, the network-reconstruction algorithm that we described earlier seems to mostly be effective when denoising subtractive noise. However, when denoising additive noise (for both +ER and +WS), the edge weights in a reconstructed network can result in ROC curves with an area under the curve (AUC) that is as small as 0.5. For instance, as we show in the histogram in Figure 8b, when we denoise CALTECH with +ER noise, the false edges are assigned weights that are significantly larger than those of the true edges when we reconstruct the observed network using latent motifs that we learn from the corrupted network (see Figure 8h). Consequently, we obtain an AUC of 0.5 for our classification. There is a simple explanation of this result. The Markov-chain Monte Carlo (MCMC) sampling algorithm, which incrementally

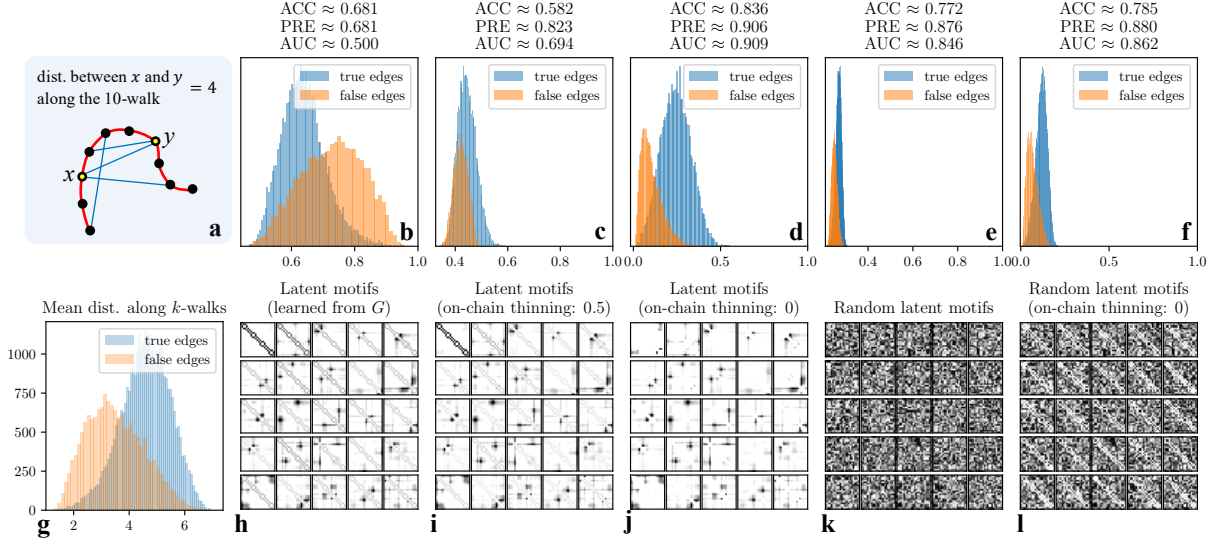


FIGURE 8. Denoising CALTECH corrupted by 50% additive noise of type ER. There are 16,656 true (i.e., original) edges and 7,854 false (i.e., added) edges to correctly classify. As we illustrate in panel **a**, when a  $k$ -walk connects two nodes  $x$  and  $y$ , we define the distance between  $x$  and  $y$  along the  $k$ -walk to be the shortest-path distance between  $x$  and  $y$ . During reconstruction, we sample a sequence of  $k$ -walks in a network using a Markov-chain Monte Carlo (MCMC) algorithm (see Algorithm MP in the SI). Suppose that this sequence is  $\mathbf{x}_1, \dots, \mathbf{x}_T$ . We compute the mean of the distances between  $x$  and  $y$  along the  $k$ -walk  $\mathbf{x}_t$  for all  $t \in \{1, \dots, T\}$  such that  $\mathbf{x}_t$  connects  $x$  and  $y$ . In panel **g**, we show the histogram of the mean distances along the  $k$ -walks  $\mathbf{x}_1, \dots, \mathbf{x}_T$  between the two ends of true edges and the two ends of false edges. In panels **b–f**, we show histograms of edge weights for various reconstructions using 21-node latent motifs (as weighted adjacency matrices) in panels **h–l**. We learn the 25 latent motifs in panel **h** from the corrupted network. We multiply the on-chain edge weights of these latent motifs by a thinning parameter of  $\xi = 0.5$  and  $\xi = 0$  to obtain the matrices in panels **i** and **j**, respectively. We randomly choose the latent motifs in panel **k** by drawing each entry of its  $k \times k$  weighted adjacency matrix independently and uniformly from  $[0, 1]$ . Setting the on-chain entries to 0 of such random latent motifs gives the matrices in panel **l**. The classification accuracy (ACC) and precision (PRE) use the optimal threshold for truncating weighted edges in the reconstruction that we compute from a uniformly randomly chosen training set of edges (with 50% of the edges in the observed network). The area under the curve (AUC) refers to the area under the receiver-operating characteristic (ROC) curve.

evolves a specified  $k$ -walk, that we use throughout the denoising process tends to connect false edges using a smaller number of edges than it uses to connect true edges. In other words, if there is an edge between nodes  $x$  and  $y$  in an additively corrupted network and we uniformly randomly sample a  $k$ -walk that uses both  $x$  and  $y$ , then the number of edges between these two nodes along the sampled  $k$ -walk tends to be small if the edge between  $x$  and  $y$  is false and tends to be large if it is true (see Figure 8a). This indicates that there are not many ways to connect the two ends of a false edge using a  $k$ -walk that avoids using that false edge. Consequently, of the edges between nodes in a uniformly sampled  $k$ -walk in an additively corrupted network, false edges are more likely to appear as on-chain edges than as off-chain edges. When we consider subtractive noise, an analogous observation holds for true non-edges and false non-edges.

To address this issue, we modify our network-reconstruction algorithm for the specific purpose of network denoising by thinning out the on-chain edge weights of latent motifs prior to the reconstruction. To do this, we multiply the weights of on-chain edges in the latent motifs and in all sampled mesoscale patches by a scalar chain-edge thinning parameter  $\xi \in [0, 1]$ . For instance,

the latent motifs in panels **i** and **j** in Figure 8 use  $\xi = 0.5$  and  $\xi = 0$ , respectively. As we see in the histograms in panels **c** and **d**, the negative edges in the resulting reconstruction have significantly smaller weights than the positive edges. For example, with  $\xi = 0$ , this results in a classification AUC of 0.91.

In Figure 9, we compare the performance of our network-denoising method to the performance of several existing approaches. We use four classical approaches (the JACCARD INDEX, PREFERENTIAL ATTACHMENT, the ADAMIC-ADAR INDEX, and a SPECTRAL EMBEDDING) [12, 20] and two more recent methods (DEEPWALK [28] and NODE2VEC [32]) that are based on network embeddings. Let  $N(x)$  denote the set of neighbors of node  $x$  in a network. For the JACCARD INDEX, PREFERENTIAL ATTACHMENT, and the ADAMIC-ADAR INDEX, the confidence score (which plays the same role as an edge weight in a reconstructed network) that the nodes  $x$  and  $y$  are adjacent via a true edge is  $|N(x) \cap N(y)|/|N(x) \cup N(y)|$ ,  $|N(x)| \cdot |N(y)|$ , and  $\sum_{z \in N(x) \cap N(y)} 1/\ln |N(z)|$ , respectively.

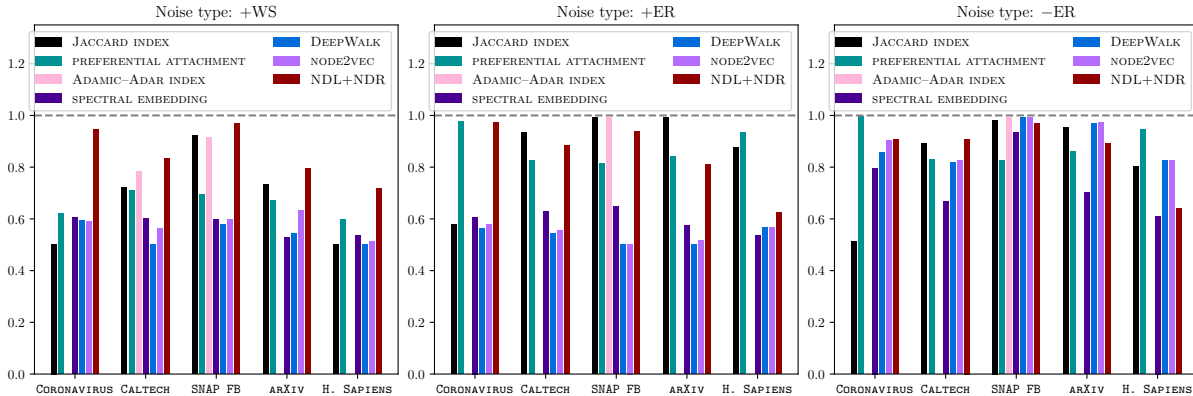


FIGURE 9. Application of our NDL and NDR algorithms to network denoising with additive and subtractive noise on a variety of networks from empirical data sets. In our experiments with subtractive noise, we corrupt a network by removing 50% of its edges uniformly at random. We seek to classify the removed edges and the non-edges as true edges and false edges, respectively. In our experiments with additive noise, we corrupt a network by uniformly randomly adding 50% of the number of its edges or 1,000 random edges for all but one network (we add 30,000 random edges for H. SAPIENS) that we generated using the WS model. We seek to classify the edges and non-edges in the resulting corrupted network as ‘negative’ (i.e., false edges) or ‘positive’ (i.e., true edges). To perform classification in a network, we first use NDL to learn latent motifs from a corrupted network and then reconstruct the networks using NDR to assign a confidence value to each potential edge. We then use these confidence values to infer the correct labeling of potential edges in the uncorrupted network. Importantly, we never use information from the original networks. For each network, we report AUC scores of the ROC curves. See Figure 13 in the SI for accuracy, precision, and recall scores.

We show results in the forms of means of the AUC of the ROC curves for five independent runs of each method. The ADAMIC-ADAR INDEX is not defined for nodes with self-edges, so we do not use it for networks with self-edges (such as ARXIV, CORONAVIRUS, and H. SAPIENS). For our method, we apply NDL at scale  $k = 21$  with  $r \in \{2, 25\}$  to learn latent motifs from the corrupted networks and apply NDR with the chain-edge thinning parameter  $\xi \in \{0, 1\}$ . A thinning parameter of  $\xi = 1$  corresponds to network reconstruction with unchanged latent motifs and mesoscale patches (see Figure 8h), whereas  $\xi = 0$  removes all of the on-chain edges (see Figure 8j).

The existing methods JACCARD INDEX and PREFERENTIAL ATTACHMENT seem to work well for noise types +ER and -ER. For instance, the high performance of PREFERENTIAL ATTACHMENT for CORONAVIRUS with noise type +ER indicates that the product of the degrees of two nodes that are attached via a true edge is larger than the product of the degrees of two nodes that are attached via a false edge. To illustrate why this is the case, consider a star network with five leaves (i.e., degree-1 nodes). In this network, a uniformly randomly chosen non-edge is always attached to two degree-1 nodes, but a uniformly randomly chosen edge is always attached to one degree-5 node (i.e., the center node) and one degree-1 node. As in this star example, all real-world networks that we consider are sparse (with edge densities of at most 0.057, which is the density for CALTECH). One can approximately uniformly randomly choose a non-edge from such sparse networks by choosing two nodes uniformly at random. However, as in the star example, uniformly choosing an edge may induce a bias towards choosing at least one large-degree node.

Our method outperforms all of the other examined methods for denoising +WS structured noise. For example, when we add 1,000 false edges that we generate from the WS model to CORONAVIRUS (which has 2,463 true edges), our method yields an AUC of 0.94. We obtain the second best AUC (of only 0.61) using PREFERENTIAL ATTACHMENT. There are at least two confounding factors to consider in the high accuracy of our network denoising method. First, as we noted before, false edges are more likely to appear as on-chain edges than as off-chain edges in a subgraph that one samples by a uniformly random  $k$ -walk. Consequently, the mean distance between two nodes along  $k$ -walks tends to be larger when they form a true edge than when they form a false edge (as shown in Figure 8a). This distance already somewhat distinguishes the true edges and the false edges. Consequently, we see in Figure 8k,l that we can reasonably successfully denoise the network CALTECH with additive noise of type +ER using randomized latent motifs (in which each we draw each entry of their weighted adjacency matrices independently and uniformly from  $[0, 1]$ ), regardless of whether the on-chain thinning parameter is  $\xi = 1$  (see Figure 8k) or  $\xi = 0$  (see Figure 8l). Second, knowing the exact subgraph mesoscale structure (i.e., the latent motifs of the original network, which by definition does not have false edges) improves the denoising accuracy, which one can infer directly from the observed network (which has false edges) because of the low-rank nature of the examined mesoscale structures of the social and PPI networks (see Figure 5a). Specifically, because NDL learns a small number of latent motifs that are able to successfully give an approximate basis for all mesoscale patches, they should not be affected significantly by noise.

**Conclusions.** We introduced a mesoscale network structure, which we call *latent motifs*, that consists of  $k$ -node subgraphs that are building blocks of all connected  $k$ -node subgraphs of a network. In contrast to motifs [7], which are used frequently to capture overrepresented  $k$ -node subgraphs in a network, nonnegative linear combinations of our latent motifs approximate  $k$ -node subgraphs that are induced by uniformly random  $k$ -paths in a network. We also established theoretically that one can approximate an entire network accurately if one has a dictionary of latent motifs that can accurately approximate the network’s mesoscale structures.

Our computational experiments in Figures 2, 3, and 4 demonstrated that latent motifs can have distinctive network structures at various mesoscales. Our computational experiments in Figures 5, 8, and 9 illustrated that various social, collaboration and PPI networks have low-rank [24] mesoscale structures, in the sense that a few (e.g.,  $r = 25$ , but see Figure 5 for other choices of  $r$ ) latent motifs that we learn using NDL are able to reconstruct, infer, and denoise the edges in an entire network by employing our NDR algorithm. We hypothesize that such low-rank mesoscale structures are a common feature of networks beyond the social, collaboration, and PPI networks that we examined. As we have illustrated in this paper, one can leverage mesoscale

structures to perform important tasks like network denoising, so it is important in future studies to explore the level of generality of our insights.

Notions of motifs have been extended to more complicated network structures, such as temporal networks (in which nodes, edges, and edge weights can change with time) [34] and multilayer networks (in which, e.g., nodes can be adjacent via multiple types of relationships) [33]. We did not consider latent motifs in these generalized network structures in our work, but it is clearly of interest to extend our approach and algorithms to these situations.

#### ACKNOWLEDGEMENTS

HL was supported by the National Science Foundation through grants 2206296 and 2010035. JV was supported by the National Science Foundation through grant 1740325.

#### REFERENCES

- [1] Paul Erdős and Alfréd Rényi. “On random graphs. I”. *Publicationes Mathematicae* 6.18 (1959), pp. 290–297.
- [2] William M. Rand. “Objective criteria for the evaluation of clustering methods”. *Journal of the American Statistical Association* 66.336 (1971), pp. 846–850.
- [3] Paul W. Holland, Kathryn Blackmond Laskey, and Samuel Leinhardt. “Stochastic block-models: First steps”. *Social Networks* 5.2 (1983), pp. 109–137.
- [4] Duncan J. Watts and Steven H. Strogatz. “Collective dynamics of ‘small-world’ networks”. *Nature* 393.6684 (1998), pp. 440–442.
- [5] Albert-László Barabási and Réka Albert. “Emergence of scaling in random networks”. *Science* 286.5439 (1999), pp. 509–512.
- [6] Daniel D. Lee and H. Sebastian Seung. “Learning the parts of objects by non-negative matrix factorization”. *Nature* 401.6755 (1999), pp. 788–791.
- [7] Ron Milo, Shai Shen-Orr, Shalev Itzkovitz, Nadav Kashtan, Dmitri Chklovskii, and Uri Alon. “Network motifs: Simple building blocks of complex networks”. *Science* 298.5594 (2002), pp. 824–827.
- [8] Gavin C. Conant and Andreas Wagner. “Convergent evolution of gene circuits”. *Nature Genetics* 34.3 (2003), pp. 264–266.
- [9] Olaf Sporns, Rolf Kötter, and Karl J. Friston. “Motifs in brain networks”. *PLoS Biology* 2.11 (2004), e369.
- [10] Michael Elad and Michal Aharon. “Image denoising via sparse and redundant representations over learned dictionaries”. *IEEE Transactions on Image Processing* 15.12 (2006), pp. 3736–3745.
- [11] Uri Alon. “Network motifs: Theory and experimental approaches”. *Nature Reviews Genetics* 8.6 (2007), pp. 450–461.
- [12] David Liben-Nowell and Jon Kleinberg. “The link-prediction problem for social networks”. *Journal of the American Society for Information Science and Technology* 58.7 (2007), pp. 1019–1031.
- [13] Julien Mairal, Michael Elad, and Guillermo Sapiro. “Sparse representation for color image restoration”. *IEEE Transactions on Image Processing* 17.1 (2007), pp. 53–69.
- [14] Vincent D. Blondel, Jean-Loup Guillaume, Renaud Lambiotte, and Etienne Lefebvre. “Fast unfolding of communities in large networks”. *Journal of Statistical Mechanics: Theory and Experiment* 2008.10 (2008), P10008.
- [15] Krzysztof Juszczyszyn, Przemyslaw Kazienko, and Bogdan Gabrys. “Temporal changes in local topology of an email-based social network”. *Computing and Informatics* 28.6 (2009), pp. 763–779.



- [16] Gabriel Peyré. “Sparse modeling of textures”. *Journal of Mathematical Imaging and Vision* 34.1 (2009), pp. 17–31.
- [17] Mason A. Porter, Jukka-Pekka Onnela, and Peter J. Mucha. “Communities in networks”. *Notices of the American Mathematical Society* 56.9 (2009), pp. 1082–1097, 1164–1166.
- [18] Takaaki Ohnishi, Hideki Takayasu, and Misako Takayasu. “Network motifs in an inter-firm network”. *Journal of Economic Interaction and Coordination* 5.2 (2010), pp. 171–180.
- [19] Jason M. K. Rip, Kevin S. McCann, Denis H. Lynn, and Sonia Fawcett. “An experimental test of a fundamental food web motif”. *Proceedings of the Royal Society B: Biological Sciences* 277.1688 (2010), pp. 1743–1749.
- [20] Mohammad Al Hasan and Mohammed J. Zaki. “A survey of link prediction in social networks”. *Social Network Data Analytics*. Springer, 2011, pp. 243–275.
- [21] Aditya Krishna Menon and Charles Elkan. “Link prediction via matrix factorization”. *Machine Learning and Knowledge Discovery in Databases*. Ed. by Dimitrios Gunopulos, Thomas Hofmann, Donato Malerba, and Michalis Vazirgiannis. Heidelberg, Germany: Springer-Verlag, 2011, pp. 437–452.
- [22] Veronica Red, Eric D. Kelsic, Peter J. Mucha, and Mason A. Porter. “Comparing community structure to characteristics in online collegiate social networks”. *SIAM Review* 53 (2011), pp. 526–543.
- [23] Jure Leskovec and Julian J. McAuley. “Learning to discover social circles in ego networks”. *Advances in Neural Information Processing Systems*. 2012, pp. 539–547.
- [24] Ivan Markovsky and Konstantin Usevich. *Low Rank Approximation*. Heidelberg, Germany: Springer-Verlag, 2012.
- [25] Jukka-Pekka Onnela, Daniel J. Fenn, Stephen Reid, Mason A. Porter, Peter J. Mucha, Mark D. Fricker, and Nick S. Jones. “Taxonomies of networks from community structure”. *Physical Review E* 86.3 (2012), p. 036104.
- [26] Amanda L. Traud, Peter J. Mucha, and Mason A. Porter. “Social structure of Facebook networks”. *Physica A* 391.16 (2012), pp. 4165–4180.
- [27] Xu Hong-lin, Yan Han-bing, Gao Cui-fang, and Zhu Ping. “Social network analysis based on network motifs”. *Journal of Applied Mathematics* 2014 (2014), p. 874708.
- [28] Bryan Perozzi, Rami Al-Rfou, and Steven Skiena. “DeepWalk: Online learning of social representations”. *Proceedings of the 20th ACM SIGKDD International Conference on Knowledge Discovery and Data Mining*. 2014, pp. 701–710.
- [29] Konstantin Ristl, Sebastian J. Plitzko, and Barbara Drossel. “Complex response of a food-web module to symmetric and asymmetric migration between several patches”. *Journal of Theoretical Biology* 354 (2014), pp. 54–59.
- [30] Lucas G. S. Jeub, Prakash Balachandran, Mason A. Porter, Peter J. Mucha, and Michael W. Mahoney. “Think locally, act locally: Detection of small, medium-sized, and large communities in large networks”. *Physical Review E* 91 (1 2015), p. 012821.
- [31] Santo Fortunato and Darko Hric. “Community detection in networks: A user guide”. *Physics Reports* 659 (2016), pp. 1–44.
- [32] Aditya Grover and Jure Leskovec. “NODE2VEC: Scalable feature learning for networks”. 2016, pp. 855–864.
- [33] Federico Battiston, Vincenzo Nicosia, Mario Chavez, and Vito Latora. “Multilayer motif analysis of brain networks”. *Chaos: An Interdisciplinary Journal of Nonlinear Science* 27.4 (2017), p. 047404.
- [34] Ashwin Paranjape, Austin R Benson, and Jure Leskovec. “Motifs in temporal networks”. *Proceedings of the tenth ACM international conference on web search and data mining*. 2017, pp. 601–610.

- [35] Ankit N. Khambhati, Ann E. Sizemore, Richard F. Betzel, and Danielle S. Bassett. “Modeling and interpreting mesoscale network dynamics”. *NeuroImage* 180 (2018), pp. 337–349.
- [36] Mark E. J. Newman. *Networks*. Second. Oxford, UK: Oxford University Press, 2018.
- [37] Frank W. Takes, Walter A. Kosters, Boyd Witte, and Eelke M. Heemskerk. “Multiplex network motifs as building blocks of corporate networks”. *Applied Network Science* 3.1 (2018), pp. 1–22.
- [38] Fernanda B. Correia, Edgar D. Coelho, José L. Oliveira, and Joel P. Arrais. “Handling noise in protein interaction networks”. *BioMed Research International* 2019 (2019), pp. 1–13.
- [39] Katja Kovács István A. and Luck, Kerstin Spirohn, Yang Wang, Carl Pollis, Sadie Schlabach, Wenting Bian, Dae-Kyum Kim, Nishka Kishore, and Tong Hao. “Network-based prediction of protein interactions”. *Nature Communications* 10.1 (2019), p. 1240.
- [40] Hanbaek Lyu, Facundo Memoli, and David Sivakoff. “Sampling random graph homomorphisms and applications to network data analysis”. *arXiv:1910.09483* (2019).
- [41] Rose Oughtred, Chris Stark, Bobby-Joe Breitkreutz, Jennifer Rust, Lorrie Boucher, Christie Chang, Nadine Kolas, Lara O’Donnell, Genie Leung, and Rochelle McAdam. “The BioGRID interaction database: 2019 update”. *Nucleic Acids Research* 47.D1 (2019), pp. D529–D541.
- [42] David E. Gordon, Gwendolyn M. Jang, Mehdi Bouhaddou, Jiewei Xu, Kirsten Obernier, Kris M. White, Matthew J. O’Meara, Veronica V. Rezelj, Jeffrey Z. Guo, and Danielle L. Swaney. “A SARS-CoV-2 protein interaction map reveals targets for drug repurposing”. *Nature* 583 (2020), pp. 1–13.
- [43] Roger Guimerà. “One model to rule them all in network science?” *Proceedings of the National Academy of Sciences of the United States of America* 117.41 (2020), pp. 25195–25197.
- [44] Jure Leskovec and Andrej Krevl. “SNAP Datasets: Stanford Large Network Dataset Collection”. Available at <http://snap.stanford.edu/data>. 2020.
- [45] Hanbaek Lyu, Deanna Needell, and Laura Balzano. “Online matrix factorization for Markovian data and applications to network dictionary learning”. *Journal of Machine Learning Research* 21 (2020), pp. 1–49.
- [46] C. Seshadhri, Aneesh Sharma, Andrew Stolman, and Ashish Goel. “The impossibility of low-rank representations for triangle-rich complex networks”. *Proceedings of the National Academy of Sciences of the United States of America* 117.11 (2020), pp. 5631–5637.
- [47] theBiogrid.org. “Coronavirus PPI network” (2020). Retrieved from <https://wiki.thebiogrid.org/doku.php/covid> (downloaded 24 July 2020, Ver. 3.5.187.tab3).
- [48] Alice C. Schwarze and Mason A. Porter. “Motifs for processes on networks”. *SIAM Journal on Applied Dynamical Systems* 20.4 (2021), pp. 2516–2557.
- [49] Tao Zhou. “Progresses and challenges in link prediction”. *iScience* 24.11 (2021), p. 103217.

## METHODS

We briefly discuss our algorithms for network dictionary learning (NDL) and network denoising and reconstruction (NDR). We also provide a detailed description of the employed real-world and synthetic networks.

In this section, we restrict our discussion to networks that one can represent as a graph  $G = (V, E)$  with a node-set  $V$  and an edge set  $E$  without directed edges or multi-edges (but possibly with self-edges). In our SI, we give an extended discussion that applies to more general types of networks. Specifically, in that discussion, we no longer restrict edges to have binary weights; instead, the weights may be continuous-valued. See Section B.1 of the SI.

**Motif sampling and mesoscale patches of networks.** Natural candidates for the mesoscale patches of a network are its connected  $k$ -node subgraphs. These subgraphs have  $k$  nodes that

inherit their adjacency structures from the original networks from which we draw them. It is convenient to consider the  $k \times k$  adjacency matrices of these subgraphs, as it allows us to perform computations on the space of subgraphs. However, we need to address two issues to do this. First, because the same  $k$ -node subgraph can have multiple (specifically,  $k!$ ) different representations as an adjacency matrix (depending on the ordering of its nodes), we need an unambiguous way to choose an ordering of its nodes. Second, because most real-world networks are sparse [36], independently choosing a set of  $k$  nodes from a network may yield only a few edges and may thus often result in a disconnected subgraph. Therefore, we need an efficient sampling algorithm to guarantee that we obtain connected  $k$ -node subgraphs when we sample from sparse networks.

We employ an approach that is based on *motif sampling* [40] both to choose an ordering of the nodes in a  $k$ -node subgraph and to ensure that we sample connected subgraphs from sparse networks. The key idea is to consider the random  $k$ -node subgraph that we obtain by first sampling a copy of a ‘template’ subgraph uniformly at random and including all edges between the sampled nodes of the network. We take such a template to be a ‘ $k$ -path’. A sequence  $\mathbf{x} = (x_1, \dots, x_k)$  of  $k$  (not necessarily distinct) nodes is a  $k$ -walk if  $x_i$  and  $x_{i+1}$  are adjacent for all  $i \in \{1, \dots, k-1\}$ . A  $k$ -walk is a  $k$ -path if all nodes in the walk are distinct (see Figure 1). For each  $k$ -path  $\mathbf{x} = (x_1, \dots, x_k)$ , we define the corresponding mesoscale patch of a network to be the  $k \times k$  matrix  $A_{\mathbf{x}}$  such that  $A_{\mathbf{x}}(i, j) = 1$  if nodes  $x_i$  and  $x_j$  are adjacent and  $A_{\mathbf{x}}(i, j) = 0$  if they are not adjacent. This is the adjacency matrix of the  $k$ -node subgraph of the network with nodes  $x_1, \dots, x_k$ . One can use one of the Markov-chain Monte Carlo (MCMC) algorithms for motif sampling from [40] to efficiently and uniformly randomly sample a  $k$ -walk from a sparse network. By only accepting samples in which the  $k$ -walk has  $k$  distinct nodes (i.e., so that it is  $k$ -path), we efficiently sample a uniformly random  $k$ -path from a network, as long as  $k$  is not too large. If  $k$  is too large, one has to ‘reject’ too many samples of  $k$ -walks that are not  $k$ -paths. The expected number of rejected samples is approximately the number of  $k$ -walks divided by the number of  $k$ -paths. The number of  $k$ -walks in a network grows monotonically with  $k$ , but the number of  $k$ -paths can decrease with  $k$  and it becomes identically 0 if  $k$  exceeds the shortest-path diameter of the network. (See Section C of the SI for a detailed discussion.) Consequently, by repeatedly sampling  $k$ -paths  $\mathbf{x}$ , we obtain a data set of mesoscale patches  $A_{\mathbf{x}}$  of a network.

**Algorithm for network dictionary learning.** We now present the basic structure of the algorithms that we employ for *network dictionary learning* (NDL) [45]. Suppose that we compute all possible  $k$ -paths  $\mathbf{x}_1, \dots, \mathbf{x}_M$  and their corresponding mesoscale patches  $A_{\mathbf{x}_t}$  (which are  $k \times k$  binary matrices) for  $t \in \{1, \dots, M\}$  of a network. We column-wise vectorize (i.e., we place the second column underneath the first column and so on; see Algorithm A4 in the SI) each of these  $k \times k$  mesoscale patches to obtain a  $k^2 \times M$  data matrix  $X$ . We then apply nonnegative matrix factorization (NMF) [6] to obtain a  $k^2 \times r$  nonnegative matrix  $W$  for some fixed integer  $r \geq 1$  to yield an approximate factorization  $X \approx WH$  for some nonnegative matrix  $H$ . From this procedure, we approximate each column of  $X$  by the nonnegative linear combination of the  $r$  columns of  $W$ ; its coefficients are the entries of the corresponding column of  $H$ . If we let  $\mathcal{L}_i$  be the  $k \times k$  matrix that we obtain by reshaping the  $i^{\text{th}}$  column of  $W$  (using Algorithm A5 in SI), then  $\mathcal{L}_1, \dots, \mathcal{L}_r$  are the learned latent motifs; they form a network dictionary. The set of these latent motifs is an approximate basis (but not a subset) of the set  $A_{\mathbf{x}_1}, \dots, A_{\mathbf{x}_M}$  of mesoscale patches. For instance, latent motifs have entries that take continuous values between 0 and 1, but mesoscale patches have binary entries. We can regard each  $\mathcal{L}_i$  as the  $k$ -node weighted network with node set  $\{1, \dots, k\}$  and weighted adjacency matrix  $\mathcal{L}_i$ . See Figure 2 for an illustration of latent motifs as weighted networks.

The scheme in the paragraph above requires us to store all possible mesoscale patches of a network, entailing a memory requirement that is at least of order  $k^2 M$ , where  $M$  denotes the total

number of mesoscale patches in a network. Because  $M$  scales with the size of the network from which we sample subgraphs, we need unbounded memory to handle arbitrarily large networks. To address this issue, Algorithm **NDL** implements the above scheme in the setting of ‘online learning’, where subsets (so-called ‘minibatches’) of data arrive in a sequential manner and one does not store previous subsets of the data before processing new subsets. Specifically, at each iteration  $t = 1, 2, \dots, T$ , we process a sample matrix  $X_t$  that is smaller than the full matrix  $X$  and includes only  $N \ll M$  mesoscale patches, where one can take  $N$  to be independent of the network size. Instead of a standard NMF algorithm for a fixed matrix [50], we use an ‘online’ NMF algorithm [53, 45] that one can use on sequences of matrices, where the intermediate dictionary matrices  $W_t$  that we obtain by factoring the sample matrix  $X_t$  typically improve as we iterate (see [53, 45]). In Algorithm **NDL** in the SI, we give a complete implementation of the NDL algorithm.

**Algorithm for network denoising and reconstruction.** Suppose that we have an image  $\gamma$  of size  $k \times k$  pixels and a set of ‘basis images’  $\beta_1, \dots, \beta_r$  of the same size. We can ‘reconstruct’ the image  $\gamma$  using the basis images  $\beta_1, \dots, \beta_r$  by finding nonnegative coefficients  $a_1, \dots, a_r$  such that the linear combination  $\hat{\gamma} = a_1\beta_1 + \dots + a_r\beta_r$  is as close as possible to  $\gamma$ . The basis images determine what shapes and colors of the original image to capture in the reconstruction  $\hat{\gamma}$ . In the standard pipeline for image denoising and reconstruction [10, 51, 52], one assumes that the size  $k \times k$  of the square ‘patches’ is much smaller than the full image  $\gamma$ . One can then sample a large number of  $k \times k$  overlapping patches  $\gamma_1, \dots, \gamma_M$  of the image  $\gamma$  and obtain their best linear approximations  $\hat{\gamma}_1, \dots, \hat{\gamma}_M$  of them using the basis images  $\beta_1, \dots, \beta_r$ . Because the  $k \times k$  patches  $\gamma_1, \dots, \gamma_M$  overlap, each pixel  $(I, J)$  of  $\gamma$  can occur in multiple instances of  $\gamma_1, \dots, \gamma_M$ . Therefore, we take the mean of the corresponding values in the mesoscale reconstruction  $\hat{\gamma}_0$  as the value of the pixel  $(I, J)$  in the global reconstruction  $\hat{\gamma}$ .

As an illustration, consider reconstructing the color image in Figure 10a in two ways, which yield the images in panels b and c. In panel d, we show the dictionary with 25 basis images of size  $21 \times 21$  pixels. We uniformly randomly choose the color of each pixel from all possible colors (which we represent as vectors in  $[0, 256]^3$  for red–green–blue (RGB) weights). The basis images do not include any information about the original image in panel a, so the linear approximation of the  $21 \times 21$  mesoscale patches of the image in panel a using the basis images in panel d may be inaccurate. However, when we reconstruct the entire image from panel a using the basis images in panel d, we do observe some basic geometric information from the original image. We show the image that results from this reconstruction in panel b. Importantly, the image reconstruction in b uses both the basis images and the original image that one seeks to reconstruct. Unfortunately, the colors have averaged out to be neutral, so the reconstructed image is monochrome. Using a smaller (e.g.,  $5 \times 5$ ) randomly generated (with each pixel again taking an independently and uniformly chosen color) basis-image set for reconstruction results in a similar monochrome (but sharper) reconstructed image. Notably, one can learn the basis images in panel e from the image in panel f using nonnegative matrix factorization (NMF) [6]. The image in f is in black and white, and thus so are the images in e. The corresponding reconstruction in panel c has nicely captured shapes from the original image, although we have lost the color information in the original image in panel a and the reconstruction in panel d is thus in black and white.

A network analog of the above patch-based image reconstruction proceeds as follows. Given a network  $G = (V, E)$  and latent motifs  $(\mathcal{L}_1, \dots, \mathcal{L}_r)$  (which we do not necessarily compute from  $G$ ; see Figure 10), we obtain a weighted network  $G_{\text{recons}}$  using the same node set  $V$  and a weighted adjacency matrix  $A_{\text{recons}} : V^2 \rightarrow \mathbb{R}$ . To do this, we first uniformly randomly sample a large number  $T$  of  $k$ -walks  $\mathbf{x}_1, \dots, \mathbf{x}_T : \{1, \dots, k\} \rightarrow V$  in  $G$ . We then determine the corresponding mesoscale patches  $A_{\mathbf{x}_1}, \dots, A_{\mathbf{x}_T}$  of  $G$ , which are  $k \times k$  unweighted matrices. We then approximate

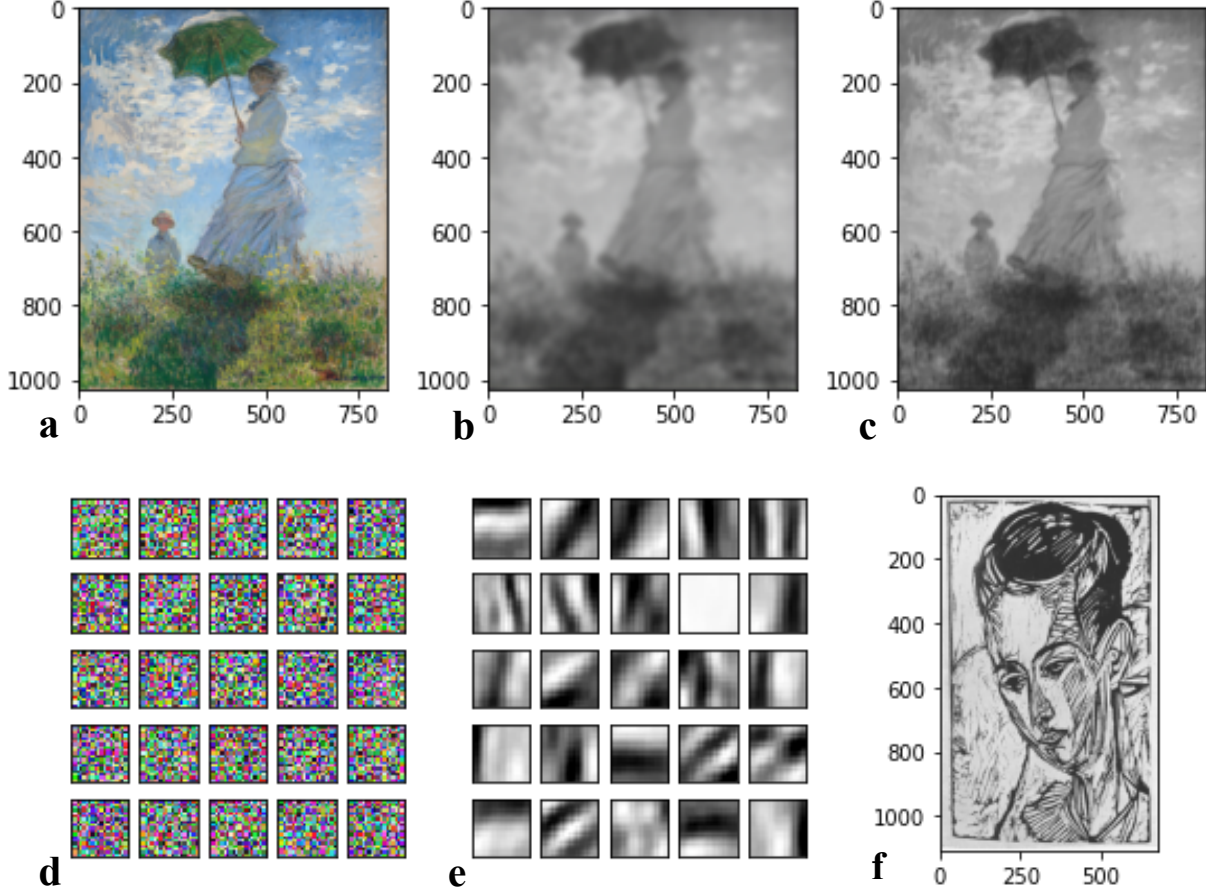


FIGURE 10. **a** image WOMAN WITH A PARASOL - MADAME MONET AND HER SON (Claude Monet, 1875). We show reconstructions of it in **b** and **c**. The image in panel **b** is a reconstruction of the image in panel **a** using the dictionary with 25 basis images of size  $21 \times 21$  pixels in panel **d**. We uniformly randomly choose the color of each pixel from all possible colors (which we represent as vectors in  $[0, 256]^3$  for red–green–blue (RGB) weights). The image in panel **d** is a reconstruction of the image in panel **a** using the dictionary with 25 basis images of size  $21 \times 21$  pixels in panel **e**. We learn this basis from the image in panel **f** using NMF. The image in panel **f** is from the collection DIE GRAPHIK ERNST LUDWIG KIRCHNERS BIS 1924, VON GUSTAV SCHIEFLER BAND I BIS 1916 (Accession Number 2007.141.9, Ernst Ludwig Kirchner, 1926). [We use the images in panels **a** and **f** with permission from the National Gallery of Art in Washington, DC, USA.]

each mesoscale patch  $A_{\mathbf{x}_t}$  by a nonnegative linear combination  $\hat{A}_{\mathbf{x}_t}$  of the latent motifs  $\mathcal{L}_i$ . We seek to ‘replace’ each  $A_{\mathbf{x}_t}$  with  $\hat{A}_{\mathbf{x}_t}$  to construct the weighted adjacency matrix  $A_{\text{recons}}$ . To do this, we define  $A_{\text{recons}}(x, y)$  for each  $x, y \in V$  as the mean of  $\hat{A}_{\mathbf{x}_t}(a, b)$  over all  $t \in \{1, \dots, T\}$  and all  $a, b \in \{1, \dots, k\}$  such that  $\mathbf{x}_t(a) = x$  and  $\mathbf{x}_t(b) = y$ . Our network denoising and reconstruction (NDR) algorithm (see Algorithm **NDR**) builds on this idea. See Section **E** of the SI for more details.

**Comparison of our work with the prior research in [45].** Recently, Lyu et al. [45] proposed a preliminary approach for the algorithms that we propose in the present work — the NDL algorithm with  $k$ -walk sampling and the network-reconstruction — as an application to showcase a theoretical result about the convergence of online NMF for data samples that are not independently and identically distributed (IID) [45, Thm. 1]. A notable limitation of the NDL algorithm in [45] is that one cannot interpret the elements of a network dictionary as latent

motifs and one thus cannot associate them directly with mesoscale structures in networks. Additionally, Lyu et al. [45] does not include any theoretical analysis of either the convergence or the correctness of network reconstruction, so it was unclear from that work whether or not one can reconstruct a network using the low-rank mesoscale structure that is encoded in a network dictionary. Moreover, one cannot use the network-reconstruction algorithm that was proposed in [45] to denoise additive noise unless one knows in advance that the noise is additive (rather than subtractive) before denoising (see [45, Rmk. 4.]). In the present paper, we build substantially on the research in [45] and provide a much more complete computational and theoretical framework to analyze low-rank mesoscale structure of networks. In particular, we overcome all of the aforementioned limitations. In Table 1, we summarize the key differences between the present work and the recent paper by Lyu et al. [45].

<b>NDL</b>	Sampling	Latent motifs	Convergence	Efficient MCMC
Lyu et al. [45]	$k$ -walks	✗	Non-bipartite networks	✗
The present work	$k$ -paths (Alg. RM)	✓	Non-bipartite and bipartite networks (Thm. 7.4, Thm. 7.7)	✓ (Prop. 7.2)

<b>NDR</b>	Sampling	Reconstruction	Denoising	Convergence	Error bound
Lyu et al. [45]	$k$ -walks	✓	✗	✗	✗
The present work	$k$ -walks $k$ -paths	✓	✓	✓ (Thm. 7.10)	✓ (Thm. 7.10)

TABLE 1. A comparison of the contributions in the present work with those in Lyu et al. [45]. In the SI, we give the statements and proofs of the proposition and theorems in this table.

The most significant theoretical advance that we make in the present paper concerns the relationship between global reconstruction error and an approximation error of mesoscale patches by latent motifs, with an explicit dependence on the number of nodes in subgraphs at the mesoscale that we state in Theorem 7.10(iii) of our SI. Informally, Theorem 7.10(iii) states that one can accurately reconstruct a network if one has a dictionary of latent motifs that can accurately approximate mesoscale patches of a network. We illustrate this theoretical result with supporting experiments in Figure 7. A crucial part of our proof of Theorem 7.10 (iii) is our use of an explicit formula for the limiting reconstructed network as the number of iterations that one uses for network reconstruction tends to infinity. We state this explicit formula for the limiting reconstructed network, which is also a novel contribution of the present paper, in Theorem 7.10(ii).

We now elaborate on the use of  $k$ -path sampling in our new NDL algorithm to ensure the interpretability of the network dictionary elements as latent motifs. The NDL algorithm in [45] used the  $k$ -walk motif-sampling algorithm of [40]. That algorithm samples a sequence of  $k$  nodes (which are not necessarily distinct) in which the  $i$ th node is adjacent to the  $(i + 1)$ th node for all  $i \in \{1, \dots, k - 1\}$ . The  $k$ -walks that sample  $k \times k$  subgraph adjacency matrices can have overlapping nodes, so some of the  $k \times k$  adjacency matrices can correspond to subgraphs with fewer than  $k$  nodes. If there are a large number of such subgraphs of a network, then the  $k$ -node latent motifs that one learns from the set of subgraph adjacency matrices can have misleading patterns that may not exist in any  $k$ -node subgraph of the network. This situation occurs in the network CORONAVIRUS PPI, where one obtains clusters of large-degree nodes from the learned

latent motifs if one uses  $k$ -walk sampling. However, this misleading result arises from the  $k$ -walk visiting the same large-degree node many times, rather than because  $k$  distinct nodes of the network actually exhibit this type of connection (see Figure 11). To resolve this issue in the present paper, during the dictionary-learning phase, we combine MCMC  $k$ -walk sampling with rejection sampling so that we use only  $k$ -walks with  $k$  distinct nodes (i.e., we use  $k$ -paths). Consequently, we now learn the  $k$ -node latent motifs only from  $k \times k$  adjacency matrices that correspond to  $k$ -node subgraphs of the network. This guarantees that any network structure (e.g., large-degree nodes, communities, and so on) in the latent motifs must also exist in the network at scale  $k$ .

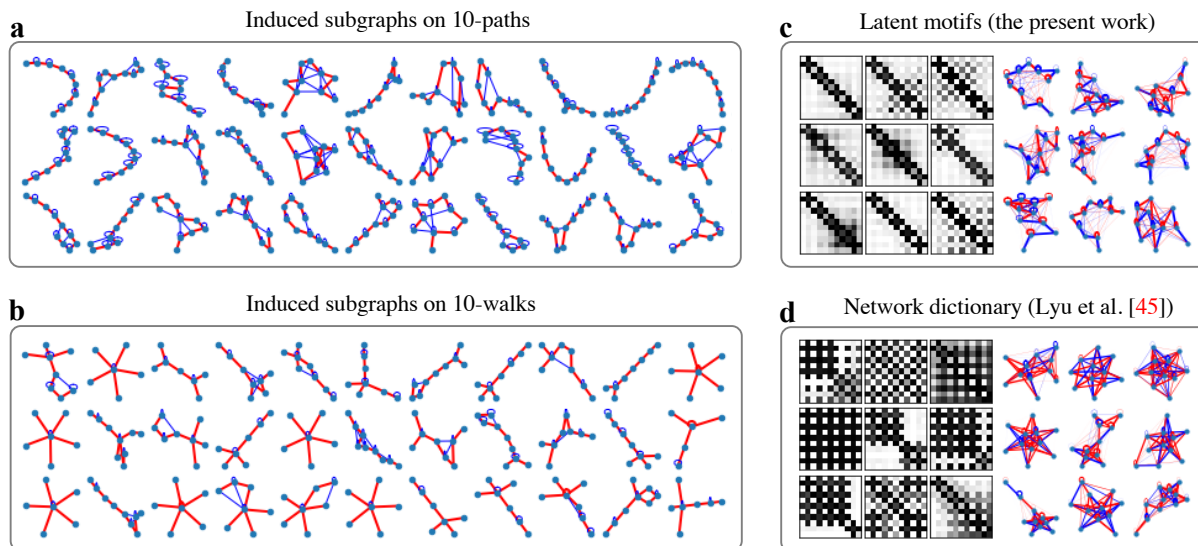


FIGURE 11. comparison of subgraphs of **CORONAVIRUS** PPI that are induced by node sets that we sample using **a** uniformly random  $k$ -paths and **b** uniformly random  $k$ -walks with  $k = 10$ . We also compare the network dictionary with  $r = 9$  latent motifs of **CORONAVIRUS** PPI that we determine using **c** the NDL algorithm (see Algorithm **NDL**) in the present work to **d** the network dictionary that we determine using the NDL algorithm from [45]. We also show the weighted adjacency matrices of the latent motifs. The 10-walks in the network tend to visit the same nodes many times. Consequently, one cannot regard the  $10 \times 10$  mesoscale patches that correspond to those walks as the adjacency matrices of  $k$ -node subgraphs of the network. Additionally, the networks in the network dictionary in panel **d** have clusters of several large-degree nodes, even though the original network does not possess such mesoscale structures.

**Data sets.** We examine the following eight real-world networks:

- (1) **CALTECH**: This connected network, which is part of the **FACEBOOK100** data set [26] (and which was studied previously as part of the **FACEBOOK5** data set [22]), has 762 nodes and 16,651 edges. The nodes represent users in the Facebook network of Caltech on one day in fall 2005, and the edges encode Facebook ‘friendships’ between these accounts.
- (2) **MIT**: This connected network, which is part of the **FACEBOOK100** data set [26], has 6,402 nodes and 251,230 edges. The nodes represent user accounts in the Facebook network of MIT on one day in fall 2005, and the edges encode Facebook ‘friendships’ between these accounts.
- (3) **UCLA**: This connected network, which is part of the **FACEBOOK100** data set [26], has 20,453 nodes and 747,604 edges. The nodes represent user accounts in the Facebook

network of UCLA on one day in fall 2005, and the edges encode Facebook ‘friendships’ between these accounts.

- (4) **HARVARD**: This connected network, which is part of the FACEBOOK100 data set [26], has 15,086 nodes and 824,595 edges. The nodes represent user accounts in the Facebook network of Harvard on one day in fall 2005, and the edges represent Facebook ‘friendships’ between these accounts.
- (5) **SNAP FACEBOOK** (with the shorthand **SNAP FB**) [23]: This connected network has 4,039 nodes and 88,234 edges. This network is a Facebook network that has been used as an example for edge inference [32]. The nodes represent user accounts in the Facebook network on one day in 2012, and the edges represent Facebook ‘friendships’ between these accounts.
- (6) **ARXIV ASTRO-PH** (with the shorthand **ARXIV**) [44, 32]: This network has 18,722 nodes and 198,110 edges. Its largest connected component has 17,903 nodes and 197,031 edges. We use the complete network in our experiments. This network is a collaboration network between authors of astrophysics papers that were posted to the arXiv preprint server. The nodes represent scientists and the edges indicate coauthorship relationships. This network has 60 self-edges; these edges encode single-author papers.
- (7) **CORONAVIRUS PPI** (with the shorthand **CORONAVIRUS**): This connected network is curated by [theBiogrid.org](http://theBiogrid.org) [41, 47, 42] from 142 publications and preprints. It has 1,536 proteins that are related to coronaviruses and 2,463 protein–protein interactions (in the form of physical contacts) between them. This network is the largest connected component of the Coronavirus PPI network that we downloaded on 24 July 2020; in total, there are 1,555 proteins and 2,481 interactions. Of the 2,481 interactions, 1,536 of them are for SARS-CoV-2 and were reported by 44 publications and preprints; the rest are related to coronaviruses that cause Severe Acute Respiratory Syndrome (SARS) or Middle Eastern Respiratory Syndrome (MERS).
- (8) **HOMO SAPIENS PPI** (with the shorthand **H. SAPIENS**) [41, 54, 32]: This network has 24,407 nodes and 390,420 edges. Its largest connected component has 24,379 nodes and 390,397 edges. We use the complete network in our experiments. The nodes represent proteins in the organism *Homo sapiens*, and the edges encode physical interactions between these proteins.

We now describe the eight synthetic networks that we examine:

- (9) **ER<sub>1</sub>** and **ER<sub>2</sub>**: An Erdős–Rényi (ER) network [1, 36], which we denote by  $ER(n, p)$ , is a random-graph model. The parameter  $n$  is the number of nodes and the parameter  $p$  is the independent, homogeneous probability that each pair of distinct nodes has an edge between them. The network **ER<sub>1</sub>** is an individual graph that we draw from  $ER(5000, 0.01)$ , and **ER<sub>2</sub>** is an individual graph that we draw from  $ER(5000, 0.02)$ .
- (10) **WS<sub>1</sub>** and **WS<sub>2</sub>**: A Watts–Strogatz (WS) network, which we denote by  $WS(n, k, p)$ , is a random-graph model to study the small-world phenomenon [4, 36]. In the version of WS networks that we use, we start with an  $n$ -node ring network in which each node is adjacent to its  $k$  nearest neighbors. With independent probability  $p$ , we then remove and rewire each edge so that it connects a pair of distinct nodes that we choose uniformly at random. The network **WS<sub>1</sub>** is an individual graph that we draw from  $WS(5000, 50, 0.05)$ , and **WS<sub>2</sub>** is an individual graph that we draw from  $WS(5000, 50, 0.10)$ .
- (11) **BA<sub>1</sub>** and **BA<sub>2</sub>**: A Barabási–Albert (BA) network, which we denote by  $BA(n, n_0)$ , is a random-graph model with a linear preferential-attachment mechanism [5, 36]. In the version of BA networks that we use, we start with  $n_0$  isolated nodes and we introduce



new nodes with  $n_0$  new edges each that attach preferentially (with a probability that is proportional to node degree) to existing nodes until we obtain a network with  $n$  nodes. The network  $\text{BA}_1$  is an individual graph that we draw from  $\text{BA}(5000, 25)$ , and  $\text{BA}_2$  is an individual graph that we draw from  $\text{BA}(5000, 50)$ .

- (12) **SBM<sub>1</sub>** and **SBM<sub>2</sub>**: We use stochastic-block-model (SBM) networks in which each block is an ER network [3]. Fix disjoint finite sets  $C_1 \cup \dots \cup C_{k_0}$  and a  $k_0 \times k_0$  matrix  $B$  whose entries are real numbers between 0 and 1. An SBM network, which we denote by  $\text{SBM}(C_1, \dots, C_{k_0}, B)$ , has the node set  $V = C_1 \cup \dots \cup C_{k_0}$ . For each node pair  $(x, y)$ , there is an edge between  $x$  and  $y$  with independent probabilities  $B[i_0, j_0]$ , with indices  $i_0, j_0 \in \{1, \dots, k_0\}$  such that  $x \in C_{i_0}$  and  $y \in C_{j_0}$ . If  $k_0 = 1$  and  $B$  has a constant  $p$  in all entries, this SBM specializes to the Erdős–Rényi (ER) random-graph model  $\text{ER}(n, p)$  with  $n = |C_1|$ . The networks **SBM<sub>1</sub>** and **SBM<sub>2</sub>** are individual graphs that we draw from  $\text{SBM}(C_1, \dots, C_{k_0}, B)$  with  $|C_1| = |C_2| = |C_3| = 1,000$ , where  $B$  is the  $3 \times 3$  matrix whose diagonal entries are 0.5 in both cases and whose off-diagonal entries are 0.001 for **SBM<sub>1</sub>** and 0.1 for **SBM<sub>2</sub>**. Both networks have 3,000 nodes; **SBM<sub>1</sub>** has 752,450 edges and **SBM<sub>2</sub>** has 1,049,365 edges.

**Types of noise.** We now describe the three noise types that we consider in our network-denoising experiments (see Figures 8 and 9). These noise types are as follows:

- (1) (Noise type: –ER) Given a network  $G = (V, E)$ , we choose a spanning tree  $T$  of  $G$  (such a tree includes all nodes of  $G$ ) uniformly at random from all possible spanning trees. Let  $E_0$  denote the set of all edges in  $G$  that are not in the edge set of  $T$ . We then obtain a corrupted network  $G'$  by uniformly randomly removing half of the edges in  $E_0$  from  $G$ . Note that  $G'$  is guaranteed to be connected.
- (2) (Noise type: +ER) Given a network  $G = (V, E)$ , we uniformly randomly choose a set  $E_2$  of pairs of non-adjacent nodes in  $G$  of size  $|E_2| = \lfloor |E|/2 \rfloor$ . The corrupted network is  $G' = (V, E \cup E_2)$ , and we note that 50% of the edges in  $G'$  are new.
- (3) (Noise type: +WS) Given a network  $G = (V, E)$ , fix integers  $n_0 \in \{1, \dots, |V|\}$  and  $k \in \{1, \dots, n_0\}$  and fix a real number  $p \in [0, 1]$ . We uniformly randomly choose a subset  $V_0 \subseteq V$  (with  $|V_0| = n_0$ ) of the nodes of  $G$ . We generate a network  $H = (V_0, E_3)$  from the Watts–Strogatz model  $\text{WS}(n_0, k, p)$  using the node set  $V_0$ . We then obtain the corrupted network  $G' = (V, E \cup E_3)$ , which has  $|E_3| = n_0 \lfloor k/2 \rfloor$  new edges. If  $G$  is

**CALTECH**, **SNAP FB**, **ARXIV**, or **CORONAVIRUS**, we use the parameters  $n_0 = 100$ ,  $k = 20$ , and  $p = 0.3$ . In this case,  $G'$  has 1,000 new edges. If  $G$  is **H. SAPIENS**, we use the parameters  $n_0 = 500$ ,  $k = 120$ , and  $p = 0.3$ . In this case,  $G'$  has 30,000 new edges.

**Data availability.** The datasets generated during the current study are available in the repository [https://github.com/HanbaekLyu/NDL\\_paper](https://github.com/HanbaekLyu/NDL_paper). For datasets of real-world networks analysed during the current study, see the ‘Data sets’ section in our Methods.

**Code availability.** Our code for the main algorithms and simulations is publicly available in the repository [https://github.com/HanbaekLyu/NDL\\_paper](https://github.com/HanbaekLyu/NDL_paper). We also provide a user-friendly version as a PYTHON package NDLEARN at <https://github.com/jvendrow/Network-Dictionary-Learning>.

## REFERENCES

- [50] Daniel D. Lee and H. Sebastian Seung. “Algorithms for non-negative matrix factorization”. *Advances in Neural Information Processing Systems*. 2001, pp. 556–562.

- [51] Julien Mairal, Michael Elad, and Guillermo Sapiro. “Sparse learned representations for image restoration”. *Proceedings of the 4th World Conference of the International Association for Statistical Computing* (2008), p. 118.
- [52] Julien Mairal, Francis Bach, Jean Ponce, Guillermo Sapiro, and Andrew Zisserman. “Non-local sparse models for image restoration”. *IEEE 12th International Conference on Computer Vision* (2009), pp. 2272–2279.
- [53] Julien Mairal, Francis Bach, Jean Ponce, and Guillermo Sapiro. “Online learning for matrix factorization and sparse coding”. *Journal of Machine Learning Research* 11 (2010), pp. 19–60.
- [54] theBiogrid.org. “Homo sapiens PPI network” (2020). Retrieved from <https://wiki.thebiogrid.org/doku.php/covid> (downloaded 24 July 2020, Ver. 3.5.180.tab2).

**Supplementary Information:**  
**LEARNING LOW-RANK LATENT MESOSCALE STRUCTURES IN NETWORKS**

APPENDIX A. OVERVIEW

In this supplement, we present our algorithms for network dictionary learning (NDL) and network denoising and reconstruction (NDR), and we prove theoretical results about their convergence and error bounds. We give the complete NDL algorithm (see Algorithm [NDL](#)) in Section [D](#), and we give the complete NDR algorithm (see Algorithm [NDR](#)) in Section [E](#). We introduce the notion of ‘latent motif dominance’ in Section [D.2](#) to measure the significance of each latent motif that we learn from a network. In Section [7](#), we give a rigorous analysis of the NDL and NDR algorithms.

APPENDIX B. PROBLEM FORMULATION FOR NETWORK DICTIONARY LEARNING (NDL)

**B.1. Definitions and notation.** To facilitate our discussions, we use terminology and notation from [[65](#), Ch. 3]. In the main manuscript, we described a network as a graph  $G = (V, E)$  with a node set  $V$  and an edge set  $E$  without directed or multi-edges, but possibly with self-edges. One can characterize the edge set  $E$  of  $\mathcal{G}$  using an *adjacency matrix*  $A_G : V^2 \rightarrow \{0, 1\}$ , where  $A(x, y) = \mathbb{1}(\{x, y\} \in E)$  for each  $x, y \in V$ . The function  $\mathbb{1}(S)$  denotes the indicator of the event  $S$ ; it takes the value 1 if  $S$  occurs and takes the value 0 if it does not occur. In this supplementary information, we formulate our NDL framework in the more general setting in which edges in a network may have weights. Although one can extend the above definition of networks to include weighted edges by adjoining an additional entry to  $G = (V, E)$  for edge weights, it is convenient to extend the range of adjacency matrices from  $\{0, 1\}$  to the interval  $[0, \infty)$ .

We define a *network* as a pair  $\mathcal{G} = (V, A_G)$  with node set  $V$  and a *weight matrix* (which is also often called a ‘weighted adjacency matrix’)  $A_G : V^2 \rightarrow [0, \infty)$  that encodes the weights of the contacts between nodes. For simplicity, we often drop the subscript  $\mathcal{G}$  in  $A_G$  and denote it as  $A$ . A graph  $G = (V, E)$  determines a unique network  $\mathcal{G} = (V, A_G)$ , where  $A_G$  is the adjacency matrix of  $G$ . The set  $V(\mathcal{G})$  is the node set of the network  $\mathcal{G}$ , which has *size*  $|V(\mathcal{G})|$ , where  $|S|$  is the number of elements in the set  $S$ . A pair  $(x, y)$  of nodes in  $\mathcal{G}$  is called a *directed edge* if  $A(x, y) > 0$  and it is called a *self-edge* if  $x = y$  and  $A(x, x) > 0$ . We say that a network  $\mathcal{G} = (V, A)$  is *symmetric* if its weight matrix is symmetric (i.e.,  $A(x, y) = A(y, x)$  for all  $x, y \in V$ ) and we say that it is *binary* (i.e., unweighted) if  $A(x, y) \in \{0, 1\}$  for all  $x, y \in V$ . Given a symmetric network  $\mathcal{G} = (V, A)$ , an unordered pair  $\{x, y\}$  of nodes in  $\mathcal{G}$  is an *edge* if  $A(x, y) = A(y, x) > 0$ . The network  $\mathcal{G}$  is *bipartite* if it admits a ‘bipartition’, which is a partition  $V = V_1 \cup V_2$  of the node set  $V$  such that  $V = V_1 \cup V_2$  and  $A(x, y) = 0$  if  $x, y \in V_1$  or  $x, y \in V_2$  for each  $x, y \in V$ . If two networks  $\mathcal{G} = (V, A)$  and  $\mathcal{G}' = (V', A')$  satisfy  $V' \subseteq V$  and  $A'(x, y) \leq A(x, y)$  for all  $x, y \in V'$ , then we say that  $\mathcal{G}'$  is a *subgraph* of  $\mathcal{G}$  and write  $\mathcal{G}' \subseteq \mathcal{G}$ . If  $A'(x, y) = A(x, y)$  for all  $x, y \in V'$ , then we say that  $\mathcal{G}'$  is an *induced subgraph* of  $\mathcal{G}$  that is induced by the node set  $V'$ .

For an integer  $k \geq 2$  and nodes  $x, y \in V$ , we refer to a sequence  $(x_1, \dots, x_k)$  of (not necessarily distinct) nodes in  $\mathcal{G}$  as a *k-walk from x to y* if  $A(x_i, x_{i+1}) > 0$  for all  $i \in \{1, \dots, k-1\}$  and  $(x_1, x_k) = (x, y)$ . A *k-walk*  $(x_1, \dots, x_k)$  is a *k-path* if all nodes  $x_1, \dots, x_k$  are distinct. We say that the network  $\mathcal{G}$  is *connected* if for any nodes  $x, y \in V$ , there exists a *k-path* from  $x$  to  $y$  for

some  $k \geq 1$ . If  $\mathcal{G}$  is connected, then for any two distinct nodes  $x, y \in V$ , we define  $d_{\mathcal{G}}(x, y)$  to be the smallest possible integer  $k \geq 1$  such that there exists a  $k$ -walk from  $x$  to  $y$ . The quantity  $d_{\mathcal{G}}(x, y)$  is called the *shortest-path distance* between  $x$  and  $y$ . The maximum of  $d_{\mathcal{G}}(x, y)$  over all node pairs  $(x, y)$  is the *shortest-path diameter*  $\text{diam}(\mathcal{G})$  of  $\mathcal{G}$ . It equals the minimum number of edges in a walk in  $\mathcal{G}$  that connects  $x$  and  $y$ .

Suppose that we are given  $N$  elements  $\mathbf{v}_1, \dots, \mathbf{v}_m$  in some vector space. When we say that we take their *mean*, we refer to their sample mean  $\bar{\mathbf{v}} = N^{-1} \sum_{i=1}^N \mathbf{v}_i$ . When we say that we take a *weighted average* of them, we refer to the expectation  $\sum_{i=1}^N \mathbf{v}_i p_i$ , where  $(p_1, \dots, p_N)$  is a probability distribution on the set of  $N$  elements.

**B.2. Homomorphisms between networks and motif sampling.** The ability to sample from a complex data set according to a known probability distribution (e.g., a uniform one) is a crucial ingredient in dictionary-learning problems. For instance, in image-processing applications [10, 51, 52], it is straightforward to uniformly randomly sample a  $k \times k$  patch from an image. However, it is not straightforward to uniformly randomly sample a connected  $k$ -node subgraph of a network [70, 58, 60, 59]. For our purpose of developing dictionary learning for networks, we use motif sampling, which was introduced recently in [40]. In motif sampling, instead of directly sampling a connected subgraph, one samples a random function from the node set of a smaller network (i.e., a motif) into the node set of a target network that preserves adjacency relations, and one then uses the subgraph that is induced by the nodes in the image of the function. As we discuss below, such a function between networks is a homomorphism.

Fix an integer  $k \geq 1$  and a weight matrix  $A_F : [k]^2 \rightarrow [0, \infty)$ , where we use the shorthand notation  $[k] = \{1, \dots, k\}$ . We use the term *motif* for the corresponding network  $F = ([k], A_F)$ . A motif is a network, and we use motifs to sample from a given (and much larger) network. The type of motif that particularly interests us is a *k-chain*, for which  $A_F = \mathbb{1}(\{(1, 2), (2, 3), \dots, (k-1, k)\})$ . A *k-chain* is a directed path with node set  $[k]$ . For a general  $k$ -node motif  $F = ([k], A_F)$  and a network  $\mathcal{G} = (V, A)$ , we define the probability distribution  $\pi_{F \rightarrow \mathcal{G}}$  on the set  $V^{[k]}$  of all node maps (i.e., functions between node sets)  $\mathbf{x} : [k] \rightarrow V$  by

$$\pi_{F \rightarrow \mathcal{G}}(\mathbf{x}) := \frac{1}{Z} \left( \prod_{i,j \in \{1, \dots, k\}} A(\mathbf{x}(i), \mathbf{x}(j))^{A_F(i,j)} \right), \quad (1)$$

where  $Z = Z(F, \mathcal{G})$  is a normalization constant that we call the *homomorphism density* of  $F$  in  $\mathcal{G}$  [65]. A node map  $\mathbf{x} : [k] \rightarrow V$  a *homomorphism*  $F \rightarrow \mathcal{G}$  if  $\pi_{F \rightarrow \mathcal{G}}(\mathbf{x}) > 0$ , which is the case if and only if  $A(\mathbf{x}(a), \mathbf{x}(b)) > 0$  for all  $a, b \in [k]$  with  $A_F(a, b) > 0$  (with the convention that  $\zeta^0 = 1$  for all  $\zeta \in \mathbb{R}$ ). Informally, this means that if  $(i, j)$  is a directed edge in  $F$ , then  $(\mathbf{x}(i), \mathbf{x}(j))$  is a directed edge in  $\mathcal{G}$ . Motif sampling refers to the problem of sampling a random homomorphism  $\mathbf{x} : F \rightarrow \mathcal{G}$  according to the distribution (1).

For our goal of learning interpretable latent motifs, it is important to sample a homomorphism  $\mathbf{x} : F \rightarrow \mathcal{G}$  such that  $\mathbf{x}$  is injective. This ensures that the nodes  $\mathbf{x}(1), \dots, \mathbf{x}(k)$  in  $V$  that correspond to nodes  $1, \dots, k$  in the motif  $F$  through the homomorphism  $\mathbf{x}$  are all distinct. When  $\mathbf{x} : F \rightarrow \mathcal{G}$  is an injective homomorphism, we denote  $\mathbf{x} : F \hookrightarrow \mathcal{G}$ . Using the subgraph of  $\mathcal{G}$  that is induced by the node set  $\{\mathbf{x}(1), \dots, \mathbf{x}(k)\}$  when  $\mathbf{x}$  is injective returns a  $k$ -node subgraph of  $\mathcal{G}$ . For convenience, we define the probability distribution

$$\pi_{F \hookrightarrow \mathcal{G}}(\mathbf{x}) := C \pi_{F \rightarrow \mathcal{G}}(\mathbf{x}) \cdot \mathbb{1}(\mathbf{x}(1), \dots, \mathbf{x}(k) \text{ are distinct}), \quad (2)$$

where  $C > 0$  is a normalization constant. Injective motif sampling refers to the problem of sampling a random injective homomorphism  $\mathbf{x} : F \hookrightarrow \mathcal{G}$  according to the distribution (2). The probability distribution (2) is well-defined as long as there exists an injective homomorphism

$\mathbf{x} : F \rightarrow \mathcal{G}$ . For instance, if  $F$  is a  $k$ -chain motif and  $k$  is larger than the shortest-path diameter of  $\mathcal{G}$ , then there is no injective homomorphism  $\mathbf{x} : F \rightarrow \mathcal{G}$  and the probability distribution (2) is not well-defined. As a special case of interest, for a symmetric and binary motif  $F$  and a network  $\mathcal{G}$ , the distributions  $\pi_{F \rightarrow \mathcal{G}}$  and  $\pi_{F \hookrightarrow \mathcal{G}}$  are the uniform distribution among all homomorphisms  $F \rightarrow \mathcal{G}$  and among all injective homomorphisms  $F \hookrightarrow \mathcal{G}$ , respectively. That is,

$$F, \mathcal{G} \text{ are symmetric and binary} \implies \begin{aligned} \pi_{F \rightarrow \mathcal{G}} &= \text{Uniform}(\{\mathbf{x} : F \rightarrow \mathcal{G}\}) \\ \pi_{F \hookrightarrow \mathcal{G}} &= \text{Uniform}(\{\mathbf{x} : F \hookrightarrow \mathcal{G}\}), \end{aligned} \quad (3)$$

which is the case for all of our examples in the main manuscript. In Section C, we discuss three Markov-chain Monte Carlo (MCMC) algorithms for motif sampling and propose corresponding algorithms for injective motif sampling by combining them with rejection sampling.

**B.3. Mesoscale patches of networks.** A homomorphism  $F \rightarrow \mathcal{G}$  is a node map  $V(F) \rightarrow V(\mathcal{G})$  that maps the edges of  $F$  to edges of  $\mathcal{G}$ , so it maps  $F$  onto a subgraph of  $\mathcal{G}$ . It thereby maps  $F$  ‘into’  $\mathcal{G}$ . For each homomorphism  $\mathbf{x} : F \rightarrow \mathcal{G}$  from a motif  $F = ([k], A_F)$  into a network  $\mathcal{G} = (V, A)$ , we define a  $k \times k$  matrix

$$A_{\mathbf{x}}(a, b) := A(\mathbf{x}(a), \mathbf{x}(b)) \quad \text{for all } a, b \in \{1, \dots, k\}. \quad (4)$$

We say that  $A_{\mathbf{x}}$  in (4) is the *mesoscale patch* of  $\mathcal{G}$  that is induced by the homomorphism  $\mathbf{x} : F \rightarrow \mathcal{G}$ , which is specified uniquely by the homomorphism  $\mathbf{x} : F \rightarrow \mathcal{G}$  and the weight matrix  $A$ . Given a  $k \times k$  matrix  $B$  and a homomorphism  $\mathbf{x} : F \rightarrow \mathcal{G}$ , we say that the  $(a, b)$  entries of  $B$  are *on-chain* if  $A_F(a, b) > 0$  and *off-chain* otherwise. The condition  $A_F(a, b) > 0$  implies that  $A(\mathbf{x}(a), \mathbf{x}(b)) > 0$  by the definition of the homomorphism  $\mathbf{x}$ , so the on-chain entries of  $A_{\mathbf{x}}$  are always positive (and are always 1 if  $\mathcal{G}$  is unweighted). However, the off-chain entries of  $A_{\mathbf{x}}$  are not necessarily positive, so they encode meaningful information about a network that one ‘detects’ with the homomorphism  $\mathbf{x} : F \rightarrow \mathcal{G}$ . As an illustration, suppose that  $F$  is the 6-chain motif and that  $\mathcal{G} = (V, A)$  is an undirected and binary graph. For any homomorphism  $\mathbf{x} : F \rightarrow \mathcal{G}$ , we have

$$A_{\mathbf{x}} = \begin{bmatrix} 0 & 1 & * & * & * & * \\ 1 & 0 & 1 & * & * & * \\ * & 1 & 0 & 1 & * & * \\ * & * & 1 & 0 & 1 & * \\ * & * & * & 1 & 0 & 1 \\ * & * & * & * & 1 & 0 \end{bmatrix},$$

where each entry  $*$  of  $A_{\mathbf{x}}$  is either 0 or 1. In this example, the entries that we mark as 1 are the on-chain entries of  $A_{\mathbf{x}}$  and the other entries are off-chain entries.

Let  $\mathcal{G}_{\mathbf{x}}$  denote the induced subgraph of  $\mathcal{G}$  whose node set is the image  $\text{Im}(\mathbf{x}_t) = \{\mathbf{x}(a) \mid a \in \{1, \dots, k\}\}$  of the homomorphism  $\mathbf{x} : F \rightarrow \mathcal{G}$ . If  $\mathbf{x}$  has  $k$  distinct nodes in its image, then the weight matrix of  $\mathcal{G}_{\mathbf{x}}$  is exactly the mesoscale patch  $A_{\mathbf{x}}$ . However, this is not the case when  $\mathbf{x}$  has fewer than  $k$  distinct nodes. In that situation, we cannot interpret the mesoscale patch  $A_{\mathbf{x}}$  as the weight matrix of the induced subgraph  $\mathcal{G}_{\mathbf{x}}$  of  $\mathcal{G}$ . (For example, see Figure 11 in the main manuscript.) This motivates us to sample an injective homomorphism  $\mathbf{x} : F \rightarrow \mathcal{G}$  according to the distribution (2), instead of according to the distribution (1).

**B.4. Problem formulation for network dictionary learning (NDL).** The goal of the *NDL problem* is to learn, for a fixed integer  $r \geq 1$ , a set of  $r$  nonnegative matrices  $\mathcal{L}_1, \dots, \mathcal{L}_r$ , of size  $k \times k$  and Frobenius norms of at most 1, such that

$$A_{\mathbf{x}} \approx a_1(\mathbf{x})\mathcal{L}_1 + \dots + a_r(\mathbf{x})\mathcal{L}_r \quad (5)$$

for each injective homomorphism  $\mathbf{x} : F \hookrightarrow \mathcal{G}$  for some coefficients  $a_1(\mathbf{x}), \dots, a_r(\mathbf{x}) \geq 0$ . For each homomorphism  $\mathbf{x} : F \rightarrow \mathcal{G}$ , this implies that one can approximate the mesoscale patch  $A_{\mathbf{x}}$

of  $\mathcal{G}$  that is induced by  $\mathbf{x}$  as a linear combination of the  $r$  matrices  $\mathcal{L}_1, \dots, \mathcal{L}_r$ . We say that the tuple  $(\mathcal{L}_1, \dots, \mathcal{L}_r)$  is a *network dictionary* for  $\mathcal{G}$ , and we say that each  $\mathcal{L}_i$  is a *latent motif* of  $\mathcal{G}$ . We identify a network dictionary  $(\mathcal{L}_1, \dots, \mathcal{L}_r)$  with the nonnegative matrix  $W \in \mathbb{R}_{\geq 0}^{k^2 \times r}$  whose  $j^{\text{th}}$  column is the vectorization of the  $j^{\text{th}}$  latent motif  $\mathcal{L}_j$  for  $j \in \{1, \dots, r\}$ . The choice of vectorization  $\mathbb{R}^{k \times k} \rightarrow \mathbb{R}^{k^2}$  is arbitrary, but we use a column-wise vectorization in Algorithm A4. One can interpret each  $\mathcal{L}_i$  as the  $k$ -node weighted network with node set  $\{1, \dots, k\}$  and weight matrix  $\mathcal{L}_i$ . See Figure 2 in the main manuscript for plots of latent motifs as weighted networks.

For the latent motifs  $\mathcal{L}_i$  to be interpretable as subgraphs of  $\mathcal{G}$ , it is crucial that we require both their entries and the coefficients  $a_i(\mathbf{x})$  to be nonnegative. The nonnegativity constraint on each latent motif  $\mathcal{L}_i$  allows one to interpret each  $\mathcal{L}_i$  as the weight matrix of a  $k$ -node network. Additionally, because the coefficients  $a_j(\mathbf{x})$  are also nonnegative, the approximate decomposition (5) implies that  $a_i(\mathbf{x})\mathcal{L}_i \lesssim A_{\mathbf{x}}$ . Therefore, if  $a_i(\mathbf{x}) > 0$ , any network structure (e.g., large-degree nodes, communities, and so on) in the latent motif  $\mathcal{L}_i$  must also exist in  $A_{\mathbf{x}}$ . Therefore, one can consider the latent motifs as approximate  $k$ -node subgraphs  $\mathcal{G}$  that exhibit ‘typical’ network structures of  $\mathcal{G}$  at scale  $k$ . In the spirit of Lee and Seung [6], one can view the latent motifs as ‘parts’<sup>1</sup> of a network  $\mathcal{G}$ .

As a more precise formulation of (5), consider the stochastic optimization problem

$$\arg \min_{\substack{\mathcal{L}_1, \dots, \mathcal{L}_r \in \mathbb{R}_{\geq 0}^{k \times k} \\ \|\mathcal{L}_1\|_F, \dots, \|\mathcal{L}_r\|_F \leq 1}} \mathbb{E}_{\mathbf{x} \sim \pi_{F \hookrightarrow \mathcal{G}}} \left[ \inf_{a_1(\mathbf{x}), \dots, a_r(\mathbf{x}) \geq 0} \left\| A_{\mathbf{x}} - \sum_{i=1}^r a_i(\mathbf{x}) \mathcal{L}_i \right\|_F \right], \quad (6)$$

where  $\pi_{F \hookrightarrow \mathcal{G}}$  is the probability distribution that we defined in (2) and  $\|\cdot\|_F$  denotes the matrix Frobenius norm. The choice of the probability distribution  $\pi_{F \hookrightarrow \mathcal{G}}$  for the injective homomorphisms  $\mathbf{x} : F \hookrightarrow \mathcal{G}$  is natural because it becomes the uniform distribution on the set of all injective homomorphisms  $F \hookrightarrow \mathcal{G}$  when the adjacency matrices for  $\mathcal{G}$  and  $F$  are both unweighted. Exactly solving the NDL optimization problem (6) is computationally difficult because the objective function in it is non-convex and it is not obvious how to sample an injective homomorphism  $F \hookrightarrow \mathcal{G}$  according to the distribution  $\pi_{F \hookrightarrow \mathcal{G}}$  that we defined in (2). In Section D, we provide an algorithm for NDL that approximately solves (6).

**B.5. Overview of our algorithms and their theoretical guarantees.** We overview our algorithms and their theoretical guarantees. Our main theoretical results (which are all novel) are Theorems 7.4 and 7.7 for NDL and Theorems 7.10 and 7.14 for NDR. We summarize our algorithms and main results in Table 2, and we compare and contrast them with the results in [45].

**Algorithm NDL:** Given a network  $\mathcal{G}$ , the NDL algorithm (see Algorithm NDL) computes a sequence  $(W_t)_{t \geq 0}$  of network dictionaries (which take the form of  $k^2 \times r$  matrices) of latent motifs.

**Algorithm NDR:** Given a network  $\mathcal{G}$ , a network dictionary  $W$ , and a threshold parameter  $\theta > 0$ , the NDR algorithm (see Algorithm NDR) computes a sequence of weighted networks  $\mathcal{G}_{\text{recons}}$  and binary (i.e., unweighted) networks  $\mathcal{G}_{\text{recons}}(\theta)$ .

**Theorem 7.4:** Given a non-bipartite network  $\mathcal{G}$  and a choice of the parameters in Algorithm NDL, we prove that the sequence  $(W_t)_{t \geq 0}$  of network dictionaries converges almost surely to the set of stationary points of the associated objective function in (6).

<sup>1</sup>Lee and Seung [6] discussed a similar nonnegative decomposition in which the  $A_{\mathbf{x}}$  are images of faces. In that scenario, the learned factors capture parts of human faces (such as eyes, noses, and mouths).

<b>NDL</b>	Sampling	Convergence		Efficient MCMC
Lyu et al. [45]	$k$ -walks	Non-bipartite networks		$\times$
The present work	$k$ -paths (Alg. <b>RM</b> )	Non-bipartite networks (Thm. <b>7.4</b> )	Bipartite networks (Thm. <b>7.7</b> )	$\checkmark$ (Prop. <b>7.2</b> )

<b>NDR</b>	Sampling	denoising	Convergence	Error bound
Lyu et al. [45]	$k$ -walks	F	$\times$	$\times$
The present work	$k$ -walks	F, T	$\checkmark$ (Thm. <b>7.10(i)-(ii)</b> )	$\checkmark$ (Thm. <b>7.10(iii)</b> )
	$k$ -paths		(Thm. <b>7.14(i)-(ii)</b> )	(Thm. <b>7.14(iii)</b> )

TABLE 2. A comparison of the algorithms and theoretical contributions of the present work with those in [45]. In the table for NDR, **denoising** refers to the Boolean variable in our NDR algorithm (see Algorithm **NDR**). The special case of the NDR algorithm with  $k$ -walk sampling (i.e.,  $\text{InjHom} = \text{F}$ ) and **denoising** = F corresponds to the network-reconstruction algorithm in [45].

**Theorem 7.7:** Given a bipartite network  $\mathcal{G}$  and a choice of the parameters in Algorithm **NDL**, we prove a convergence result that is analogous to the one in Theorem 7.4.

**Theorem 7.10:** Given a non-bipartite target network  $\mathcal{G}$  and a network dictionary  $W$ , we show that (i) the sequence of weighted reconstructed networks  $\mathcal{G}_{\text{recons}}$  that we obtain using the NDR algorithm (see Algorithm **NDR**) converges almost surely to some limiting network, and (ii) we obtain a closed-form expression of this limiting network. We also show that (iii) a suitable Jaccard reconstruction error between the original network  $\mathcal{G}$  and the limiting reconstructed network satisfies

$$\text{Jaccard reconstruction error} \leq \frac{\text{mesoscale approximation error}}{2(k-1)},$$

where  $k$  denotes the mesoscale parameter (i.e., the number of nodes in a  $k$ -chain motif) and the mesoscale approximation error is the mean  $L_1$  distance between the  $k \times k$  mesoscale patches of  $\mathcal{G}$  and their nonnegative linear approximations from the latent motifs in  $W$ .

**Theorem 7.14:** We show a convergence result that is analogous to the one in Theorem 7.14 for a bipartite target network  $\mathcal{G}$ .

#### APPENDIX C. MARKOV-CHAIN MONTE CARLO (MCMC) MOTIF-SAMPLING ALGORITHMS

We mentioned in Section B.4 that one of the main difficulties in solving the optimization problem (6) is to directly sample an injective homomorphism  $\mathbf{x} : F \hookrightarrow \mathcal{G}$  from the distribution  $\pi_{F \hookrightarrow \mathcal{G}}$  (see (2)). To overcome this difficulty, we use the Markov-chain Monte Carlo (MCMC) algorithms that were introduced in [40]. Although the algorithms in [40] apply to networks with edge weights and/or node weights, we only use the simplified forms of them that we give in Algorithms **MP** and **MG**. Algorithm **MP** with the option `AcceptProb = Approximate` is a novel algorithm of the present paper. Using these MCMC sampling algorithms, we generate a sequence  $(\mathbf{x}_t)_{t \geq 0}$  of homomorphisms  $F \rightarrow \mathcal{G}$  such that the distribution of  $\mathbf{x}_t$  converges to  $\pi_{F \rightarrow \mathcal{G}}$  under some mild conditions on  $\mathcal{G}$  and  $F$  [45, Thm. 5.7].

Once we have an iterative motif-sampling algorithm, we combine it with a standard rejection-sampling algorithm to shrink the support of the probability distribution  $\pi_{F \rightarrow \mathcal{G}}$  to that of injective

homomorphisms  $\mathbf{x} : F \hookrightarrow \mathcal{G}$ . (See, e.g., [57] for background information about rejection sampling.) The key idea is to ignore (i.e., ‘reject’) the unwanted instances in the trajectory  $(\mathbf{x}_t)_{t \geq 0}$ . In our case, the instances that we reject are the homomorphisms  $\mathbf{x}_t$  that are not injective. That is, we reject situations in which  $\mathbf{x}_t(1), \dots, \mathbf{x}_t(k)$  are not all distinct. We state our algorithm for injective motif sampling in Algorithm **RM**.

---

**Algorithm RM.** Injective motif sampling
 

---

- 1: **Input:** Network  $\mathcal{G} = (V, A)$ , motif  $F = ([k], A_F)$ , and homomorphism  $\mathbf{x} : F \rightarrow \mathcal{G}$
  - 2: **While:**  $\mathbf{x} : F \rightarrow \mathcal{G}$  is injective (i.e.,  $\mathbf{x}'(1), \dots, \mathbf{x}'(k)$  are distinct)
  - 3:     Update  $\mathbf{x}$  to a new homomorphism  $F \rightarrow \mathcal{G}$  using either Algorithm **MP** or Algorithm **MG**
  - 4: **Output:** Injective homomorphism  $\mathbf{x} : F \hookrightarrow \mathcal{G}$
- 

Algorithm **RM** restricts the state space of the MCMC motif-sampling algorithms (see Algorithms **MG** and **MP**) onto the subset of injective homomorphisms  $F \hookrightarrow \mathcal{G}$ . By the strong Markov property, this restriction is a Markov chain. Therefore, Algorithm **RM** is an MCMC algorithm for the injective motif-sampling problem. (See Proposition 7.3 for details.) When there are only a few injective homomorphisms  $F \hookrightarrow \mathcal{G}$  relative to the number of homomorphisms  $F \rightarrow \mathcal{G}$ , the rejection step (i.e., the while loop) in Algorithm **RM** may take a while to terminate. (It is inversely proportional to the probability that a random homomorphism under the probability distribution  $\pi_{F \rightarrow \mathcal{G}}$  is injective.) For example, this is the case when  $\mathcal{G}$  is the network **CORONAVIRUS PPI** and  $F$  is a  $k$ -chain motif with  $k \geq 21$ .

We now give more details about the MCMC algorithms that we employ for non-injective motif sampling. In the *pivot chain* (see Algorithm **MP** with `AcceptProb=Exact`), for each update  $\mathbf{x}_t \mapsto \mathbf{x}_{t+1}$ , the *pivot*  $\mathbf{x}_t(1)$  first performs a random-walk move on  $\mathcal{G}$  (see (7)) to move to a new node  $\mathbf{x}_{t+1}(1) \in V$ . It accepts this move with a suitable acceptance probability (see (8)) according to the Metropolis–Hastings algorithm (see, e.g., [69, Sec. 3.2]), so the stationary distribution is exactly the target distribution. After the move  $\mathbf{x}_t(1) \mapsto \mathbf{x}_{t+1}(1)$ , we sample each  $\mathbf{x}_{t+1}(i) \in V$  for  $i \in \{2, 3, \dots, k\}$  successively from the conditional distribution (9). This ensures that the desired distribution  $\pi_{F \rightarrow \mathcal{G}}$  in (1) is a stationary distribution of the resulting Markov chain. In the *Glauber chain*, we select one node  $i \in [k]$  of  $F$  uniformly at random, and we resample its location  $\mathbf{x}_t(i) \in V(\mathcal{G})$  at time  $t$  to  $\ell = \mathbf{x}_{t+1}(i) \in V$  from the conditional distribution (10) (see Figure 12a). See [69, Sec. 3.3] for discussions of the Metropolis–Hastings algorithm and Glauber-chain MCMC sampling.

Let  $\Delta$  denote the maximum degree (i.e., number of neighbors) of the nodes of the network  $\mathcal{G} = (V, A)$ . We also say that the network  $\mathcal{G}$  itself has a maximum degree of  $\Delta$ . The Glauber chain has an efficient local update (with a computational complexity of  $O(\Delta)$ ). It converges quickly to the stationary distribution  $\pi_{F \rightarrow \mathcal{G}}$  only for networks that are dense enough so that two homomorphisms that differ at one node have a probability of at least  $1/(2\Delta)$  to coincide after a single Glauber-chain update. See [40, Thm. 6.1] for a precise statement of this fact.

The pivot chain (see Algorithm **MP** with `AcceptProb = Exact`) has more computationally expensive local updates than the Glauber chain. The pivot chain has a computational complexity of  $O(\Delta^{k-1})$  (as discussed in [40, Remark 5.6]), but it converges as fast as a ‘lazy’ random walk on a network. (In a lazy random walk, each move has a chance to be rejected; see [40, Thm. 6.2].) In our computational experiments, we find that the Glauber chain is slow, especially for sparse networks (e.g., for **COVID PPI**, which has an edge density of 0.0010, and **UCLA**, which has an edge density of 0.0037) and that the pivot chain is too expensive to compute for chain motifs with  $k \geq 21$ . As a compromise, to simultaneously have low computational complexity and fast convergence (which is as fast as the standard random walk), we employ an approximate



---

**Algorithm MP.** Pivot-Chain Update

---

- 1: **Input:** Symmetric network  $\mathcal{G} = (V, A)$ , a  $k$ -chain motif  $F = ([k], A_F)$ , and homomorphism  $\mathbf{x} : F \rightarrow \mathcal{G}$
- 2: **Parameters:**  $\text{AcceptProb} \in \{\text{Exact}, \text{Approximate}\}$
- 3: **Do:**  $\mathbf{x}' \leftarrow \mathbf{x}$
- 4:     **If**  $\sum_{c \in V} A(\mathbf{x}(1), c) = 0$ : **Terminate**
- 5:     **Else:**
- 6:         Sample  $\ell \in V$  at random from the distribution

$$p_1(w) = \frac{A(\mathbf{x}(1), w)}{\sum_{c \in V} A(\mathbf{x}(1), c)}, \quad w \in V \quad (7)$$

- 7:     Compute the acceptance probability  $\alpha \in [0, 1]$  by

$$\alpha \leftarrow \begin{cases} \min \left( \frac{\sum_{c \in [n]} A^{k-1}(\ell, c)}{\sum_{c \in [n]} A^{k-1}(\mathbf{x}(1), c)} \frac{\sum_{c \in V} A(c, \mathbf{x}(1))}{\sum_{c \in V} A(\mathbf{x}(1), c)}, 1 \right), & \text{if } \text{AcceptProb} = \text{Exact} \\ \min \left( \frac{\sum_{c \in V} A(c, \mathbf{x}(1))}{\sum_{c \in V} A(\mathbf{x}(1), c)}, 1 \right), & \text{if } \text{AcceptProb} = \text{Approximate} \end{cases} \quad (8)$$

- 8:     Sample  $U \in [0, 1]$  uniformly at random, independently of everything else
- 9:      $\ell \leftarrow \mathbf{x}(1)$  if  $U > \lambda$  and  $\mathbf{x}'(1) \leftarrow \ell$
- 10:    **For**  $i = 2, 3, \dots, k$ :
- 11:         Sample  $\mathbf{x}'(i) \in V$  from the distribution

$$p_i(w) = \frac{A(\mathbf{x}(i-1), w)}{\sum_{c \in V} A(\mathbf{x}(i-1), c)}, \quad w \in V \quad (9)$$

- 12: **Output:** Homomorphism  $\mathbf{x}' : F \rightarrow \mathcal{G}$
- 

**Algorithm MG.** Glauber-Chain Update

---

- 1: **Input:** Network  $\mathcal{G} = (V, A)$ , a  $k$ -chain motif  $F = ([k], A_F)$ , and homomorphism  $\mathbf{x} : F \rightarrow \mathcal{G}$
- 2: **Do:** Sample  $v \in [k]$  uniformly at random
- 3:     Sample  $z \in V$  at random from the distribution

$$p(w) = \frac{1}{Z} \left( \prod_{u \in [k]} A(\mathbf{x}(u), w)^{A_F(u, v)} \right) \left( \prod_{u \in [k]} A(w, \mathbf{x}(u))^{A_F(v, u)} \right), \quad w \in V \quad (10)$$

where  $Z = \sum_{c \in V} \left( \prod_{u \in [k]} A(\mathbf{x}(u), c)^{A_F(u, v)} \right) \left( \prod_{u \in [k]} A(c, \mathbf{x}(u))^{A_F(v, u)} \right)$  is the normalization constant

- 4:     Define a new homomorphism  $\mathbf{x}' : F \rightarrow \mathcal{G}$  by  $\mathbf{x}'(w) = z$  if  $w = v$  and  $\mathbf{x}'(w) = \mathbf{x}(w)$  otherwise
  - 5: **Output:** Homomorphism  $\mathbf{x}' : F \rightarrow \mathcal{G}$
-

pivot chain, which is Algorithm **MP** with the option `AcceptProb = Approximate`. Specifically, we compute the acceptance probability  $\alpha$  in (8) only approximately and thereby reduce the computational cost to  $O(\Delta)$ . Our compromise, which we discuss in the next paragraph, is that the stationary distribution of the approximate pivot chain may be slightly different from our target distribution  $\pi_{F \rightarrow \mathcal{G}}$ .

Define a probability distribution  $\hat{\pi}_{F \rightarrow \mathcal{G}}$  on the set of all node maps  $\mathbf{x} : [k] \rightarrow V$  as

$$\hat{\pi}_{F \rightarrow \mathcal{G}}(\mathbf{x}) := \frac{\prod_{i=1}^k A(\mathbf{x}(i-1), \mathbf{x}(i))}{|V| \sum_{y_2, \dots, y_k \in V} A(\mathbf{x}(1), y_2) \prod_{i=3}^k A(y_{i-1}, y_i)}. \quad (11)$$

According to Proposition 7.2, the stationary distribution of the approximate pivot chain is (11). The distribution (11) is different from the desired target distribution  $\pi_{F \rightarrow \mathcal{G}}$ . Specifically,  $\pi_{F \rightarrow \mathcal{G}}(\mathbf{x})$  is proportional only to the numerator in (11) and the sum in the denominator in (11) is a weighted count of the homomorphisms  $\mathbf{y} : F \rightarrow \mathcal{G}$  for which  $\mathbf{y}(1) = \mathbf{x}(1)$ . Therefore, under  $\hat{\pi}_{F \rightarrow \mathcal{G}}$ , we penalize the probability of each homomorphism  $\mathbf{x} : F \rightarrow \mathcal{G}$  according to the number of  $k$ -step walks in  $\mathcal{G}$  that start from  $\mathbf{x}(1) \in V$ . (The exact acceptance probability in (8) neutralizes this penalty.) It follows that  $\hat{\pi}_{F \rightarrow \mathcal{G}}$  is close to  $\pi_{F \rightarrow \mathcal{G}}$  when the  $k$ -step-walk counts that start from each node in  $\mathcal{G}$  do not differ too much for different nodes. For example, on degree-regular networks like lattices, such counts do not depend on the starting node, and it thus follows that  $\hat{\pi}_{F \rightarrow \mathcal{G}} = \pi_{F \rightarrow \mathcal{G}}$ . Nevertheless, despite the potential discrepancy between  $\pi_{F \rightarrow \mathcal{G}}$  and  $\hat{\pi}_{F \rightarrow \mathcal{G}}$ , the approximate pivot chain gives good results for the reconstruction and denoising experiments that we showed in Figures 5 and 9 in the main manuscript.

#### APPENDIX D. ALGORITHM FOR NETWORK DICTIONARY LEARNING (NDL)

**D.1. Algorithm overview and statement.** The essential idea behind our algorithm for NDL (see Algorithm **NDL**) is as follows. Suppose that we compute all possible injective homomorphisms  $\mathbf{x}_1, \dots, \mathbf{x}_M : F \hookrightarrow \mathcal{G}$  and their corresponding mesoscale patches  $A_{\mathbf{x}_t}$  for  $t \in \{1, \dots, M\}$ . These  $M$  mesoscale patches of  $\mathcal{G}$  form the data set (a so-called ‘batch’) in which we apply a dictionary-learning algorithm. To do this, we column-wise vectorize each of these  $k \times k$  matrices (using Algorithm **A4**) and obtain a  $k^2 \times M$  data matrix  $X$ , and we then apply nonnegative matrix factorization (NMF) [6] to obtain a  $k^2 \times r$  nonnegative matrix  $W$  for some fixed integer  $r \geq 1$  to yield an approximate factorization  $X \approx WH$  for some nonnegative matrix  $H$ . From this procedure, we approximate each column of  $X$  by the nonnegative linear combination of the  $r$  columns of  $W$  with coefficients that are given by entries of the  $r^{\text{th}}$  column of  $H$ . Therefore, if we let  $\mathcal{L}_i$  be the  $k \times k$  matrix that we obtain by reshaping the  $i^{\text{th}}$  column of  $W$  (using Algorithm **A5**), then  $(\mathcal{L}_1, \dots, \mathcal{L}_r)$  is an approximate solution of (6). We give the precise meaning of ‘approximate solution’ in Theorems 7.4 and 7.7.

The scheme in the paragraph above requires one to store all  $M$  mesoscale patches, entailing a memory requirement that is at least of order  $k^2 M$ , where  $M$  is the number of all possible injective homomorphisms  $F \hookrightarrow \mathcal{G}$ . Because  $M$  grows with the size of  $\mathcal{G}$ , we need unbounded memory to handle arbitrarily large networks. To address this issue, Algorithm **NDL** implements the above scheme in the setting of ‘online learning’, where subsets (so-called ‘minibatches’) of data arrive in a sequential manner and one does not store previous subsets of the data before processing new subsets. Specifically, at each iteration  $t = 1, 2, \dots, T$ , we process a sample matrix  $X_t$  that is smaller than the full matrix  $X$  and includes only  $N \ll M$  mesoscale patches, where one can take  $N$  to be independent of the network size. Instead of using a standard NMF algorithm for a fixed matrix [50], we use an ‘online’ NMF algorithm [53, 45] that one can use on sequences of matrices, where the intermediate dictionary matrices  $W_t$  that we obtain by factoring the sample

**Algorithm NDL.** Network Dictionary Learning (NDL)

- 
- 1: **Input:** Network  $\mathcal{G} = (V, A)$
  - 2: **Parameters:**  $F = ([k], A_F)$  (a  $k$ -chain motif),  $T \in \mathbb{N}$  (the number of iterations),  $N \in \mathbb{N}$  (the number of homomorphisms per iteration),  $r \in \mathbb{N}$  (the number of latent motifs),  $\lambda \geq 0$  (the coefficient of an  $L_1$ -regularizer)
  - 3: **Options:**  $\text{MCMC} \in \{\text{Pivot}, \text{PivotApprox}, \text{Glauber}\}$
  - 4: **Requirement:** There exists at least one injective homomorphism  $F \hookrightarrow \mathcal{G}$
  - 5: **Initialization:**
  - 6: Sample a homomorphism  $\mathbf{x} : F \rightarrow \mathcal{G}$  using the rejection sampling (see Algorithm A3)
  - 7:  $W = (k^2 \times r)$  matrix of independent entries that we sample uniformly from  $[0, 1]$
  - 8:  $P_0 =$  matrix of size  $r \times r$  whose entries are 0
  - 9:  $Q_0 =$  matrix of size  $r \times k^2$  whose entries are 0
  - 10: **For**  $t = 1, 2, \dots, T$ :
  - 11: *MCMC update and sampling mesoscale patches:*
  - 12: Successively generate  $N$  injective homomorphisms  $\mathbf{x}_{N(t-1)+1}, \mathbf{x}_{N(t-1)+2}, \dots, \mathbf{x}_{Nt}$  by applying Algorithm RM with
 

Algorithm MP with <code>AcceptProb = Exact</code>	if	<code>MCMC = Pivot</code>
Algorithm MP with <code>AcceptProb = Approximate</code>	if	<code>MCMC = PivotApprox</code>
Algorithm MG with <code>AcceptProb = Glauber</code>	if	<code>MCMC = Glauber</code>
  - 13: **For**  $s = N(t-1) + 1, \dots, Nt$ :
  - 14:  $A_{\mathbf{x}_s} \leftarrow k \times k$  mesoscale patch of  $\mathcal{G}$  that is induced by  $\mathbf{x}_s$  (see (4))
  - 15:  $X_t \leftarrow k^2 \times N$  matrix whose  $j^{\text{th}}$  column is  $\text{vec}(A_{\mathbf{x}_\ell})$  with  $\ell = N(t-1) + j$   
(where  $\text{vec}(\cdot)$  denotes the vectorization operator that we defined in Algorithm A4)
  - 16: *Single iteration of online nonnegative matrix factorization:*

$$\begin{cases} H_t \leftarrow \arg \min_{H \in \mathbb{R}_{\geq 0}^{r \times N}} \|X_t - W_{t-1}H\|_F^2 + \lambda \|H\|_1 & \text{(using Algorithm A1)} \\ P_t \leftarrow (1 - t^{-1})P_{t-1} + t^{-1}H_tH_t^T \\ Q_t \leftarrow (1 - t^{-1})Q_{t-1} + t^{-1}H_tX_t^T \\ W_t \leftarrow \arg \min_{W \in \mathcal{C}^{\text{dict}} \subseteq \mathbb{R}_{\geq 0}^{k^2 \times r}} (\text{tr}(WP_tW^T) - 2\text{tr}(WQ_t)) & \text{(using Algorithm A2)}, \end{cases} \quad (12)$$

where  $\mathcal{C}^{\text{dict}} = \{W \in \mathbb{R}_{\geq 0}^{k^2 \times r} \mid \text{columns of } W \text{ have a Frobenius norm of at most } 1\}$
  - 17: **Output:** Network dictionary  $W_T \in \mathbb{R}_{\geq 0}^{k^2 \times r}$
- 

matrix  $X_t$  typically improves as we iterate (see [53, 45]). In Algorithm NDL, we give a complete implementation of the NDL algorithm.

We now explain how our NDL algorithm works. It combines one of the three MCMC algorithms — a pivot chain (in which we use Algorithm MP with `AcceptProb = Exact`), an approximate pivot chain (in which we use Algorithm MP with `AcceptProb = Approximate`), and a Glauber chain (in which we use Algorithm MG) — for injective motif sampling that we presented in Section C with the online NMF algorithm from [45]. Suppose that we have an undirected and unweighted graph  $\mathcal{G} = (V, A)$  and a  $k$ -chain motif  $F = ([k], A_F)$ . Furthermore, assume that we satisfy the requirement in Algorithm NDL that there exists at least one injective homomorphism  $F \hookrightarrow \mathcal{G}$ . At each iteration  $t = 1, 2, \dots, T$ , the injective motif-sampling algorithm generates

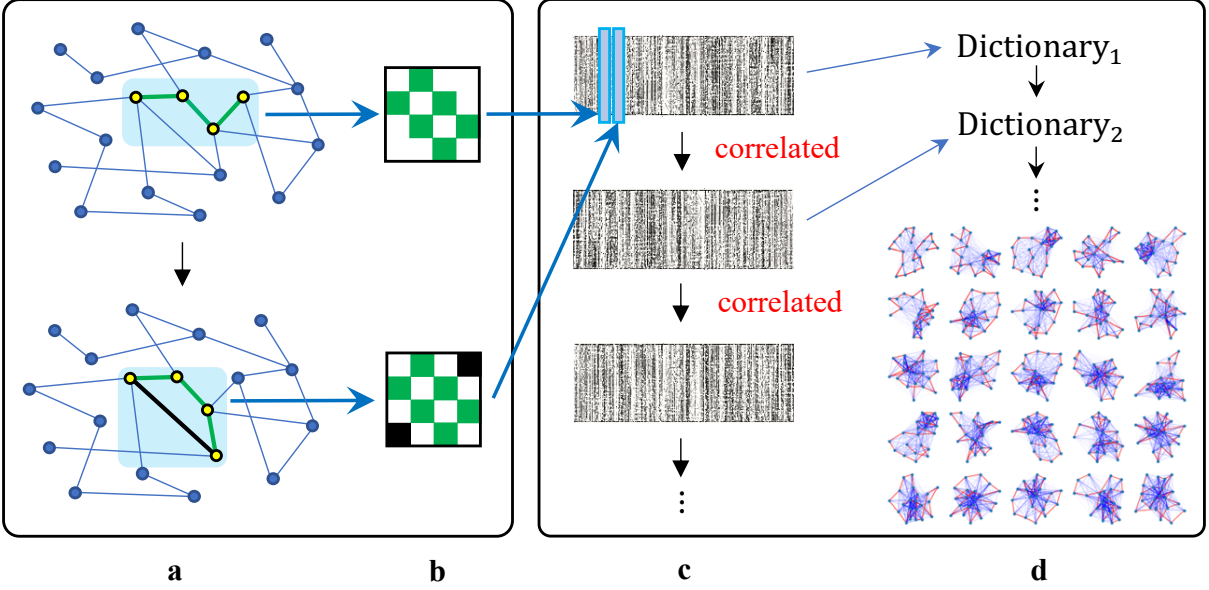


FIGURE 12. Illustration of our network dictionary learning (NDL) algorithm (see Algorithm NDL). (a) Homomorphisms  $\mathbf{x}_t : F \rightarrow \mathcal{G}$  from a  $k$ -chain motif into a target network  $\mathcal{G}$  evolve as a Markov chain to yield a sequence of  $k$ -chain subgraphs (the green edges) in  $\mathcal{G}$ . (b) Each copy of the  $k$ -chain motif in  $\mathcal{G}$  induces a  $k$ -node subgraph (i.e., the mesoscale patch  $A_{\mathbf{x}_t}$  that we defined in (4)). (c) We form a sequence of matrices  $X_t$  of size  $k^2 \times N$ , where the  $N$  columns of each  $X_t$  are vectorizations of the  $N$  consecutive  $k \times k$  mesoscale patches in panel b. (d) Using an online nonnegative matrix factorization (NMF) algorithm, we progressively learn the desired number of latent motifs as the data matrix of mesoscale patches  $X_t$  arrives.

a sequence  $\mathbf{x}_s : F \rightarrow \mathcal{G}$  of  $N$  injective homomorphisms and corresponding mesoscale patches  $A_{\mathbf{x}_s}$  (see Figure 12a), which we summarize as the  $k^2 \times N$  data matrix  $X_t$ . The online NMF algorithm in (12) learns a nonnegative factor matrix  $W_t$  of size  $k^2 \times r$  by improving the previous factor matrix  $W_{t-1}$  by using the new data matrix  $X_t$ . It is an ‘online’ NMF algorithm because it factorizes a sequence  $(X_t)_{t \in \{1, \dots, T\}}$  of data matrices, rather than a single matrix as in conventional NMF algorithms [50]. As it proceeds, the algorithm only needs to store auxiliary matrices  $P_t$  and  $Q_t$  of fixed sizes  $r \times r$  and  $r \times k^2$ , respectively; it does not need the previous data matrices  $X_1, \dots, X_{t-1}$ . Therefore, NDL is efficient in memory and scales well with network size. Moreover, it is applicable to time-dependent networks because of its online nature, although we do not study such networks in the present paper.

In (12), we solve convex optimization problems to find matrices  $H_t \in \mathbb{R}^{r \times N}$  and  $W_t \in \mathbb{R}^{k^2 \times r}$ . The subproblem in (12) of computing  $H_t$  is a ‘coding problem’. Given two matrices  $X_t$  and  $W_{t-1}$ , we seek to find a factor matrix (i.e., a ‘code matrix’)  $H_t$  such that  $X_t \approx W_{t-1}H_t$ . The parameter  $\lambda \geq 0$  is an  $L_1$ -regularizer, which encourages  $H_t$  to have a small  $L_1$  norm. One can solve the coding problem efficiently by using Algorithm A1 or one of a variety of existing algorithms (e.g., layer-wise adaptive-rate scaling (LARS) [56], LASSO [55], or feature-sign search [61]). The second and third lines in (12) update the ‘aggregate matrices’  $P_{t-1} \in \mathbb{R}^{r \times r}$  and  $Q_{t-1} \in \mathbb{R}^{r \times k^2}$  by taking a weighted average of them with the new information  $X_t H_t^T \in \mathbb{R}^{r \times r}$  and  $H_t X_t^T$ , respectively. We weight the old aggregate matrices by  $1 - t^{-1}$  and the new information by  $t^{-1}$ . By induction, we obtain  $P_t = t^{-1} \sum_{s=1}^t H_s H_s^T$  and  $Q_t = t^{-1} \sum_{s=1}^t H_s X_s^T$ . We use the updated aggregate matrices,  $P_t$  and  $Q_t$ , in the subproblem in (12) of computing  $W_t$ . This problem is called the ‘dictionary-update problem’ and yields  $W_t$ . This is a constrained quadratic problem;

we can solve it using projected gradient descent (see Algorithm A2). In all of our experiments, we take the compact and convex constraint set  $\mathbb{R}_{\geq 0}^{k^2 \times r}$  to be the set of  $W \in \mathbb{R}_{\geq 0}^{k^2 \times r}$  whose columns have a Frobenius norm of at most 1 (as required in (6)).

**D.2. Dominance scores of latent motifs.** In this subsection, we introduce a quantitative measurement of the ‘prevalence’ of latent motifs in the network dictionary  $W_T$  that we compute using NDL (see Algorithm NDL) for a network  $\mathcal{G}$ .

Given a network  $\mathcal{G}$  and a  $k$ -chain motif, recall that the output of the NDL algorithm is a network dictionary  $W_T$  of  $r$  latent motifs  $\mathcal{L}_1, \dots, \mathcal{L}_r$  of size  $k \times k$ . Recall as well that the NDL algorithm yields data matrices  $X_1, \dots, X_T$  of size  $k^2 \times N$ . Suppose that we have code matrices  $H_1^*, \dots, H_T^*$  such that  $X_t \approx W_T H_t^*$  for all  $t \in \{1, \dots, T\}$ . More precisely, we let

$$H_t^* := \arg \min_{H \geq 0} (\|X_t - W_T H\|^2 + \lambda \|H\|_1), \quad (13)$$

where we take the arg min over all  $H \in \mathbb{R}_{\geq 0}^{k^2 \times N}$ . The columns of  $H_t^*$  encode how to nonnegatively combine the latent motifs in  $W_T$  to approximate the mesoscale patches in  $X_t \in \mathbb{R}_{\geq 0}^{k^2 \times N}$ , so the rows of  $H_t^*$  encode the linear coefficients of each latent motif in  $W_T$  that we use for approximating the columns of  $X_t$ . Consequently, the means of the Euclidean norms of the rows of  $H_t^*$  for each  $t \in \{1, \dots, T\}$  encode the mean prevalences of the latent motifs in  $W_T$  in  $\mathcal{G}$ . This motivates us to consider the mean Gramian matrix [64]

$$P_T^* := \frac{1}{T} \sum_{t=1}^T H_t^* (H_t^*)^T \in \mathbb{R}^{r \times r}.$$

The square root of the diagonal entries of  $P_T^*$  yield the mean prevalences of the latent motifs in  $W_T$  in  $\mathcal{G}$ .

Computing  $P_T^*$  requires us to store the previous data matrices  $X_1, \dots, X_T$  and determine  $H_1^*, \dots, H_T^*$  by solving (13) for  $t \in \{1, \dots, T\}$ . This way of computing  $P_T^*$  is very expensive with respect to both memory and computational requirements. To address this issue, we use the aggregate matrix  $P_T$  that we compute as part of Algorithm NDL. It then does not require any extra computation. Note that

$$P_T = \frac{1}{T} \sum_{t=1}^T H_t H_t^T,$$

where  $H_t = \arg \min_{H \geq 0} (\|X_t - W_{t-1} H\|^2 + \lambda \|H\|_1) \in \mathbb{R}_{\geq 0}^{r \times N}$  is the code matrix. The matrix  $P_T$  is an approximation of  $P_T^*$  because the defining equation of  $H_t$  is the same as that of  $H_t^*$  in (13) with  $W_T$  replaced by  $W_{t-1}$ . The approximation error of using  $P_T$  instead of  $P_T^*$  vanishes as  $T \rightarrow \infty$  under mild conditions.

Specifically, under the hypotheses of Theorems 7.4 and 7.7, the network dictionary  $W_t$  converges almost surely to some limiting dictionary. It follows that  $\|P_T^* - P_T\|_F \rightarrow 0$  almost surely as  $T \rightarrow \infty$ .

## APPENDIX E. ALGORITHM FOR NETWORK DENOISING AND RECONSTRUCTION (NDR)

**E.1. Algorithm overview and statement.** The standard pipeline for image denoising and reconstruction [10, 51, 52] is to uniformly randomly sample a large number of  $k \times k$  overlapping patches of an image and then average their associated approximations at each pixel to obtain a reconstructed version of the original image. A network analog of this pipeline proceeds as follows. Given a network  $\mathcal{G} = (V, A)$ , a  $k$ -chain motif  $F = ([k], A_F)$ , and a network dictionary with latent motifs  $(\mathcal{L}_1, \dots, \mathcal{L}_r)$ , we compute a weighted network  $\mathcal{G}_{\text{recons}} = (V, A_{\text{recons}})$ . To do this, we first

uniformly randomly sample a large number  $T$  of (not necessarily injective) homomorphisms  $\mathbf{x}_t : F \rightarrow \mathcal{G}$  and determine the corresponding mesoscale patches  $A_{\mathbf{x}_0}, \dots, A_{\mathbf{x}_T}$  using (4). We then approximate each mesoscale patch  $A_{\mathbf{x}_t}$  by a nonnegative linear combination  $\hat{A}_{\mathbf{x}_t}$  of the latent motifs  $\mathcal{L}_i$ . Finally, for each  $x, y \in V$ , we define  $A_{\text{recons}}(x, y)$  as the mean of  $\hat{A}_{\mathbf{x}_t}(a, b)$  over all  $t = \{0, \dots, T\}$  and all  $a, b \in \{1, \dots, k\}$  such that  $\mathbf{x}_t(a) = x$  and  $\mathbf{x}_t(b) = y$ .

Our network denoising and reconstruction (NDR) algorithm (see Algorithm **NDR**) builds on the idea in the preceding paragraph. Suppose that we have a network  $\mathcal{G} = (V, A)$ , a  $k$ -chain motif  $F = ([k], A_F)$ , and a network dictionary  $W$  that consists of  $r$  nonnegative  $k \times k$  matrices  $\mathcal{L}_1, \dots, \mathcal{L}_r$ . We provide two options to reconstruct  $\mathcal{G}$ . In one option, we use uniformly random homomorphisms from the distribution  $\pi_{F \rightarrow \mathcal{G}}$  in (1) (option **InjHom = F**). In the other option, we use only the injective homomorphisms, which means that we instead use the distribution  $\pi_{F \hookrightarrow \mathcal{G}}$  in (2) (option **InjHom = T**). The latter option has a larger computational cost, but it has better theoretical properties with respect to the NDL algorithm (see Algorithm **NDL**). To sketch how the NDR algorithm with **InjHom = F** works, suppose that we sample homomorphisms  $\mathbf{x}_0, \dots, \mathbf{x}_T$  from the distribution  $\pi_{F \rightarrow \mathcal{G}}$ . For each  $t \geq 0$ , we approximate the mesoscale patch  $A_{\mathbf{x}_t}$  (see (4)) by a nonnegative linear combination of latent motifs  $\mathcal{L}_i$  and we then take the mean of the values of each entry  $A(a, b)$  for all  $t \in \{1, \dots, T\}$ . However, because sampling a homomorphism  $\mathbf{x}_t : F \rightarrow \mathcal{G}$  from  $\pi_{F \rightarrow \mathcal{G}}$  is not as straightforward as uniformly randomly sampling  $k \times k$  patches of an image, we generate a sequence  $(\mathbf{x}_t)_{t \in \{0, \dots, T\}}$  of homomorphisms using an MCMC motif-sampling algorithms (see Algorithms **MG** and **MP**). The NDR algorithm with **InjHom = T** works similarly, but it uses injective homomorphisms that are generated from the injective motif-sampling algorithm (see Algorithm **RM**).

For network reconstruction, it is important to sample homomorphisms  $\mathbf{x}_1, \dots, \mathbf{x}_T : F \rightarrow \mathcal{G}$  that cover an entire network  $\mathcal{G}$  (or at least a large portion of it). A node  $x$  of  $\mathcal{G}$  is ‘covered’ by the homomorphisms  $\mathbf{x}_1, \dots, \mathbf{x}_T$  if it is contained in the image of  $\mathbf{x}_t$  for some  $t \in \{1, \dots, T\}$ . In Proposition 7.9, we show that one can cover all nodes in  $\mathcal{G}$  by the images of injective homomorphisms  $F \hookrightarrow \mathcal{G}$  if  $2(k-1) \leq \text{diam}(\mathcal{G})$  if  $\mathcal{G}$  is symmetric and connected. However, even when this inequality is satisfied, we have to sample more homomorphisms using one of our MCMC motif-sampling algorithms (see Algorithms **MG** and **MP**) to cover the same portion of the network  $\mathcal{G}$  than when we use all sampled homomorphisms. This gives a computational advantage of using **InjHom = F** instead of **InjHom = T** in our NDR algorithm.

Despite the above computational disadvantage of using **InjHom = T**, this choice has a nice theoretical advantage. Recall that the NDL algorithm (see Algorithm **NDL**) computes latent motifs  $\mathcal{L}_1, \dots, \mathcal{L}_r$  from mesoscale patches  $A_{\mathbf{y}_1}, \dots, A_{\mathbf{y}_M}$  of  $\mathcal{G}$  for injective homomorphisms  $\mathbf{y}_t : F \rightarrow \mathcal{G}$  for  $t \in \{1, \dots, M\}$  so that they give an approximate solution of (6). Consequently, when linearly approximating a mesoscale patch  $A_{\mathbf{x}}$  of  $\mathcal{G}$ , these latent motifs  $\mathcal{L}_1, \dots, \mathcal{L}_r$  are less effective if the homomorphism  $\mathbf{x}$  is non-injective than if  $\mathbf{x}$  is injective. We need to linearly approximate multiple mesoscale patches  $A_{\mathbf{x}_1}, \dots, A_{\mathbf{x}_T}$  for homomorphisms  $\mathbf{x}_t : F \rightarrow \mathcal{G}$  for  $t \in \{1, \dots, T\}$ , so we expect the reconstructed network that we obtain using Algorithm **NDR** with only injective homomorphisms to be more accurate than when using all sampled homomorphisms. In Theorem 7.10(iii), we obtain an upper bound for the Jaccard reconstruction error (which we define in (30)). This upper bound is optimized by the latent motifs that we obtain with the NDL algorithm using only injective homomorphisms. Therefore, NDR algorithm with option **InjHom = T** has a theoretical advantage over the NDR algorithm with option **InjHom = F**.

As in the first line of (12), the problem of determining  $H_t$  in line 15 of Algorithm **NDR** is a standard convex problem, which one can solve by using Algorithm **A1**. There are two variants of the NDR algorithm. The variant is specified by the Boolean variable **denoising**. The NDR algorithm with **denoising = F** is identical to the network-reconstruction algorithm in [45], except

---

**Algorithm NDR.** Network Denoising and Reconstruction (NDR)

---

- 1: **Input:** Network  $\mathcal{G} = (V, A)$ , and network dictionary  $W \in \mathbb{R}_{\geq 0}^{k^2 \times r}$
- 2: **Parameters:**  $F = ([k], A_F)$  (a  $k$ -chain motif),  $T \in \mathbb{N}$  (number of iterations),  $\lambda \geq 0$  (the coefficient of an  $L_1$ -regularizer),  $\theta \in [0, 1]$  (an edge threshold)
- 3: **Options:**  $\text{denoising} \in \{\text{T}, \text{F}\}$ ,  $\text{MCMC} \in \{\text{Pivot}, \text{PivotApprox}, \text{Glauber}\}$ ,  $\text{InjHom} \in \{\text{T}, \text{F}\}$
- 4: **Requirement:** There exists at least one homomorphism  $F \rightarrow \mathcal{G}$
- 5: **Initialization:**
- 6:  $A_{\text{recons}}, A_{\text{count}} : V^2 \rightarrow \{0\}$  (matrices with 0 entries)
- 7: Sample a (not necessarily injective) homomorphism  $\mathbf{x}_0 : F \rightarrow \mathcal{G}$  by the rejection sampling in Algorithm A3
- 8: **For**  $t = 1, 2, \dots, T$ :
- 9: *MCMC update and mesoscale patch extraction:*
- 10:  $\mathbf{x}_t \leftarrow$  Updated homomorphism that we obtain by applying
 

Algorithm MP with AcceptProb = Exact	if	MCMC = Pivot
Algorithm MP with AcceptProb = Approximate	if	MCMC = PivotApprox
Algorithm MG with AcceptProb = Glauber	if	MCMC = Glauber
- (If  $\text{InjHom} = \text{T}$ , set  $\mathbf{x}_t \leftarrow$  Updated injective homomorphism from applying Algorithm RM with the specified MCMC algorithm)
- 11:  $A_{\mathbf{x}_t} \leftarrow k \times k$  mesoscale patch of  $\mathcal{G}$  that is induced by  $\mathbf{x}_t$  (see (4))
- 12:  $X_t \leftarrow k^2 \times 1$  matrix that we obtain by vectorizing  $A_{\mathbf{x}_t}$  (using Algorithm A4)
- 13: *Mesoscale reconstruction:*
- 14: 
$$\begin{cases} \tilde{X}_t \leftarrow X_t \text{ and } \tilde{W} \leftarrow W & \text{if } \text{denoising} = \text{F} \\ \tilde{X}_t \leftarrow (X_t)_{\text{off}} \text{ and } \tilde{W} \leftarrow (W)_{\text{off}} \text{ using Algorithm 2a} & \text{if } \text{denoising} = \text{T} \end{cases}$$
- 15:  $H_t \leftarrow \arg \min_{H \in \mathbb{R}_{\geq 0}^{r \times 1}} (\|\tilde{X}_t - \tilde{W}H\|_F^2 + \lambda \|H\|_1)$  and  $\hat{X}_t \leftarrow \tilde{W}H_t$
- 16:  $\hat{A}_{\mathbf{x}_t; W} \leftarrow k \times k$  matrix that we obtain by reshaping the  $k^2 \times 1$  matrix  $\hat{X}_t$  using Algorithm A5
- 17: *Update global reconstruction:*
- 18: **For**  $a, b \in \{1, \dots, k\}$ :
- 19: **If** ( $\text{denoising} = \text{F}$  or  $A_F(a, b) = 0$ ):
 

$A_{\text{count}}(\mathbf{x}_t(a), \mathbf{x}_t(b)) \leftarrow A_{\text{count}}(\mathbf{x}_t(a), \mathbf{x}_t(b)) + 1$
$j \leftarrow A_{\text{count}}(\mathbf{x}_t(a), \mathbf{x}_t(b))$
$A_{\text{recons}}(\mathbf{x}_t(a), \mathbf{x}_t(b)) \leftarrow (1 - j^{-1})A_{\text{recons}}(\mathbf{x}_t(a), \mathbf{x}_t(b)) + j^{-1}\hat{A}_{\mathbf{x}_t; W}(\mathbf{x}_t(a), \mathbf{x}_t(b))$
- 20: **Output:** Reconstructed networks  $\mathcal{G}_{\text{recons}} = (V, A_{\text{recons}})$ 

---

**Algorithm 2a.** Off-Chain Projection

**Input:** Matrix  $Y \in \mathbb{R}^{k^2 \times m}$ , motif  $F = ([k], A_F)$

**Do:** Let  $Y'$  be a  $k \times k \times m$  tensor that we obtain by reshaping each column of  $Y$  using Algorithm A5

Let  $Y''$  be a  $k \times k \times m$  tensor that we obtain from  $Y'$  by

$$Y''(a, b, c) = Y'(a, b, c) \mathbb{1}(A_F(a, b) = 0) \quad \text{for all } a, b \in \{1, \dots, k\} \text{ and } c \in \{1, \dots, m\}$$

Let  $Y_{\text{off}}$  be a  $k^2 \times m$  matrix that we obtain from  $Y''$  by vectorizing each of its slices using Algorithm A4:  $Y''[:, :, c]$  for all  $c \in \{1, \dots, m\}$

**Output:** Matrix  $(Y)_{\text{off}} \in \mathbb{R}^{k^2 \times m}$

for the thresholding step. The NDR algorithm with `denoising = T` is a new variant of NDR that we present in this work for the purpose of network denoising.

**E.2. Further discussion of the denoising variant of the NDR algorithm.** We now give a detailed discussion of Algorithm NDR with `denoising = T` for network-denoising applications. Recall that our network-denoising problem is to reconstruct a true network  $\mathcal{G}_{\text{true}} = (V, A)$  from an observed network  $\mathcal{G}_{\text{obs}} = (V, A')$ . The scheme that we used to produce Figure 9 is the following:

- D.1** Learn a network dictionary  $W \in \mathbb{R}_{\geq 0}^{k^2 \times r}$  from an observed network  $\mathcal{G}_{\text{obs}} = (V, A)$  using NDL (see Algorithm NDL).
- D.2** Compute a reconstructed network  $\mathcal{G}_{\text{recons}} = (V, A_{\text{recons}})$  using NDR (see Algorithm NDR) with inputs  $\mathcal{G}_{\text{obs}} = (V, A)$  and  $W$ .
- D.3** Fix an edge threshold  $\theta \in [0, 1]$ . If  $\mathcal{G}_{\text{obs}}$  is  $\mathcal{G}_{\text{true}}$  with additive (respectively, subtractive) noise, we classify each edge (respectively, non-edge)  $\{x, y\}$  as ‘positive’ if and only if  $A_{\text{recons}}(x, y) > \theta$ .

As was discussed in [45, Remark 4], a limitation of using NDR with `denoising = F` for network denoising is that the meaning of successful classification for subtractive-noise cases is an ‘inversion’ of its meaning for additive-noise cases. Specifically, [45] used network denoising with NDR for additive noise, but it is necessary to classify each non-edge  $\{x, y\}$  as ‘positive’ if  $A_{\text{recons}}(x, y) < \theta$ . In the experiment in Figure 8 in the main manuscript, we noted that NDR with `denoising = F` may assign large weights to false edges and small weights to true edges. Our NDR algorithm with `denoising = T` addresses this directionality issue and allows us to use the unified classification scheme above for both additive and subtractive noise.

The idea behind NDR with `denoising = T` is to handle an issue that occurs when denoising additive noise for sparse real-world networks but does not arise in the image-denoising setting. Suppose that we obtain  $\mathcal{G}_{\text{obs}}$  by adding some false edges to a sparse unweighted network  $\mathcal{G}_{\text{true}}$ . The on-chain entries of the mesoscale patches  $A_{\mathbf{x}}$  are always equal to 1. Therefore, the latent motifs that we learn from  $\mathcal{G}_{\text{obs}}$  have constant on-chain entries (see, e.g., Figure 2 in the main manuscript). Consequently, a linear approximation of the mesoscale patches  $A_{\mathbf{x}}$  of  $\mathcal{G}_{\text{obs}}$  of the latent motifs that we learn from  $\mathcal{G}_{\text{obs}}$  cannot distinguish between true and false on-chain entries. Furthermore, because  $\mathcal{G}_{\text{obs}}$  is sparse, there are many fewer positive off-chain entries in  $A_{\mathbf{x}}$  than on-chain entries of  $A_{\mathbf{x}}$ . Therefore, in a reconstruction, linear approximations of  $A_{\mathbf{x}}$  with the latent motifs are likely to assign larger weights to on-chain entries of  $A_{\mathbf{x}}$  than to off-chain entries. The resulting reconstruction of  $\mathcal{G}_{\text{obs}}$  is thus similar to  $\mathcal{G}_{\text{obs}}$ , and it is very hard to detect false edges in  $\mathcal{G}_{\text{obs}}$ . Using the option `denoising = T` prevents this issue by ignoring all on-chain entries both for each sampled mesoscale patch  $A_{\mathbf{x}}$  and for each latent motif in the network dictionary  $W$  that we use for denoising.



## APPENDIX F. EXPERIMENTAL DETAILS

F.1. **Figure 1.** In Figure 1, we show six subgraphs that are induced by approximately uniformly random samples of  $k$ -paths with  $k = 20$  (red edges) from the networks CALTECH, UCLA, ER<sub>1</sub>, BA<sub>2</sub>, WS<sub>2</sub>, and SBM<sub>1</sub>. To sample such  $k$ -paths, we use Algorithm MP with `AcceptProb = Approximate`. The red edges in each subgraph designate edges in the sampled  $k$ -paths (i.e., on-chain edges), and the blue edges designate edges (the off-chain edges) that connect non-adjacent nodes on sampled paths.

F.2. **Figure 2.** In Figure 2, we illustrate latent motifs that we learn from the networks UCLA and CALTECH and we compare them to an image dictionary. The image in panel a is from the collection DIE GRAPHIK ERNST LUDWIG KIRCHNERS BIS 1924, VON GUSTAV SCHIEFLER BAND I BIS 1916 (Accession Number 2007.141.9, Ernst Ludwig Kirchner, 1926). We use this image with permission from the National Gallery of Art in Washington, DC, USA.<sup>2</sup> We use a  $k$ -chain motif with the corresponding network  $F = ([k], A_F)$ , a scale  $k = 21$  for  $T = 100$  iterations,  $N = 100$  injective homomorphisms per iteration,  $r = 25$  latent motifs, an  $L_1$ -regularizer with coefficient  $\lambda = 1$ , and the MCMC motif-sampling algorithm `MCMC = PivotApprox`. The image dictionary for the artwork CYCLE in Figure 2 uses an algorithm that is similar to Algorithm NDL, except that we uniformly randomly sample  $21 \times 21$  square patches of the image instead of  $k \times k$  mesoscale patches of a network.

F.3. **Figure 3.** In Figure 3, we compare box plots of community sizes of 10,000 randomly sampled subgraphs that are induced by approximately uniformly random paths of  $k = 21$  (using Algorithm MP with `AcceptProb = Approximate`.) nodes (in red) to the corresponding box plots of  $r = 25$  latent motifs of  $k = 21$  nodes for various real-world and synthetic networks. (See the Methods section of the main manuscript.) We determine latent motifs using NDL (see Algorithm NDL) with a  $k$ -chain motif with the corresponding network  $F = ([k], A_F)$  for  $T = 100$  iterations,  $N = 100$  injective homomorphisms per iteration (so we sample a total  $10^4$  injective homomorphisms), an  $L_1$ -regularizer with coefficient  $\lambda = 1$ , and the MCMC injective motif-sampling algorithm `MCMC = PivotApprox`. We determine the communities of the subgraph and the latent motifs using the locally-greedy Louvain algorithm for modularity maximization [14].

F.4. **Figure 4.** In this figure, we show latent motifs of the examined networks (which we described in the Methods section of the main manuscript) using Algorithm NDL with various parameter choices. In each column of this figure, we use a  $k$ -chain motif  $F = ([k], A_F)$  for  $T = 100$  iterations,  $N = 100$  injective homomorphisms per iteration (so we sample a total  $10^4$  injective homomorphisms), an  $L_1$ -regularizer with coefficient  $\lambda = 1$ , and the MCMC injective motif-sampling algorithm `MCMC = PivotApprox`. We specify the number  $r$  of latent motifs and the scale  $k$  in the caption Figure 4.

F.5. **Figure 5.** To generate Figure 5, we first apply the NDL algorithm (see Algorithm NDL) to each network in the figure to learn  $r = 25$  latent motifs for a  $k$ -chain motif with the corresponding network  $F = ([k], A_F)$ , a scale  $k = 21$  for  $T = 100$  iterations,  $N = 100$  injective homomorphisms per iteration, an  $L_1$ -regularizer with coefficient  $\lambda = 1$ , and the MCMC motif-sampling algorithm `MCMC = PivotApprox`. For each self-reconstruction  $X \leftarrow X$  (see the caption of Figure 5), we apply the NDR algorithm (see Algorithm NDR) to a  $k$ -chain motif  $F = ([k], A_F)$ , a scale  $k = 21$  for  $T = \lfloor n \ln n \rfloor$  iterations (where  $n$  is the number of nodes of the network),  $r = 25$  latent motifs, an  $L_1$ -regularizer with coefficient  $\lambda = 0$  (i.e., no regularization), the MCMC motif-sampling algorithm `MCMC = PivotApprox`, and `denoising = F`. For each cross-reconstruction  $Y \leftarrow X$  (see

<sup>2</sup>See <https://www.nga.gov/notices/open-access-policy.html> for the open-access policy of the National Gallery of Art.

the caption of Figure 5), we apply the NDR algorithm (see Algorithm **NDR**) to a  $k$ -chain motif  $F = ([k], A_F)$ , a scale  $k = 21$  for  $T = (1+3\cdot\mathbb{1}(n < 1000))[n \ln n]$  iterations (where  $n$  is the number of nodes of the network), the edge threshold  $\theta = 0.4$ , an  $L_1$ -regularizer with coefficient  $\lambda = 1$ , the MCMC motif-sampling algorithm  $\text{MCMC} = \text{PivotApprox}$ , and  $\text{denoising} = \text{InjHom} = \text{F}$ . We use several choices of the number  $r$  of latent motifs; we indicate them in the caption of Figure 5.

In the main manuscript, we made several claims based on the reconstruction accuracies in Figure 5 in conjunction with the latent motifs in Figures 2, 4, 14, and 16. We now justify these claims.

- (1) The mesoscale structure of the network **CALTECH** is rather different from those of the networks **HARVARD**, **UCLA**, and **MIT** at scale  $k = 21$ .
  - In Figure 5c, we observe that the accuracy of the cross-reconstruction  $Y \leftarrow X$  is consistently higher for  $X \in \{\text{UCLA}, \text{HARVARD}, \text{MIT}\}$  than for  $X = \text{CALTECH}$  for all values of  $r$ . For instance, for  $r = 9$ , we can reconstruct **UCLA** with more than 90% accuracy and we can reconstruct **HARVARD** and **MIT** with more than 80% accuracy. However, the latent motifs that we learn from **CALTECH** for  $r = 9$  gives only about 80% accuracy for reconstructing **UCLA** and only about 70% accuracy for reconstructing **MIT** and **UCLA**. This indicates that **CALTECH** has a significantly different mesoscale structure than the other three universities' Facebook networks at scale  $k = 21$ . Indeed, from Figures 2, 4, and 14, we see that the  $r = 25$  latent motifs of **CALTECH** at scale  $k = 21$  have larger off-chain entries than those of **UCLA**, **MIT**, and **HARVARD**.
- (2) The mesoscale structure of **CALTECH** at scale  $k = 21$  has a higher dimension than those of the other three universities' Facebook networks.
  - Consider the cross-reconstructions  $\text{CALTECH} \leftarrow X$  for  $X \in \{\text{UCLA}, \text{HARVARD}, \text{MIT}\}$  in Figure 5b. The accuracy with  $r = 9$  for the latent motifs that we learn from **CALTECH** is as low as 64%. By contrast, it is 80% or higher for the self-reconstructions  $X \leftarrow X$  for the Facebook networks of the other universities. In other words,  $r = 9$  latent motifs at scale  $k = 21$  do not approximate the mesoscale structures of **CALTECH** as well as those of the other three universities' Facebook networks. This indicates that the dimension of the mesoscale structures of **CALTECH** at scale  $k = 21$  is larger than those of the other three universities' Facebook networks.
- (3) The network **BA**<sub>2</sub> is better than the networks **ER**<sub>2</sub>, **WS**<sub>2</sub>, and **SBM**<sub>2</sub> at capturing the mesoscale structures of **MIT**, **HARVARD**, and **UCLA** at scale  $k = 21$ . However, for  $r \in \{9, 15, 25, 49\}$ , the network **SBM**<sub>2</sub> captures the mesoscale structure of **CALTECH** better than all but one of the seven other networks in Figure 5b. (The only exception is **CALTECH** itself.)
  - From the reconstruction accuracies for  $Y \leftarrow X$  in Figure 5b,c, where  $X$  is one of the four synthetic networks (**ER**<sub>2</sub>, **WS**<sub>2</sub>, **BA**<sub>2</sub>, and **SBM**<sub>2</sub>), we observe that the two **BA** networks have higher accuracies than the networks from the **ER** and **WS** models for  $Y \in \{\text{UCLA}, \text{HARVARD}, \text{MIT}\}$ . This suggests that the mesoscale structures of **UCLA**, **HARVARD**, and **MIT** are more similar in some respects to those of **BA**<sub>2</sub> than to those of **ER**<sub>2</sub>, **WS**<sub>2</sub>, and **SBM**<sub>2</sub>. The latent motifs of **BA**<sub>2</sub> in Figures 4 and 16 at  $k \in \{11, 21\}$  have characteristics that we also observe in **UCLA**, **HARVARD**, and **MIT**. (Specifically, they have nodes that are adjacent to many other nodes and off-chain entries that are much smaller (so they are lighter in color) than the on-chain entries.) By contrast, in Figure 17, we see that the latent motifs of **ER**<sub>2</sub> have sparse but seemingly randomly distributed off-chain connections and that the ones for **WS**<sub>2</sub> have strongly interconnected communities of about 10 nodes (as indicated by the diagonal block of black entries). These patterns differ from the ones that we observe in the latent motifs of **UCLA**, **MIT**, and **HARVARD** (see Figure 14). For the claim about **SBM**<sub>2</sub>, observe that the cross-reconstruction accuracy  $\text{CALTECH} \leftarrow \text{SBM}_2$

in Figure 5 dominates that of all other  $\text{CALTECH} \leftarrow X$  except  $X = \text{CALTECH}$ . Also, the theoretical lower bound of the Jaccard reconstruction accuracy for  $\text{CALTECH} \leftarrow \text{SBM}_2$  in Figure 7b dominates that of all other  $\text{CALTECH} \leftarrow X$  except  $X = \text{CALTECH}$ .

- (4) If we uniformly randomly sample a walk of  $k = 21$  nodes, we are more likely to obtain communities with 10 or more nodes in the induced subgraph for  $\text{CALTECH}$  than for  $\text{UCLA}$ ,  $\text{HARVARD}$ , and  $\text{MIT}$ .
- This observation manifests directly from the box plots in Figure 3 for community sizes in latent motifs and subgraphs that are induced by  $k$ -paths. We can also indirectly justify this observation. From the reconstruction accuracies for  $Y \leftarrow X$  in Figure 5b,c, where  $X$  is one of the four synthetic networks ( $\text{ER}_2$ ,  $\text{WS}_2$ ,  $\text{BA}_2$ , and  $\text{SBM}_2$ ), we observe that  $\text{WS}_2$  outperform both BA and ER networks in reconstructing  $\text{CALTECH}$ , but they are one of the lowest-performing networks for reconstructing the Facebook networks of the other three universities. In other words, the nonnegative linear combinations of the latent motifs of  $\text{WS}_2$  better approximate the mesoscale patches of  $\text{CALTECH}$  than the mesoscale patches of  $\text{UCLA}$ ,  $\text{HARVARD}$ , and  $\text{MIT}$ . Recall that most latent motifs of  $\text{WS}_2$  at scale  $k = 21$  have blocks of black entries of size  $10 \times 10$  or larger (see Figure 16); these correspond to adjacency matrices of communities with 10 or more nodes. It seems that this community structure is more likely to occur in subgraphs that are induced from uniformly random samples of  $k = 21$ -node walks in  $\text{CALTECH}$  than from such samples in  $\text{UCLA}$ ,  $\text{HARVARD}$ , or  $\text{MIT}$ .

6.6. **Figure 6.** In Figure 6, we compare the degree distributions (which we show as histograms) and the mean local clustering coefficients of the original and the reconstructed networks using  $r$  latent motifs at scale  $k = 21$ . We conduct this experiment for the five networks in Figure 5a. In panel a, we use the unweighted reconstructed networks for  $\text{CALTECH}$  with  $r \in \{9, 16, 25, 64\}$  latent motifs that we used to compute the self-reconstruction accuracy in 5b. In panels b–e, we use the unweighted reconstructed networks for  $\text{CORONAVIRUS}$ ,  $\text{H. SAPIENS}$ ,  $\text{SNAP FB}$ , and  $\text{ARXIV}$  with  $r = 25$  latent motifs that we used to compute the self-reconstruction accuracy in Figures 5b–e.

6.7. **Figure 7.** For each experiment  $Y \leftarrow X$  in Figures 7b–e, we plot

$$1 - \frac{\mathbb{E}_{\mathbf{x} \sim \pi} [\|A_{\mathbf{x}} - \hat{A}_{\mathbf{x};W}\|_1]}{2(k-1)}, \quad (14)$$

where  $k = 21$  and  $W$  is the network dictionary of  $r = 25$  latent motifs in network  $X$  that we determine using our NDL algorithm (see Algorithm NDL) for a  $k$ -chain motif with the corresponding network  $F = ([k], A_F)$  for  $T = 100$  iterations,  $N = 100$  injective homomorphisms per iteration, an  $L_1$ -regularizer with coefficient  $\lambda = 1$ , and the MCMC motif-sampling algorithm  $\text{MCMC} = \text{PivotApprox}$ . The distribution  $\pi$  is the stationary distribution  $\hat{\pi}_{F \hookrightarrow \mathcal{G}}$  (see (16)) of the MCMC injective motif-sampling algorithm (see Algorithm RM and Proposition 7.9). For each mesoscale patch  $A_{\mathbf{x}} \in \mathbb{R}^{k \times k}$ , we compute the linear approximation  $\hat{A}_{\mathbf{x};W}$  (see line 16 of Algorithm NDL). We approximate the expectation in the numerator of (14) using a Monte Carlo method. Specifically, from the convergence result in Proposition 7.3, we have

$$\mathbb{E}_{\mathbf{x} \sim \pi} [\|A_{\mathbf{x}} - \hat{A}_{\mathbf{x};W}\|_1] = \lim_{N \rightarrow \infty} \frac{1}{N} \sum_{t=1}^N \|A_{\mathbf{x}_t} - \hat{A}_{\mathbf{x}_t;W}\|_1, \quad (15)$$

where  $(\mathbf{x}_t)_{t \geq 0}$  is a sequence of injective homomorphisms  $F \hookrightarrow \mathcal{G}$  that we sample using the MCMC injective motif-sampling algorithm (see Algorithm RM). We use the finite sample mean  $\frac{1}{N} \sum_{t=1}^N \|A_{\mathbf{x}_t} - \hat{A}_{\mathbf{x}_t;W}\|_1$  with  $N = 10^4$  as a proxy of the expectation in the left-hand side of (15).

6.8. **Figure 8.** In Figure 8, we show histograms of various statistics of true and false edges when denoising the network **CALTECH** after corrupting it with 50% additive noise of type +ER.

We say that a  $k$ -walk  $\mathbf{x}_t$  ‘visits’ an edge between distinct nodes  $x$  and  $y$  if there exist indices  $a$  and  $b$  such that  $1 \leq a < b \leq k$  with  $\mathbf{x}_t(a) = x$  and  $\mathbf{x}_t(b) = y$ . We define the ‘distance’ between nodes  $x$  and  $y$  along the  $k$ -walk  $\mathbf{x}_t$  that visits the edge between them by the minimum value of  $|i - j|$ , where  $i$  and  $j$  are integers in  $\{1, \dots, k\}$  such that  $\mathbf{x}_t(i) = x$  and  $\mathbf{x}_t(j) = y$ . (See the illustration in panel **a**.) We then compute the mean of such distances between  $x$  and  $y$  for all  $t \in \{1, \dots, T\}$  such that  $\mathbf{x}_t$  visits the edge between  $x$  and  $y$ . In panel **g**, we show the histogram of the mean distances along the  $k$ -walks  $\mathbf{x}_1, \dots, \mathbf{x}_T$  between the two ends of true edges and the two ends of false edges.

We compute the  $r = 25$  latent motifs in panel **h** using NDL (see Algorithm **NDL**) with a  $k$ -chain motif  $F = ([k], A_F)$  for  $T = 100$  iterations,  $N = 100$  injective homomorphisms per iteration (so we sample a total  $10^4$  injective homomorphisms), an  $L_1$ -regularizer with coefficient  $\lambda = 1$ , and the MCMC injective motif-sampling algorithm **MCMC = PivotApprox**.

For our reconstructions of the corrupted network **CALTECH** in panels **b–f** using the corresponding latent motifs in panels **h–l**, respectively, we apply the NDR algorithm (see Algorithm **NDR**) to a  $k$ -chain motif  $F = ([k], A_F)$ , a scale  $k = 21$  for  $T = 2 \times 10^5$  iterations,  $N = 100$  homomorphisms per iteration,  $r = 25$  latent motifs, an  $L_1$ -regularizer with coefficient  $\lambda = 0$  (i.e., no regularization), the MCMC motif-sampling algorithm **MCMC = PivotApprox**, **InjHom = F**, and **denoising = F**.

6.9. **Figure 9.** To generate Figure 9, we first apply the NDL algorithm (see Algorithm **NDL**) to each corrupted network in the figure to learn  $r = 25$  latent motifs for a  $k$ -chain motif  $F = ([k], A_F)$ , a scale  $k = 21$  for  $T = 400$  iterations,  $N = 1,000$  homomorphisms per iteration, an  $L_1$ -regularizer with coefficient  $\lambda = 1$ , and the MCMC motif-sampling algorithm **MCMC = PivotApprox**. The NDR algorithm (see Algorithm **NDR**) that we use to generate the results in Figure 9 uses  $r \in \{2, 25\}$  latent motifs for a  $k$ -chain motif  $F = ([k], A_F)$ , a scale  $k = 21$  for  $T = 4 \times 10^5$  iterations for **H. SAPIENS** and  $T = 2 \times 10^5$  iterations for all other networks, an  $L_1$ -regularizer with coefficient  $\lambda = 1$ , the MCMC motif-sampling algorithm **MCMC = PivotApprox**, **InjHom = F**, and **denoising**  $\in \{\mathbf{T}, \mathbf{F}\}$ . For Figure 9, we do not conduct the denoising experiment for **CORONAVIRUS PPI** with  $-50\%$  noise because the resulting network (with 1,536 nodes and 1,232 edges) cannot be connected. (To be connected, its spanning trees need to have 1,535 edges.)

We implement several existing network-denoising methods — the **JACCARD INDEX**, **PREFERENTIAL ATTACHMENT**, the **ADAMIC–ADAR INDEX**, **SPECTRAL EMBEDDING**, **DEEPWALK**, and **NODE2VEC** — and compare the performance of our method to those of these existing approaches on the same problem settings. Let  $\mathcal{G} = (V, A)$  be an original network and let  $\mathcal{G}' = (V, A)$  be the associated corrupted network; for our experiment in Figure 9, they are both undirected and unweighted. In all cases, we obtain a network  $\hat{\mathcal{G}} = (V, \hat{A})$  from  $\mathcal{G}' = (V, A)$  without using  $\mathcal{G}$ . For each  $x, y \in V$ , we compute the ‘confidence score’  $\hat{A}(x, y)$  that the node pair  $(x, y)$  is an edge  $\{x, y\}$  in the original network  $\mathcal{G}$ . Let  $N(x)$  denote the set of neighbors of node  $x$  in  $\mathcal{G}'$ .

For the **JACCARD INDEX**, **PREFERENTIAL ATTACHMENT**, and the **ADAMIC–ADAR INDEX**, we compute the confidence score  $\hat{A}(x, y)$  by calculating  $|N(x) \cap N(y)| / |N(x) \cup N(y)|$ ,  $|N(x)| \cdot |N(y)|$ , and  $\sum_{z \in N(x) \cap N(y)} 1 / \log |N(z)|$ , respectively. For **SPECTRAL EMBEDDING**, **DEEPWALK**, and **NODE2VEC**, we first obtain a 128-dimensional vector representation of the nodes of a network; this is a so-called ‘node embedding’ of the network. We then use this node embedding to obtain vector representations of the edges using binary operations. (We use the Hadamard product; see [32] for details.) We then use logistic regression (but one can alternatively employ some other algorithm for binary classification) to attempt to detect the false edges. **SPECTRAL CLUSTERING** uses the top 128 eigenvectors of the combinatorial Laplacian matrix of  $\mathcal{G}'$  (which we

calculate by subtracting the adjacency matrix from the diagonal matrix of node degrees) to learn vector embeddings of the nodes. (See [63] for details.) DEEPWALK and NODE2VEC first sample sequences of random walks on  $\mathcal{G}'$  and then apply the popular word-embedding algorithm WORD2VEC [68]. In DEEPWALK, each random walk is a standard random walk on the network  $\mathcal{G}'$ . For NODE2VEC, we use the 16 choices of the return parameter  $p$  and the in-out parameter  $q$  from  $\{0.25, 0.5, 1, 2\}^2$ . In addition to the random walk-sampling in these two methods, we use the following common choices (these same choices were made in [32]) for both methods: using each node of  $\mathcal{G}'$  as a starting point, we independently sample 10 random walks of 80 steps; a context window size of 10; 1 stochastic gradient epoch; and 8 workers. See [32] for details.

For all approaches, we first split the data into a 25/25/50 split of training/validation/test sets. We then construct the network  $\hat{\mathcal{G}} = (V, \hat{A})$ . By varying the threshold parameter  $\theta$ , we construct a receiver-operating characteristic (ROC) curve that consists of points whose horizontal and vertical coordinates are the false-positive rates and true-positive rates, respectively. For denoising the noise of type  $-ER$  (respectively,  $+ER$  or  $+WS$ ), we also infer an optimal value of  $\theta$  for a 25% validation set of non-edges (respectively, edges) in  $\mathcal{G}'$  with known labels and then use that value of  $\theta$  to compute classification measures (such as accuracy and precision) for the test set.

**6.10. Figure 10.** In Figure 10, we illustrate cross-reconstruction experiments for images using mesoscale patches of size  $21 \times 21$ . The image that we seek to reconstruct is **WOMAN WITH A PARASOL - MADAME MONET AND HER SON** (Claude Monet, 1875), which we show in panel **a**. The image in panel **b** is a reconstruction of the image in panel **a** using the dictionary with 25 basis images of size  $21 \times 21$  pixels in panel **c**, where we choose the color of each pixel uniformly at random from all possible colors (which we represent as vectors in  $[0, 256]^3$  for red-green-blue (RGB) weights). The image in panel **d** is a reconstruction of the image in panel **a** using the dictionary with 25 basis images of size  $21 \times 21$  pixels in panel **e**. We learn this basis from the image in panel **f** using NMF [6]. The image in panel **f** is from the collection **DIE GRAPHIK ERNST LUDWIG KIRCHNERS BIS 1924, VON GUSTAV SCHIEFLER BAND I BIS 1916** (Accession Number 2007.141.9, Ernst Ludwig Kirchner, 1926). We use the images in **a** and **f** with permission from the National Gallery of Art in Washington, DC, USA. Their open-access policy is available at <https://www.nga.gov/notices/open-access-policy.html>.

**6.11. Figure 11.** In Figure 11, we compare  $10^4$  subgraphs (we show 33 of them) that are induced by approximately uniformly random (a)  $k$ -paths and (in panel **b**)  $k$ -walks for the network **CORONAVIRUS PPI** with  $k = 10$ . To sample  $k$ -walks, we use an MCMC  $k$ -chain motif-sampling algorithm (see Algorithm **MP** with **AcceptProb = Approximate**). To sample  $k$ -paths, we use the MCMC injective motif-sampling algorithm (see Algorithm **RM**).

To obtain the latent motifs in Figure 11c, we use the NDL Algorithm (see Algorithm **NDL**) with **MCMC = PivotApprox**. To obtain the latent motifs in Figure 11 bottom, we instead use the NDL algorithm from Lyu et al. [45]. This algorithm is equivalent to our NDL algorithm (see Algorithm **NDL**) if we use all homomorphisms from the  $k$ -chain motif  $F$  to the network  $\mathcal{G}$ , rather than only the injective ones as in Algorithm **NDL**. For the experiments in Figures 11c,d, we use a chain motif  $F = ([k], A_F)$  with  $T = 100$  iterations,  $N = 100$  injective homomorphisms per iteration (so we sample a total of  $10^4$  injective homomorphisms), and an  $L_1$ -regularizer with coefficient  $\lambda = 1$ .

**6.12. Figure 12.** This figure illustrates the key ideas of the NDL algorithm (see Algorithm **NDL**).

**6.13. Figure 13.** This figure shows the accuracy, precision, and recall scores of the network denoising-experiments in Figure 9. See Section 6.9 for details.

6.14. **Figures 14, 15, 16, 17, 18, 19, 20, and 21.** These figures show latent motifs of the examined networks (which we described in the Methods section of the main manuscript) using Algorithm **NDL** with various parameter choices. For each network, we use a  $k$ -chain motif  $F = ([k], A_F)$  for  $T = 100$  iterations,  $N = 100$  injective homomorphisms per iteration (so we sample a total  $10^4$  injective homomorphisms), an  $L_1$ -regularizer with coefficient  $\lambda = 1$ , and the MCMC injective motif-sampling algorithm **MCMC = PivotApprox**. We specify the number  $r$  of latent motifs and the scale  $k$  in the caption of each figure.

## 7. CONVERGENCE ANALYSIS

In this section, we give rigorous convergence guarantees for our main algorithms for NDL (see Theorems 7.4 and 7.7) and NDR (see Theorems 7.10 and 7.14). All of these results are novel. The recent paper by Lyu et al. [45] proposed a network-reconstruction algorithm that corresponds to our NDR algorithm **NDR** with the choice **denoising = InjHom = F**. Lyu et al. [45] did not do any theoretical analysis of this network-reconstruction algorithm. Our most significant theoretical contribution is our guarantees about the NDR algorithm (see Algorithm **NDR**). Specifically, in Theorems 7.10 and 7.14, we establish convergence, exact formulas, and error bounds of the reconstructed networks for all four choices  $(\text{denoising}, \text{InjHom}) \in \{\mathbf{T}, \mathbf{F}\}^2$  for both non-bipartite and bipartite networks. The most interesting part of these results is our bound for the global Jaccard reconstruction error in terms of the mesoscale approximation error divided by the number of nodes in the subgraphs at that mesoscale (see Theorem 7.10(iii)). Roughly speaking, this result guarantees that one can accurately reconstruct a network if one has a dictionary of latent motifs that can accurately approximate the subgraphs in the network at a fixed mesoscale. We illustrate this result with supporting experiments in Figure 7 in the main manuscript. A crucial feature of our proof of Theorem 7.10(iii) is its use of an explicit formula for the limiting reconstructed network as the number of iterations that we use for network reconstruction tends to infinity.

In [45, Corollary 6.1], Lyu et al. presented a convergence guarantee for the original NDL algorithm in [45] for non-bipartite networks  $\mathcal{G}$ . The key difference between our NDL algorithm (see Algorithm **NDL**) and the NDL algorithm in [45] is that we employ  $k$ -path motif sampling but they employ  $k$ -walk motif sampling. This results in different objective functions to minimize (see (6) for our objective function). Therefore, [45, Corollary 6.1] does not apply to our NDL algorithm (see Algorithm **NDL**). In Theorem 7.4, we establish a convergence result for our NDL algorithm. A key step in the proof of this result is the guaranteeing convergence of the MCMC injective motif-sampling algorithm (see Algorithm **RM**) for non-bipartite networks (see Proposition 7.3). In Theorem 7.7, we extend the convergence results for our NDL algorithm to bipartite networks, which was not established in [45] even for the original NDL algorithm. The key technical difficulty for bipartite networks is that Markov chains that are generated by the MCMC motif-sampling algorithms are not irreducible, so the main convergence results for online NMF in [45, Thm. 1] are not applicable. Our proof of Theorem 7.7 uses a careful coupling argument between two reducible classes of Markov chains.

Let  $F = ([k], A_F)$  be a  $k$ -chain motif, and let  $G = (V, A)$  be a network. Let  $\Omega \subseteq V^{[k]}$  denote the set of all homomorphisms (which do not have to be injective)  $\mathbf{x} : F \rightarrow \mathcal{G}$ . Algorithm **NDL** generates three stochastic sequences. The first one is the sequence  $(\mathbf{x}_t)_{t \geq 0}$  of injective homomorphisms  $F \hookrightarrow \mathcal{G}$  that we obtain from the injective motif-sampling algorithm (see Algorithm **A3**). The second one is the sequence  $(X_t)_{t \geq 0}$  of  $k^2 \times N$  data matrices whose columns encode  $N$  mesoscale patches of  $\mathcal{G}$ . More precisely, for each  $\mathbf{y}_1, \dots, \mathbf{y}_n \in \Omega$ , we write  $\Psi(\mathbf{y}_1, \dots, \mathbf{y}_n) \in \mathbb{R}_{\geq 0}^{k^2 \times N}$  for the  $k^2 \times N$  matrix whose  $i^{\text{th}}$  column is the vectorization (using Algorithm **A4**) of the corresponding

$k \times k$  mesoscale patch  $A_{\mathbf{y}_i}$  of  $\mathcal{G}$  (see (4)). For each  $\mathbf{y}_0 \in \Omega$ , define

$$X^{(N)}(\mathbf{y}_0) := \Psi(\mathbf{y}_1, \dots, \mathbf{y}_N) \in \mathbb{R}_{\geq 0}^{k^2 \times N},$$

where we generate  $\mathbf{y}_1, \dots, \mathbf{y}_N$  iteratively using the injective motif-sampling algorithm (see Algorithm **RM**), which we initialize with the homomorphism  $\mathbf{y}_0 : F \rightarrow \mathcal{G}$ . It then follows that  $X_t = X^{(N)}(\mathbf{x}_{Nt})$  for each  $t \geq 1$ , where  $\mathbf{x}_{Nt}$  is the injective homomorphism  $F \hookrightarrow \mathcal{G}$  that we obtain after  $Nt$  applications of Algorithm **RM**. For the third (and final) sequence that we generate using Algorithm **NDL**, let  $(W_t)_{t \geq 0}$  denote the sequence of dictionary matrices, where we define each  $W_t = W_t(\mathbf{x}_0)$  via (12) with an initial homomorphism  $\mathbf{x}_0 : F \rightarrow \mathcal{G}$  that we sample using Algorithm **A3**.

**7.1. Convergence of the MCMC algorithms.** In this subsection, we establish the convergence properties of the MCMC algorithms (see Algorithms **MP** and **MG**) for sampling a  $k$ -walk according to the target distribution  $\pi_{F \rightarrow \mathcal{G}}$  (see (1)). Recall that this distribution is the uniform distribution on the set of all homomorphisms  $F \rightarrow \mathcal{G}$  when the motif  $F$  and the network  $\mathcal{G}$  are both symmetric and unweighted (see (3)).

**Proposition 7.1.** *Fix a network  $\mathcal{G} = (V, A)$  and a  $k$ -chain motif  $F = ([k], A_F)$ . Let  $(\mathbf{x}_t)_{t \geq 0}$  denote a sequence of homomorphisms  $\mathbf{x}_t : F \rightarrow \mathcal{G}$  that we generate using the exact pivot chain (in which we use Algorithm **MP** with **AcceptProb** = **Exact**) or the Glauber chain (in which we use Algorithm **MG**). Suppose that*

- (a) *The weight matrix  $A$  is ‘bidirectional’ (i.e.,  $A(x, y) > 0$  implies that  $A(y, x) > 0$  for all  $x, y \in V$ ) and that the undirected and unweighted graph  $(V, \mathbb{1}(A > 0))$  is connected and non-bipartite.*

*It then follows that  $(\mathbf{x}_t)_{t \geq 0}$  is an irreducible and aperiodic Markov chain with the unique stationary distribution  $\pi_{F \rightarrow \mathcal{G}}$  that we defined in (1).*

*Proof.* This proposition was proved rigorously in [40, Thms. 5.7 and 5.8]. In the present paper, we sketch the proof for the exact pivot chain to illustrate the main idea behind the acceptance probability in (8). The trajectory of the first node  $\mathbf{x}_t(1)$  of the homomorphism  $\mathbf{x}$  gives a standard random walk on the network  $\mathcal{G}$  that is modified by the Metropolis–Hastings algorithm (see, e.g., [69, Sec. 3.2]) so that it has the following marginal distribution as its unique stationary distribution:

$$\pi^{(1)}(x_1) = \frac{\sum_{x_2, \dots, x_k \in [n]} \prod_{i=2}^k A(x_{i-1}, x_i)}{\mathbf{Z}},$$

where the denominator  $\mathbf{Z} = \mathbf{Z}(F, \mathcal{G})$  is the normalization constant that we call the ‘homomorphism density’ of  $F$  in  $\mathcal{G}$  (see [65]) and the numerator is proportional to the probability of sampling  $x_2, \dots, x_k \in [n]$  for  $\mathbf{x}_t(2), \dots, \mathbf{x}_t(k)$ . Fix a homomorphism  $\mathbf{x} : F \rightarrow \mathcal{G}$  with  $\mathbf{x}(i) = x_i$  for  $i = 1, \dots, k$ . We then obtain

$$\begin{aligned} \mathbb{P}(\mathbf{x}_t(1) = x_1, \dots, \mathbf{x}_t(k) = x_k) &= \mathbb{P}(\mathbf{x}_t(1) = x_1) \mathbb{P}(\mathbf{x}_t(2) = x_2, \dots, \mathbf{x}_t(k) = x_k \mid \mathbf{x}_t(1) = x_1) \\ &\approx \pi^{(1)}(x_1) \frac{\prod_{i=2}^k A(x_{i-1}, x_i)}{\sum_{y_2, \dots, y_k \in [n]} \prod_{i=2}^k A(y_{i-1}, y_i)} \\ &= \frac{\prod_{i=2}^k A(x_{i-1}, x_i)}{\mathbf{Z}} = \pi_{F \rightarrow \mathcal{G}}(\mathbf{x}), \end{aligned}$$

where the approximation in the second line above becomes exact as  $t \rightarrow \infty$ .  $\square$

We now prove Proposition **7.2**, which guarantees the convergence of the approximate pivot chain and gives an explicit formula for its unique stationary distribution.

**Proposition 7.2.** Fix a network  $\mathcal{G} = (V, A)$  and a  $k$ -chain motif  $F = ([k], A_F)$ . Let  $(\mathbf{x}_t)_{t \geq 0}$  denote a sequence of homomorphisms  $\mathbf{x}_t : F \rightarrow \mathcal{G}$  that we generate using the approximate pivot chain (in which we use Algorithm **MP** with **AcceptProb** = **Approximate**). Suppose that

- (a) The weight matrix  $A$  is bidirectional (i.e.,  $A(x, y) > 0$  implies that  $A(y, x) > 0$  for all  $x, y \in V$ ) and that the undirected and unweighted graph  $(V, \mathbb{1}(A > 0))$  is connected and non-bipartite.

It then follows that  $(\mathbf{x}_t)_{t \geq 0}$  is an irreducible and aperiodic Markov chain with the unique stationary distribution  $\hat{\pi}_{F \rightarrow \mathcal{G}}$  that we defined in (11).

*Proof.* We follow the proof of [40, Thm. 5.8]. Let  $P : V^2 \rightarrow [0, 1]$  be a matrix with entries

$$P(x, y) := \frac{A(x, y)}{\sum_{c \in V} A(a, c)}, \quad x, y \in V.$$

The matrix  $P$  is the transition matrix of the standard random walk on the network  $\mathcal{G}$ . By hypothesis (a),  $P$  is irreducible and aperiodic. Using a result in [69, Ch. 9], we know that it has the unique stationary distribution

$$\pi^{(1)}(v) := \sum_{c \in V} A(v, c) / \sum_{c, c' \in V} A(c, c').$$

The approximate pivot chain generates a move  $\mathbf{x}_t(1) \mapsto \mathbf{x}_{t+1}(1)$  of the pivot according to the distribution  $P(\mathbf{x}_t(1), \cdot)$ . We accept this move independently of everything else with the approximate acceptance probability  $\alpha$  in (8). If we always accept each move of the pivot, then the pivot performs a random walk on  $\mathcal{G}$  with the unique stationary distribution  $\pi^{(1)}$ . We compute the acceptance probability  $\alpha$  using the Metropolis–Hastings algorithm (see [69, Sec. 3.3]), and we thereby modify the stationary distribution of the pivot from  $\pi^{(1)}$  to the uniform distribution on  $V$ . (See the discussion in [40, Sec. 5].) Therefore,  $(\mathbf{x}_t(1))_{t \geq 0}$  is an irreducible and aperiodic Markov chain on  $V$  that has the uniform distribution as its unique stationary distribution. Because we sample the locations  $\mathbf{x}_{t+1}(i) \in V$  of the subsequent nodes  $i = 2, 3, \dots, k$  independently, conditional on the location  $\mathbf{x}_{t+1}(1)$  of the pivot, it follows that the approximate pivot chain  $(\mathbf{x}_t)_{t \geq 0}$  is also an irreducible and aperiodic Markov chain with a unique stationary distribution, which we denote by  $\hat{\pi}_{F \rightarrow \mathcal{G}}$ .

To determine the stationary distribution  $\hat{\pi}_{F \rightarrow \mathcal{G}}$ , we decompose  $\mathbf{x}_t$  into return times of the pivot  $\mathbf{x}_t(1)$  to a fixed node  $x_1 \in V$  in  $\mathcal{G}$ . Specifically, let  $\tau(j)$  be the  $j^{\text{th}}$  return time of  $\mathbf{x}_t(1)$  to  $x_1$ . By the independence of sampling  $\mathbf{x}_t$  over  $\{2, \dots, k\}$  for each  $t$ , the strong law of large numbers yields

$$\begin{aligned} \lim_{M \rightarrow \infty} \frac{1}{M} \sum_{j=1}^M \mathbb{1}(\mathbf{x}_{\tau(j)}(2) = x_2, \dots, \mathbf{x}_{\tau(j)}(k) = x_k) \\ = \frac{\prod_{i=2}^k A(x_{i-1}, x_i)}{\sum_{y_2, \dots, y_k \in V} \prod_{i=2}^k A(x_1, y_2) A(y_2, y_3) \dots A(y_{k-1}, y_k)}. \end{aligned}$$

For each fixed homomorphism  $\mathbf{x} : F \rightarrow \mathcal{G}$ , which maps  $i \mapsto x_i$ , we use the Markov-chain ergodic theorem (see, e.g., [62, Theorem 6.2.1 and Example 6.2.4] or [66, Theorem 17.1.7]) to obtain

$$\begin{aligned} \hat{\pi}_{F \rightarrow \mathcal{G}}(\mathbf{x}) &= \lim_{N \rightarrow \infty} \frac{1}{N} \sum_{t=0}^N \mathbb{1}(\mathbf{x}_t = \mathbf{x}) \\ &= \lim_{N \rightarrow \infty} \frac{\sum_{t=0}^N \mathbb{1}(\mathbf{x}_t = \mathbf{x})}{\sum_{t=0}^N \mathbb{1}(\mathbf{x}_t(1) = x_1)} \frac{\sum_{t=0}^N \mathbb{1}(\mathbf{x}_t(1) = x_1)}{N} \end{aligned}$$



$$\begin{aligned}
&= \mathbb{P} \left( \mathbf{x}_t(2) = x_2, \dots, \mathbf{x}_t(k) = x_k \mid \mathbf{x}_t(1) = x_1 \right) \pi^{(1)}(x_1) \\
&= \frac{\prod_{i=1}^k A(x_{i-1}, x_i)}{\sum_{y_2, \dots, y_k \in V} \prod_{i=2}^k A(x_1, y_2) A(y_2, y_3) \cdots A(y_{k-1}, y_k)} \frac{1}{|V|}.
\end{aligned}$$

This proves the assertion.  $\square$

Finally, we establish the following asymptotic convergence result for the injective motif-sampling algorithm in Algorithm [RM](#).

**Proposition 7.3** (Convergence of injective motif sampling). *Fix a network  $\mathcal{G} = (V, A)$  and a  $k$ -chain motif  $F = ([k], A_F)$ . Suppose that  $\mathcal{G}$  has at least one  $k$ -path. Let  $(\mathbf{x}_t)_{t \geq 0}$  denote a sequence of injective homomorphisms  $\mathbf{x}_t : F \hookrightarrow \mathcal{G}$  that we generate using Algorithm [RM](#). Suppose that*

- (a) *The weight matrix  $A$  is bidirectional (i.e.,  $A(x, y) > 0$  implies that  $A(y, x) > 0$  for all  $x, y \in V$ ) and that the undirected and unweighted graph  $(V, \mathbb{1}(A > 0))$  is connected and non-bipartite.*
- (i) *If we use Algorithm [MG](#) or Algorithm [MP](#) with `AcceptProb = Exact` in Algorithm [RM](#), then  $(\mathbf{x}_t)_{t \geq 0}$  is an irreducible and aperiodic Markov chain with the unique stationary distribution  $\pi_{F \hookrightarrow \mathcal{G}}$  that we defined in [\(2\)](#).*
- (ii) *If we use Algorithm [MP](#) with `AcceptProb = Approximate` in Algorithm [RM](#), then  $(\mathbf{x}_t)_{t \geq 0}$  is an irreducible and aperiodic Markov chain with the unique stationary distribution  $\hat{\pi}_{F \hookrightarrow \mathcal{G}}$ , which is defined by*

$$\hat{\pi}_{F \hookrightarrow \mathcal{G}}(\mathbf{x}) = C' \hat{\pi}_{F \hookrightarrow \mathcal{G}}(\mathbf{x}) \mathbb{1}(\mathbf{x}(1), \dots, \mathbf{x}(k) \text{ are distinct}), \quad (16)$$

where  $\hat{\pi}_{F \hookrightarrow \mathcal{G}}$  is the probability distribution on the set of homomorphisms  $F \rightarrow \mathcal{G}$  in [\(11\)](#).

*Proof.* This assertion follows from standard Markov-chain theory (see, e.g., [\[69\]](#)) in conjunction with Propositions [7.1](#) and [7.2](#).  $\square$

**7.2. Convergence of the NDL algorithm.** Recall the problem statement for NDL in [\(6\)](#). Informally, we seek to learn  $r$  latent motifs  $\mathcal{L}_1, \dots, \mathcal{L}_r \in \mathbb{R}_{\geq 0}^{k \times k}$  to minimize the expectation of the error of approximating the mesoscale patch  $A_{\mathbf{x}}$  by a nonnegative combination of the motifs  $\mathcal{L}_i$ , where  $\mathbf{x} : F \hookrightarrow \mathcal{G}$  is a random injective homomorphism that we sample from the distribution  $\pi_{F \hookrightarrow \mathcal{G}}$  [\(2\)](#). We reformulate this problem as the following matrix-factorization problem, which generalizes [\(6\)](#). Let  $\mathcal{C}^{\text{dict}}$  denote the set of all matrices  $W \in \mathbb{R}_{\geq 0}^{k^2 \times r}$  whose columns have a Frobenius norm of at most 1. The matrix-factorization problem is then

$$\arg \min_{W \in \mathcal{C}^{\text{dict}} \subseteq \mathbb{R}_{\geq 0}^{k^2 \times r}} \left( f(W) := \mathbb{E}_{\mathbf{x} \sim \pi_{F \hookrightarrow \mathcal{G}}} \left[ \ell(X^{(N)}(\mathbf{x}), W) \right] \right), \quad (17)$$

where we define the loss function

$$\ell(X, W) := \inf_{H \in \mathbb{R}_{\geq 0}^{r \times N}} \|X - WH\|_F^2 + \lambda \|H\|_1, \quad X \in \mathbb{R}^{k^2 \times N}, W \in \mathbb{R}^{k^2 \times r}. \quad (18)$$

The parameters  $N \in \mathbb{N}$  and  $\lambda \geq 0$  appear in Algorithm [NDL](#). The former is the number of homomorphisms that we sample at each iteration of Algorithm [NDL](#), and the latter is the coefficient of an  $L_1$ -regularizer that we use to find the code matrix  $H_t$  in [\(12\)](#). If  $N = 1$  and  $\lambda = 0$ , then the problem [\(17\)](#) is equivalent to the problem [\(6\)](#) because  $X^{(1)}(\mathbf{x})$  and the columns of  $W$  are vectorizations (using Algorithm [A4](#)) of the mesoscale patch  $A_{\mathbf{x}}$  and the latent motifs  $\mathcal{L}_1, \dots, \mathcal{L}_r$ , respectively.

The objective function  $f$  in the optimization problem (17) for NDL is non-convex, so it is generally difficult to find a global optimum of  $f$ . However, local optima are often good enough for practical applications (such as in image restoration [10, 51]). We find that this is also the case for our network-denoising problem (see Figure 9). Theorems 7.4 and 7.7 guarantee that our NDL algorithm (see Algorithm NDL) finds a sequence  $(W_t)_{t \geq 0}$  of dictionary matrices such that almost surely  $W_t$  is asymptotically a local optimum of the objective function  $f$ .

To make precise statements about asymptotic convergence of the NDL algorithm to a local optimum of the objective function in (6), we use some notation for measures of local optimality for non-convex constrained optimization problems. Suppose that we have a differentiable objective function  $g : \mathbb{R}^p \rightarrow \mathbb{R}$  for some integer  $p \geq 1$ . Fix a parameter set  $\Theta \subseteq \mathbb{R}^p$ . We say that  $\mathbf{v}^* \in \Theta$  is a *stationary point* of  $g$  in  $\Theta$  if

$$\inf_{\mathbf{v} \in \Theta} \langle \nabla g(\mathbf{v}^*), \mathbf{v} - \mathbf{v}^* \rangle \geq 0,$$

where  $\langle \cdot, \cdot \rangle$  denotes the dot product on  $\mathbb{R}^p$ . If  $\mathbf{v}^*$  is a stationary point of  $g$  in  $\Theta$  and if it is in the interior of  $\Theta$ , then  $\|\nabla g(\mathbf{v}^*)\| = 0$ .

We are now ready to state the convergence result for our NDL algorithm (see Algorithm NDL) for non-bipartite networks.

**Theorem 7.4** (Convergence of the NDL Algorithm for Non-Bipartite Networks). *Let  $F = ([k], A_F)$  be a  $k$ -chain motif, and let  $G = (V, A)$  be a network that satisfies the following properties:*

- (a) *The weight matrix  $A$  is bidirectional (i.e.,  $A(x, y) > 0$  implies that  $A(y, x) > 0$  for all  $x, y \in V$ ) and the undirected and unweighted graph  $(V, \mathbb{1}(A > 0))$  is connected and non-bipartite.*
- (b) *For all  $t \geq 0$ , there exists a unique solution  $H_t$  in (12).*
- (c) *For all  $t \geq 0$ , the eigenvalues of the positive semidefinite matrix  $A_t$  that is defined in (12) are at least as large as some constant  $\kappa_1 > 0$ .*

*Let  $(W_t)_{t \geq 0}$  denote the sequence of dictionary matrices that we generate using Algorithm NDL. The following statements hold:*

- (i) *For  $\text{MCMC} \in \{\text{Pivot}, \text{Glauber}\}$ , we have almost surely as  $t \rightarrow \infty$  that  $W_t$  converges to the set of stationary points of the objective function  $f$  that we defined in (17). Furthermore, if  $f$  has finitely many stationary points in  $\mathcal{C}^{\text{dict}}$ , we then have that  $W_t$  converges to a single stationary point of  $f$  almost surely as  $t \rightarrow \infty$ .*
- (ii) *For  $\text{MCMC} = \text{PivotApprox}$ , we have almost surely as  $t \rightarrow \infty$  that  $W_t$  converges to the set of stationary points of the objective function*

$$\hat{f}(W) := \mathbb{E}_{\mathbf{x} \sim \hat{\pi}_{F \rightarrow G}} \left[ \ell(X^{(N)}(\mathbf{x}), W) \right],$$

*where the distribution  $\hat{\pi}_{F \rightarrow G}$  was defined in (16). Furthermore, if  $\hat{f}$  has finitely many stationary points in  $\mathcal{C}^{\text{dict}}$ , it follows that  $W_t$  converges to a single stationary point of  $\hat{f}$  almost surely as  $t \rightarrow \infty$ .*

**Remark 7.5.** Assumptions (a)–(c) in Theorem 7.4 are all reasonable and are easy to satisfy. Assumption (a) is satisfied if  $\mathcal{G}$  is undirected, unweighted, and connected, which is the case for all of the networks that we study in the present paper. Assumptions (b) and (c) are standard assumptions in the study of online dictionary learning [53, 67, 45]. For instance, (b) is a common assumption in methods such as layer-wise adaptive-rate scaling (LARS) [56] that aim to find good solutions to problems of the form (18). See [53, Sec. 4.1] and [45, Sec. 4.1] for more detailed discussions of these assumptions.

**Remark 7.6.** It is also possible to slightly modify both the optimization problem (17) and our NDL algorithm so that Theorem 7.4 holds for the modified problem and the algorithm without needing to assume (b) and (c). The modified problem is

$$\arg \min_{W \in \mathcal{C}^{\text{dict}} \subseteq \mathbb{R}_{\geq 0}^{k^2 \times r}} \left( \mathbb{E}_{\mathbf{x} \sim \pi} \left[ \inf_{H \in \mathbb{R}_{\geq 0}^{r \times N}} \|X - WH\|_F^2 + \lambda \|H\|_1 + \kappa' \|H\|_F^2 + \lambda' \|W\|_F^2 \right] \right), \quad (19)$$

where  $\pi = \hat{\pi}_{F \rightarrow \mathcal{G}}$  if  $\text{MCMC} = \text{PivotApprox}$  and  $\pi = \pi_{F \rightarrow \mathcal{G}}$  otherwise. Note that (19) is the same as (17) with additional quadratic penalization terms for both  $H$  and  $W$  in the loss function  $\ell$  (18). By contrast, consider the modification of the NDL algorithm (see Algorithm NDL) in which the objective function for  $H_t$  in (12) has the additional term  $\kappa' \|H\|_F^2$  and we replace  $P_t$  in (12) by  $P_t + \kappa' I$ . When  $\lambda' > 0$  and  $\kappa' > 0$ , the modified objective function for  $H_t$  is strictly convex, so  $H_t$  is unique. Therefore,  $H_t$  satisfies the uniqueness condition (b) in Theorem 7.4. Additionally, the smallest eigenvalue of each matrix  $P_t$  that we compute using the modified NDL algorithm has a lower bound of  $\kappa_1$  for all  $t$ , so it satisfies condition (c) in Theorem 7.4. One can then show that all parts of Theorem 7.4 for the modified problem (19) and the modified NDL algorithm hold without assumptions (b) and (c). The argument, which we omit, is almost identical to the one for Theorem 7.4.

**Proof of Theorem 7.4.** The proof of the first part of (i) is almost identical to the proof of [45, Corollary 6.1]. Because we use additional rejection sampling in Algorithm RM in conjunction to the pivot and the Glauber chains, we need to ensure that the following statements hold. First, we need the sequence of injective homomorphisms  $(\mathbf{x}_t)_{t \geq 0}$  that we sample using Algorithm RM to be an irreducible and aperiodic Markov chain on the set of injective homomorphisms  $F \hookrightarrow \mathcal{G}$ . Second, we need  $(\mathbf{x}_t)_{t \geq 0}$  to have a unique stationary distribution that coincides with  $\pi_{F \rightarrow \mathcal{G}}$  (see (2)). We prove both statements in Proposition 7.3.

To prove the first part of (ii), we can use the same essential argument as in the proof of [45, Corollary 6.1]. However, because our assertion is for the approximate pivot chain from the present article (see Algorithm MP with  $\text{AcceptProb} = \text{Approximate}$ ), we need to use Proposition 7.2 (instead of [40, Prop. 5.8]) to establish irreducibility and convergence of the associated Markov chain. The proofs of the second parts of both (i) and (ii) are identical for exact and approximate pivot chains.

We give a detailed proof of (ii). Let  $\pi = \hat{\pi}_{F \rightarrow \mathcal{G}}$  if  $\text{MCMC} = \text{PivotApprox}$  and  $\pi = \pi_{F \rightarrow \mathcal{G}}$  for  $\text{MCMC} \in \{\text{Pivot}, \text{Glauber}\}$  (see (1) and (11)). We define  $(\mathbf{x}_t)_{t \geq 0}$ ,  $(X_t)_{t \geq 1}$ , and  $(W_t)_{t \geq 0}$  as before. We use a general convergence result for online NMF for Markovian data [45, Theorem 4.1].

Observe that the matrices  $X_t \in \mathbb{R}_{\geq 0}^{k^2 \times N}$  that we compute in line 15 of Algorithm NDL do not necessarily form a Markov chain, because the forward evolution of the Markov chain depends both on the induced mesoscale patches and on the actual homomorphisms  $(\mathbf{x}_s)_{N(t-1) < s \leq Nt}$ . However, if one considers the sequence  $\bar{X}_t := (X_t, \mathbf{x}_{Nt})$ , then  $\bar{X}_t$  forms a Markov chain. Specifically, the distribution of  $X_{t+1}$  given  $X_t$  depends only on  $\mathbf{x}_{Nt}$  and  $A$ . Indeed,  $\mathbf{x}_{Nt}$  and  $A$  determine the distribution of the homomorphisms  $(\mathbf{x}_s)_{Nt < s \leq N(t+1)}$ , which in turn determine the  $k^2 \times N$  matrix  $X_{t+1}$ .

With assumption (a), [40, Theorems 5.7 and 5.8] and Proposition 7.3 imply that the Markov chain  $(\mathbf{x}_t)_{t \geq 0}$  of injective homomorphisms  $F \hookrightarrow \mathcal{G}$  is a finite-state Markov chain that is irreducible and aperiodic with a unique stationary distribution  $\pi$  (see (2)). This implies that the  $N$ -tuple of homomorphisms  $(\mathbf{x}_s)_{N(t-1) < s \leq Nt}$  also yields a finite-state, irreducible, and aperiodic chain with a unique stationary distribution. Consequently, the Markov chain  $(\bar{X}_t)_{t \geq 0}$  that we defined above is also a finite-state, irreducible, and aperiodic chain with a unique stationary distribution. In this setting, one can regard Algorithm NDL as the online NMF algorithm in [45] for the input

sequence  $X_t = \varphi(\overline{X}_t)$ , with  $t \geq 1$ , where  $\varphi(X, \mathbf{x}) = X$  is the projection onto the first coordinate. Because  $\overline{X}_t$  takes only finitely-many values, the range of  $\varphi$  is bounded. This verifies all hypotheses of [45, Theorem 4.1], so the first part of **(ii)** follows.

Now suppose that there are finitely many stationary points  $W_1^*, \dots, W_m^*$  of  $\hat{f}$  in  $\mathcal{C}^{\text{dict}}$ . Because  $\|W_{t-1} - W_t\|_F = O(1/t)$  (see [45, Prop. 7.5]), the first part of **(ii)** (which we proved above) implies that  $W_t$  converges to  $W_i^*$  for some unique index  $i \in \{1, \dots, m\}$  almost surely.  $\square$

Our second convergence result for the NDL algorithm is similar to Theorem 7.4, but it concerns the case in which the network  $\mathcal{G}$  is bipartite. Suppose that  $\mathcal{G}$  is bipartite and that  $F$  is a  $k$ -chain motif. Let  $V_1 \cup V_2 = V$  be a bipartition of  $\mathcal{G}$ . Let  $\Omega_0$  denote the set of injective homomorphisms  $F \hookrightarrow \mathcal{G}$ . We can define a subset  $\Omega_1 \subseteq \Omega_0$  of injective homomorphisms  $F \hookrightarrow \mathcal{G}$  by  $\mathbf{x} \in \Omega_1$  if and only if  $\mathbf{x}(1) \in V_1$ . Let  $\Omega_2 = \Omega_0 \setminus \Omega_1$ . Because  $\mathcal{G}$  is bipartite, neither the pivot chain nor the Glauber chain is irreducible as Markov chains with the state space  $\Omega$ . Consequently, the injective motif-sampling chains with the pivot chain or the Glauber chain (see Algorithm RM) are not irreducible on the state space  $\Omega_0$ . However, they are irreducible when we restrict them to each  $\Omega_i$  with a unique stationary distribution  $\pi_{F \hookrightarrow \mathcal{G}}^{(i)}$ . (See the proof of [40, Theorem 5.7].) More explicitly, we compute

$$\begin{aligned} \pi_{F \hookrightarrow \mathcal{G}}^{(i)}(\mathbf{x}) &:= \mathbb{P}_{\mathbf{y} \sim \pi_{F \hookrightarrow \mathcal{G}}}(\mathbf{y} = \mathbf{x} \mid \mathbf{y} \in \Omega_i) \\ &= \frac{1}{Z_i} \left( \prod_{j \in \{2, \dots, k\}} A(\mathbf{x}(j-1), \mathbf{x}(j)) \right) \mathbb{1}(\mathbf{x} \text{ is injective}) = \frac{Z_0}{Z_i} \pi_{F \hookrightarrow \mathcal{G}}(\mathbf{x}), \quad i \in \{1, 2\}, \end{aligned} \quad (20)$$

where

$$\begin{aligned} Z_i &= \sum_{\mathbf{x} \in \Omega_i} \prod_{j \in \{2, \dots, k\}} A(\mathbf{x}(j-1), \mathbf{x}(j)) \mathbb{1}(\mathbf{x} \text{ is injective}), \\ Z_0 &= \sum_{\mathbf{x} \in \Omega_0} \prod_{j \in \{2, \dots, k\}} A(\mathbf{x}(j-1), \mathbf{x}(j)) \mathbb{1}(\mathbf{x} \text{ is injective}). \end{aligned}$$

We define two associated conditional expected loss functions

$$\begin{aligned} f^{(i)}(W) &:= \mathbb{E}_{\mathbf{x} \sim \pi_{F \hookrightarrow \mathcal{G}}^{(i)}} \left[ \ell(X^{(N)}(\mathbf{x}), W) \right] \\ &= \mathbb{E}_{\mathbf{x} \sim \pi_{F \hookrightarrow \mathcal{G}}} \left[ \ell(X^{(N)}(\mathbf{x}), W) \mid \mathbf{x} \in \Omega_i \right], \quad i \in \{1, 2\}, \end{aligned} \quad (21)$$

where the equality follows from the first equality in (20). Because the Markov chain  $(\mathbf{x}_t)_{t \geq 0}$  stays in  $\Omega_i$  if it is initialized in  $\Omega_i$ , the conditional expected loss functions  $f^{(i)}$  are the natural objective function to minimize (instead of the expected loss function  $f$  in (17)). Similarly, for the approximate pivot chain, we define the distributions  $\hat{\pi}_{F \hookrightarrow \mathcal{G}}^{(i)}$  and the conditional expected loss functions  $\hat{f}^{(i)}$  as follows. For  $\hat{\pi}_{F \hookrightarrow \mathcal{G}}$  as in (11), let

$$\begin{aligned} \hat{\pi}_{F \hookrightarrow \mathcal{G}}^{(i)}(\mathbf{x}) &:= \mathbb{P}_{\mathbf{y} \sim \hat{\pi}_{F \hookrightarrow \mathcal{G}}}(\mathbf{y} = \mathbf{x} \mid \mathbf{y} \in \Omega_i) \\ &= \frac{1}{|V_i|} \left( \frac{\prod_{2 \leq j \leq k} A(\mathbf{x}(j-1), \mathbf{x}(j))}{\sum_{y_2, \dots, y_k \in V} A(\mathbf{x}(1), y_2) \prod_{i=3}^k A(y_{i-1}, y_i)} \right) = \frac{|V|}{|V_i|} \hat{\pi}_{F \hookrightarrow \mathcal{G}}(\mathbf{x}), \\ f^{(i)}(W) &:= \mathbb{E}_{\mathbf{x} \sim \hat{\pi}_{F \hookrightarrow \mathcal{G}}^{(i)}} \left[ \ell(X^{(N)}(\mathbf{x}), W) \right] \\ &= \mathbb{E}_{\mathbf{x} \sim \hat{\pi}_{F \hookrightarrow \mathcal{G}}} \left[ \ell(X^{(N)}(\mathbf{x}), W) \mid \mathbf{x} \in \Omega_i \right], \quad i \in \{1, 2\}. \end{aligned} \quad (22)$$

We now state our second convergence result for the NLD algorithm. This result is for bipartite networks. A convergence result that is analogous to the one in Theorem [NDL](#) holds for the associated conditional expected loss function. This implies that one can initialize homomorphisms in each  $\Omega_i$  and compute sequences  $W_t^{(i)}$  (with  $i \in \{1, 2\}$ ) of dictionary matrices to learn stationary points of both associated conditional expected loss functions  $f^{(i)}$ . However, when a  $k$ -chain motif  $F = ([k], A_F)$  has an even number of nodes, one only needs to compute one sequence of dictionary matrices, because one can obtain the other sequence by the algebraic operation of taking a ‘mirror image’ of a given square matrix. More precisely, define a map  $\text{Flip} : \mathbb{R}^{k^2 \times r} \rightarrow \mathbb{R}^{k^2 \times r}$  that maps  $W \mapsto \overline{W}$ , such that the  $j^{\text{th}}$  column  $\overline{W}(:, j)$  of  $\overline{W}$  is defined by

$$\overline{X}(:, j) := \text{vec} \circ \text{rev} \circ \text{reshape}(W(:, j)), \quad j \in \{1, \dots, r\},$$

where  $W(:, j)$  denotes the  $j^{\text{th}}$  column of  $W$ , the operator  $\text{reshape} : \mathbb{R}^{k^2} \rightarrow \mathbb{R}^{k \times k}$  is the reshaping operator that we defined in Algorithm [A5](#),  $\text{rev}$  maps a  $k \times k$  matrix  $K$  to the  $k \times k$  matrix  $(\overline{K}_{ab})_{1 \leq a, b \leq k}$  with entries  $\overline{K}_{ab} = K(k - a + 1, k - b + 1)$ , and  $\text{vec}$  denotes the vectorization operator in Algorithm [A4](#). Applying  $\text{Flip}$  twice gives the identity map.

**Theorem 7.7** (Convergence of the NDL Algorithm for Bipartite Networks). *Let  $F = ([k], A_F)$  be the  $k$ -chain motif, and let  $G = (V, A)$  be a network that satisfies the the following properties:*

- (a’) *A is symmetric and the undirected and unweighted graph  $(V, \mathbb{1}(A > 0))$  is connected and bipartite.*
- (b) *For all  $t \geq 0$ , there exists a unique solution  $H_t$  in [\(12\)](#).*
- (c) *For all  $t \geq 0$ , the eigenvalues of the positive semidefinite matrix  $A_t$  in [\(12\)](#) are at least as large as some constant  $\kappa_1 > 0$ .*

Let  $(W_t)_{t \geq 0}$  denote the sequence of dictionary matrices that we generate using Algorithm [NDL](#). We then have the following properties:

- (i) *Suppose that  $\text{MCMC} \in \{\text{Pivot}, \text{Glauber}\}$ . For each  $i \in \{1, 2\}$ , conditional on  $\mathbf{x}_0 \in \Omega_i$ , the sequence of dictionary matrices  $W_t$  converges almost surely as  $t \rightarrow \infty$  to the set of stationary points of the associated conditional expected loss function  $f^{(i)}$  in [\(21\)](#). If  $\text{MCMC} = \text{PivotApprox}$ , then the same statement holds with  $f^{(i)}$  replaced by the function  $\hat{f}^{(i)}$  in [\(22\)](#). If we also assume that  $f^{(i)}$  (respectively,  $\hat{f}^{(i)}$ ), with  $i \in \{1, 2\}$ , have only finitely many stationary points in  $\mathcal{C}^{\text{dict}}$ , it then follows that  $W_t$  converges almost surely to a single stationary point of  $f^{(i)}$  (respectively,  $\hat{f}^{(i)}$ ) as  $t \rightarrow \infty$ .*
- (ii) *Suppose that  $\text{MCMC} = \text{Glauber}$  in Algorithm [NDL](#) and that  $k$  is even. Assume that  $\mathbf{x}_0 \in \Omega_1$ . It then follows that, almost surely, the sequences of dictionary matrices  $W_t$  and  $\overline{W}_t$  converge simultaneously to the sets of stationary points of the expected loss functions  $f^{(1)}$  and  $f^{(2)}$ , respectively. Moreover,  $f^{(1)}(W_t) = f^{(2)}(\overline{W}_t)$  for all  $t \geq 0$ . If we also assume that  $f^{(i)}$ , with  $i \in \{1, 2\}$ , has only finitely many stationary points in  $\mathcal{C}^{\text{dict}}$ , it then follows that  $W_t$  and  $\overline{W}_t$  converge almost surely to single stationary points of  $f^{(1)}$  and  $f^{(2)}$ , respectively as  $t \rightarrow \infty$ .*

*Proof.* We first prove (i). Fix  $i \in \{1, 2\}$  and recall the conditional stationary distribution  $\pi_{F \rightarrow \mathcal{G}}^{(i)}$  from [\(20\)](#). Conditional on  $\mathbf{x}_0 \in \Omega_{i'}$ , the Markov chain  $(\mathbf{x}_t)_{t \geq 0}$  of injective homomorphisms is irreducible and aperiodic with a unique stationary distribution  $\pi_{F \rightarrow \mathcal{G}}^{(i')}$ . Recall that the conclusion of Theorem [7.4](#) holds as long as the underlying Markov chain is irreducible. Therefore,  $W_t$  converges almost surely to the set of stationary points of the associated conditional expected loss function  $f^{(i')}$  in [\(21\)](#). The same argument verifies the case with  $\text{MCMC} = \text{PivotApprox}$ .

We now verify (ii). We first establish some notation and claims. Define the notation  $\mu_i := \pi_{F \rightarrow \mathcal{G}}^{(i)}$  and suppose that  $k$  is even. For each homomorphism  $\mathbf{x} : F \rightarrow \mathcal{G}$ , we define a map

$\bar{\mathbf{x}} : [k] \rightarrow V$  by

$$\bar{\mathbf{x}}(j) := \mathbf{x}(k - j + 1) \quad \text{for all } j \in \{1, \dots, k\}.$$

Note that  $\mathbf{x}$  is injective if and only if  $\bar{\mathbf{x}}$  is injective. For even  $k$ , we have that  $\mathbf{x} \in \Omega_1$  if and only if  $\bar{\mathbf{x}} \in \Omega_2$ . Because  $A$  is symmetric, it follows that

$$\prod_{j=1}^{k-1} A(\mathbf{x}(j), \mathbf{x}(j+1)) = \prod_{j=1}^{k-1} A(\mathbf{x}(j+1), \mathbf{x}(j)) = \prod_{j=1}^{k-1} A(\bar{\mathbf{x}}(j), \bar{\mathbf{x}}(j+1)).$$

Therefore,  $Z_1 = Z_2 = Z_0/2$ . Consequently, for each  $\mathbf{x} \in \Omega_1$ , (20) implies that

$$\mu_1(\mathbf{x}) = \mu_2(\bar{\mathbf{x}}) = 2\pi_{F \hookrightarrow \mathcal{G}}(\mathbf{x}). \quad (23)$$

Consider two Glauber chains,  $(\mathbf{z}_t)_{t \geq 0}$  and  $(\mathbf{z}'_t)_{t \geq 0}$ , where  $\mathbf{z}_0 = \mathbf{y}$  and  $\mathbf{z}'_0 = \bar{\mathbf{y}}$ . We evolve these two Markov chains using a common source of randomness so that individually they have Glauber-chain trajectories; however, they also satisfy the relation  $\mathbf{z}'_t = \bar{\mathbf{z}}_t$  for all  $t \geq 0$ . Specifically, suppose that  $\mathbf{z}'_t = \bar{\mathbf{z}}_t$ . For each update  $\mathbf{z}_t \mapsto \mathbf{z}_{t+1}$  and  $\mathbf{z}'_t \mapsto \mathbf{z}'_{t+1}$ , we choose a node  $v \in [k]$  uniformly at random and sample  $z \in V$  according to the conditional distribution (10). We define

$$\begin{aligned} \mathbf{z}_{t+1}(v) &= z \quad \text{and} \quad \mathbf{z}_{t+1}(u) = \mathbf{z}_t(u) \quad \text{for } u \neq v, \\ \mathbf{z}'_{t+1}(k - v + 1) &= z \quad \text{and} \quad \mathbf{z}'_{t+1}(u) = \mathbf{z}_t(u) \quad \text{for } u \neq k - v + 1. \end{aligned}$$

The update  $\mathbf{z}_t \mapsto \mathbf{z}_{t+1}$  follows the Glauber-chain update in Algorithm MG. Additionally,  $\mathbf{z}'_{t+1} = \bar{\mathbf{z}}_{t+1}$  because

$$\begin{aligned} \mathbf{z}'_{t+1}(k - v + 1) &= z = \mathbf{z}_{t+1}(v) = \bar{\mathbf{z}}_{t+1}(k - v + 1), \\ \mathbf{z}'_{t+1}(u) &= \mathbf{z}'_t(u) = \bar{\mathbf{z}}_t(u) = \mathbf{z}_t(k - u + 1) = \mathbf{z}_{t+1}(k - u + 1) \\ &= \bar{\mathbf{z}}_{t+1}(u) \quad \text{for } u \neq k - v + 1. \end{aligned}$$

Finally, we need to verify that  $\mathbf{z}'_t \mapsto \mathbf{z}'_{t+1}$  also follows the Glauber-chain update in Algorithm MG. It suffices to check that  $z \in V$  has the same distribution as  $\mathbf{z}'_{t+1}(k - v + 1)$ . Because  $v$  is uniformly distributed on  $[k]$ , so is  $k - v + 1$ . The distribution of  $z \in V$  is determined by

$$p(z) \propto \begin{cases} A(z, \mathbf{z}_t(2)) = A(z, \bar{\mathbf{z}}_t(k - 1)), & \text{if } v = 1 \\ A(\mathbf{z}_t(v - 1), z)A(z, \mathbf{z}_t(v + 1)) \\ \quad = A(\bar{\mathbf{z}}_t(k - v), z)A(z, \bar{\mathbf{z}}_t(k - v + 2)), & \text{if } v \in \{2, \dots, k - 1\} \\ A(\mathbf{z}_t(k - 1), z) = A(\bar{\mathbf{z}}_t(2), z), & \text{if } v = k. \end{cases}$$

Because  $\mathbf{z}'_t = \bar{\mathbf{z}}_t$ , it follows that  $z$  follows the conditional distribution (10) of  $\mathbf{z}'_{t+1}(k - v + 1)$ , as desired.

For the two Glauber chains,  $\mathbf{z}_t$  and  $\mathbf{z}'_t$ , we observe that

$$\overline{X^{(N)}(\mathbf{y})} = X^{(N)}(\bar{\mathbf{y}}) \quad (24)$$

almost surely. This result follows from the facts that  $\mathbf{z}'_t = \bar{\mathbf{z}}_t$  for all  $t \geq 0$  and  $\text{rev}(A_{\mathbf{z}}) = A_{\bar{\mathbf{z}}}$  for all  $\mathbf{z} \in \Omega$ . (See (4) for the definition of  $A_{\mathbf{z}}$ .) From this, we note that

$$\begin{aligned} f^{(1)}(W) &= \mathbb{E}_{\mathbf{z} \sim \pi} \left[ \ell(X^{(N)}(\mathbf{z}), W) \mid \mathbf{z} \in \Omega_1 \right] \\ &= \mathbb{E}_{\mathbf{z} \sim \pi} \left[ \ell\left(\overline{X^{(N)}(\mathbf{z})}, \bar{W}\right) \mid \bar{\mathbf{z}} \in \Omega_2 \right] \\ &= \mathbb{E}_{\mathbf{z} \sim \pi} \left[ \ell\left(X^{(N)}(\bar{\mathbf{z}}), \bar{W}\right) \mid \bar{\mathbf{z}} \in \Omega_2 \right] \end{aligned} \quad (25)$$

$$= \mathbb{E}_{\mathbf{z} \sim \pi} \left[ \ell(X^{(N)}(\mathbf{z}), \overline{W}) \mid \mathbf{z} \in \Omega_2 \right] = f^{(2)}(\overline{W}).$$

The first and the last equalities use the second equality in (20). The second equality uses the fact that  $\ell(X, W) = \ell(\overline{X}, \overline{W})$ . The third equality follows from (24). The fourth equality follows from the change of variables  $\overline{\mathbf{z}} \mapsto \mathbf{z}$  and the fact that  $\mathbf{z} \sim \pi$  if and only if  $\overline{\mathbf{z}} \sim \pi$  (see (23)).

We are now ready to prove (ii). The first part of (ii) follows immediately from (i) and the above construction of the Glauber chains  $\mathbf{z}_t$  and  $\mathbf{z}'_t$  that satisfy  $\mathbf{z}'_t = \overline{\mathbf{z}}_t$  for all  $t \geq 0$ . Recall that the Markov chain of injective homomorphisms  $\mathbf{x}_t$  is a subsequence of  $\mathbf{z}_t$ . We also recall that  $\mathbf{z}$  is injective if and only if  $\overline{\mathbf{z}}$  is injective. Therefore,  $\overline{\mathbf{x}}_t$  is the same subsequence of  $\overline{\mathbf{z}}$ . That is, there exist integers  $t_\ell$  (with  $\ell \geq 1$ ) such that  $\mathbf{x}_\ell = \mathbf{z}_{t_\ell}$  and  $\overline{\mathbf{x}}_\ell = \overline{\mathbf{z}}_{t_\ell}$ . Now let  $W_t = W_t(\mathbf{x}_0)$  and  $W'_t = W'_t(\mathbf{x}'_0)$  denote the sequences of dictionary matrices that we compute using Algorithm **NDR** with initial (not necessarily injective) homomorphisms  $\mathbf{x}_0$  and  $\mathbf{x}'_0$ , respectively. Suppose that  $\mathbf{x}_0 \in \Omega_1$ , from which we see that  $\mathbf{x}'_0 = \overline{\mathbf{x}}_0 \in \Omega_2$ . By (i),  $W_t$  and  $W'_t$  converge almost surely to the set of stationary points of the associated conditional expected loss functions  $f^{(1)}$  and  $f^{(2)}$ , respectively. We complete the proof of the first part of (ii) by observing that, almost surely,

$$W'_t = \overline{W}_t \quad \text{for all } t \geq 0. \quad (26)$$

The second part of (ii) follows immediately from (25).

We still need to verify (26). Roughly, we argue that all  $k \times k$  mesoscale patches  $A_{\overline{\mathbf{x}}_t} = \mathbf{ref}(A_{\mathbf{x}_t})$  have a reversed row and column ordering relative to their original ordering, so  $k \times k$  latent motifs that we train on such matrices also have this reversed ordering of rows and columns. One can check this claim by induction on  $t$  together with (24) and the uniqueness assumption (b). We omit the details.  $\square$

**7.3. Convergence and reconstruction guarantees of our NDR algorithm.** We prove various theoretical guarantees for our NDR algorithm (see Algorithm **NDR**) in Theorem 7.10. Specifically, we show that the reconstructed network that we obtain using Algorithm **NDR** at iteration  $t$  converges almost surely to some limiting network as  $t \rightarrow \infty$ , and we give a closed-form expression of the limiting network. We also derive an upper bound for the global reconstruction error. Roughly, we state the bound as follows:

$$\text{Jaccard reconstruction error} \leq \frac{\text{mesoscale approximation error}}{2(k-1)},$$

where  $k$  denotes the number of nodes in a  $k$ -chain motif. The parameter  $k$  is effectively a scale parameter. In (33), we give a precise statement of the above bound.

Before stating our mathematical results, we first introduce some notation. Fix a network  $\mathcal{G} = (V, A)$ , a  $k$ -chain motif  $F = ([k], A_F)$ , and a homomorphism  $\mathbf{x} : F \rightarrow \mathcal{G}$ . In this discussion, we do not assume that a homomorphism  $F \rightarrow \mathcal{G}$  is injective, as we use all sampled homomorphisms for our network reconstruction using our NDR algorithm (see Algorithm **NDR**), unlike in our NDL algorithm (see Algorithm **NDL**) for learning latent motifs. Let **denoising** denote the Boolean variable in Algorithm **NDR**. For each matrix  $B : V^2 \rightarrow [0, \infty)$  and a node map  $\mathbf{x} : [k] \rightarrow V$ , define the  $k \times k$  matrix  $B_{\mathbf{x}}$  by

$$B_{\mathbf{x}}(a, b) := B(\mathbf{x}(a), \mathbf{x}(b)) \quad \text{for all } a, b \in \{1, \dots, k\}.$$

If  $B = A$ , then  $B_{\mathbf{x}} = A_{\mathbf{x}}$  is the same as the mesoscale patch of  $\mathcal{G}$  that is induced by  $\mathbf{x}$  (see (4)). Additionally, given a network  $\mathcal{G} = (V, A)$ , a  $k$ -chain motif  $F = ([k], A_F)$ , a homomorphism  $\mathbf{x} : F \rightarrow \mathcal{G}$ , and a nonnegative matrix  $W \in \mathbb{R}_{\geq 0}^{k^2 \times r}$ , let  $\hat{A}_{\mathbf{x}, W}$  denote the  $k \times k$  matrix that we defined in line 11 of Algorithm **NDR**. This matrix depends on the Boolean variable **denoising**. Recall that  $\hat{A}_{\mathbf{x}, W}$  is a nonnegative linear approximation of  $A_{\mathbf{x}}$  that uses  $W$ .

We introduce the event  $(x, y) \overset{\mathbf{x}}{\leftrightarrow} (a, b)$  using the following indicator function:

$$\mathbb{1}\left((x, y) \overset{\mathbf{x}}{\leftrightarrow} (a, b)\right) := \mathbb{1}(\mathbf{x}(a) = p, \mathbf{x}(b) = q) \quad (27)$$

$$\times \mathbb{1}\left(\begin{array}{l} \text{InjHom} = \mathbf{F} \\ \text{or } \mathbf{x} \text{ is injective} \end{array}\right) \mathbb{1}\left(\begin{array}{l} \text{denoising} = \mathbf{F} \\ \text{or } A_F(a, b) = 0 \end{array}\right).$$

For each homomorphism  $\mathbf{x} : F \rightarrow \mathcal{G}$  and  $x, y \in V$ , we say that the pair  $(x, y)$  is *visited by*  $(a, b)$  *through*  $\mathbf{x}$  whenever the indicator on the left-hand side of (27) is 1. Additionally,

$$N_{xy}(\mathbf{x}) := \sum_{a, b \in \{1, \dots, k\}} \mathbb{1}\left((x, y) \overset{\mathbf{x}}{\leftrightarrow} (a, b)\right) \quad (28)$$

is the total number of visits to  $(x, y)$  through  $\mathbf{x}$ . When  $N_{xy}(\mathbf{x}) > 0$ , we say that the pair  $(x, y)$  is *visited by*  $\mathbf{x}$ . In Algorithm **NDR**, observe that both  $A_{\text{count}}(x, y)$  and  $A_{\text{recons}}(x, y)$  change at iteration  $t$  if and only if  $N_{xy}(\mathbf{x}_t) > 0$ . Let

$$\Omega_{pq} := \{\mathbf{x} : F \rightarrow \mathcal{G} \mid N_{xy}(\mathbf{x}) > 0\} \quad (29)$$

denote the set of all homomorphisms  $\mathbf{x} : F \rightarrow \mathcal{G}$  that visit the pair  $(x, y)$ .

Suppose that  $\hat{\mathcal{G}} = (V, \hat{A})$  is a reconstructed network for  $\mathcal{G} = (V, A)$ . Fix a probability distribution  $\pi$  on the set of homomorphisms  $F \rightarrow \mathcal{G}$ . For a matrix  $Q : V^2 \rightarrow \mathbb{R}$ , define the weighted  $L_1$  norm

$$\|Q\|_{1, \pi} := \sum_{x, y \in V} |Q(x, y)| \mathbb{E}_{\mathbf{x} \sim \pi} [N_{xy}(\mathbf{x})].$$

We define the following two quantities:

$$\text{JD}_{\pi}(\mathcal{G}, \hat{\mathcal{G}}) := \frac{\|A - \hat{A}\|_{1, \pi}}{\|A \vee \hat{A}\|_{1, \pi}}, \quad \text{JD}(\mathcal{G}, \hat{\mathcal{G}}) := \frac{\|A - \hat{A}\|_1}{\|A \vee \hat{A}\|_1}, \quad (30)$$

where  $A \vee \hat{A}$  is defined as  $(A \vee \hat{A})(x, y) = A(x, y) \vee \hat{A}(x, y) = \max(A(x, y), \hat{A}(x, y))$  for  $x, y \in V$ . We refer to  $\text{JD}_{\pi}(\mathcal{G}, \hat{\mathcal{G}})$  as the *Jaccard distance* between  $\mathcal{G} = (V, A)$  and  $\hat{\mathcal{G}} = (V, \hat{A})$  with respect to  $\pi$ . We refer to  $\text{JD}(\mathcal{G}, \hat{\mathcal{G}})$  as the *unweighted Jaccard distance* between  $\mathcal{G} = (V, A)$  and  $\hat{\mathcal{G}} = (V, \hat{A})$ .

To make sense of the definitions in (30), consider the special case in which the weight matrices  $A$  and  $\hat{A}$  are both symmetric and binary with 0 diagonal entries (i.e., no self-edges). We also assume that  $\pi$  is the uniform distribution on the set of homomorphisms  $F \rightarrow \mathcal{G}$  and  $k = 2$ . We then have that

$$\text{JD}_{\pi}(\mathcal{G}, \hat{\mathcal{G}}) = \text{JD}(\mathcal{G}, \hat{\mathcal{G}}) = 1 - \frac{\text{number of edges in both } \mathcal{G} \text{ and } \hat{\mathcal{G}}}{\text{number of edges in } \mathcal{G} \text{ or } \hat{\mathcal{G}}}. \quad (31)$$

Observe that the fraction in the right-hand side of (31) equals the Jaccard index for the edge sets of  $\mathcal{G}$  and  $\hat{\mathcal{G}}$ . We used this Jaccard index as a reconstruction-accuracy measure in Figure 5 in the main manuscript. Consequently, it is reasonable to view the Jaccard distances  $\text{JD}_{\pi}(\mathcal{G}, \hat{\mathcal{G}})$  and  $\text{JD}(\mathcal{G}, \hat{\mathcal{G}})$ , which coincide in this case, as the ‘Jaccard reconstruction error’ of reconstructing  $\mathcal{G}$  as  $\hat{\mathcal{G}}$ .

In the following proposition, we show that, under mild conditions, the Jaccard distance  $\text{JD}_{\pi}(\mathcal{G}, \mathcal{G}')$  with respect to  $\pi$  is close to the unweighted Jaccard distance  $\text{JD}(\mathcal{G}, \mathcal{G}')$  if the weights  $\mathbb{E}_{\mathbf{x} \sim \pi} [N_{xy}(\mathbf{x})]$  do not vary much for node pairs  $(x, y) \in V^2$  with  $|\Omega_{xy}| \geq 1$ .

**Proposition 7.8.** *Let  $F = ([k], A_F)$  be a  $k$ -chain motif, and fix connected and symmetric networks  $\mathcal{G} = (V, A)$  and  $\hat{\mathcal{G}} = (V, \hat{A})$  with the same node set  $V$ . Let  $\pi$  be a probability distribution on the set of homomorphisms  $F \rightarrow \mathcal{G}$ . Suppose that the following conditions hold:*



- (a) If  $x, y \in V$  satisfies  $|\Omega_{xy}| \geq 1$ , it follows that  $\hat{A}(x, y) = 0$ ;  
(b) Consider a homomorphism  $\mathbf{x} : F \rightarrow \mathcal{G}$  with  $\pi(\mathbf{x}) > 0$ .

Let  $\rho$  denote the maximum of the ratio  $\mathbb{E}_{\mathbf{x} \sim \pi}[N_{xy}(\mathbf{x})]/\mathbb{E}_{\mathbf{x} \sim \pi}[N_{x'y'}(\mathbf{x})]$  for  $x, x', y, y' \in V$  and suppose that  $\mathbb{E}_{\mathbf{x} \sim \pi}[N_{x'y'}(\mathbf{x})] \neq 0$ . We then have that

$$\rho^{-1} \text{JD}(\mathcal{G}, \hat{\mathcal{G}}) \leq \text{JD}_{\pi}(\mathcal{G}, \hat{\mathcal{G}}) \leq \rho \text{JD}(\mathcal{G}, \hat{\mathcal{G}}).$$

*Proof.* Consider two nodes  $x, y \in V$ , and let  $d_{\mathcal{G}}(x, y)$  denote the shortest-path distance between them in  $\mathcal{G}$ . This distance is the minimum number of edges in a walk in  $\mathcal{G}$  that connects  $x$  and  $y$ . If  $d_{\mathcal{G}}(x, y) > k$ , we then have that  $A(x, y) = \hat{A}(x, y) = 0$ . Moreover, because  $\mathcal{G}$  is symmetric,  $d_{\mathcal{G}}(x, y) \leq k$  implies that there exists a homomorphism  $\mathbf{x} : F \rightarrow \mathcal{G}$ . By condition (b), it follows that  $\mathbb{E}_{\mathbf{x} \sim \pi}[N_{xy}(\mathbf{x})] > 0$  if  $d_{\mathcal{G}}(x, y) \leq k$ . Let  $c := \min_{x, y \in V, |\Omega_{pq}| \geq 1} \mathbb{E}_{\mathbf{x} \sim \pi}[N_{xy}(\mathbf{x})]$ . We then have

$$\begin{aligned} c \|A - \hat{A}\|_1 &= \sum_{x, y \in V, d_{\mathcal{G}}(x, y) \leq k} \left| A(x, y) - \hat{A}(x, y) \right| c \\ &\leq \sum_{x, y \in V, d_{\mathcal{G}}(x, y) \leq k} \left| A(x, y) - \hat{A}(x, y) \right| \mathbb{E}_{\mathbf{x} \sim \pi}[N_{xy}(\mathbf{x})] \\ &= \sum_{x, y \in V} \left| A(x, y) - \hat{A}(x, y) \right| \mathbb{E}_{\mathbf{x} \sim \pi}[N_{xy}(\mathbf{x})] = \|A - \hat{A}\|_{1, \pi}. \end{aligned}$$

If we instead take  $C := \max_{x, y \in V, |\Omega_{pq}| \geq 1} \mathbb{E}_{\mathbf{x} \sim \pi}[N_{xy}(\mathbf{x})]$ , we obtain

$$\begin{aligned} C \|A - \hat{A}\|_1 &= \sum_{x, y \in V, d_{\mathcal{G}}(x, y) \leq k} \left| A(x, y) - \hat{A}(x, y) \right| C \\ &\geq \sum_{x, y \in V, d_{\mathcal{G}}(x, y) \leq k} \left| A(x, y) - \hat{A}(x, y) \right| \mathbb{E}_{\mathbf{x} \sim \pi}[N_{xy}(\mathbf{x})] = \|A - \hat{A}\|_{1, \pi}. \end{aligned}$$

Therefore,  $C \|A - \hat{A}\|_1 \geq \|A - \hat{A}\|_{1, \pi}$ . Moreover, by using a similar argument, we obtain  $c \|A \vee \hat{A}\|_1 \leq \|A - \hat{A}\|_{1, \pi} \leq C \|A \vee \hat{A}\|_1$ . We then let  $\rho = C/c$  to complete the proof.  $\square$

**Proposition 7.9.** *Let  $G = (V, A)$  be a symmetric and connected network, and let  $F = ([k], A_F)$  be a  $k$ -chain motif. Suppose that  $2(k-1) \leq \text{diam}(\mathcal{G})$ . For each node  $x \in V$ , it then follows that there exists an injective homomorphism  $\mathbf{x} : F \hookrightarrow \mathcal{G}$  with  $x \in \{\mathbf{x}(1), \dots, \mathbf{x}(k)\}$ .*

*Proof.* Our proof proceeds by contradiction. Suppose that there is a node  $x \in V$  for which there does not exist an injective homomorphism  $\mathbf{x} : F \hookrightarrow \mathcal{G}$  with  $x \in \{\mathbf{x}(1), \dots, \mathbf{x}(k)\}$ . We will show that this implies that  $\text{diam}(\mathcal{G}) < 2(k-1)$ , which contradicts the hypothesis.

Fix two nodes  $y, z \in V$ . Consider a walk  $(y_1, \dots, y_a)$  from  $x$  to  $y$  and another walk  $(z_1, \dots, z_b)$  from  $z$  to  $x$ . We choose these walks so that the integers  $p, q \geq 1$  are as small as possible. By minimality, we then know that these walks are paths (i.e., all  $y_i$  are distinct and all  $z_i$  are distinct). If  $p \geq k$ , then  $(y_1, \dots, y_k)$  gives a  $k$ -path, so  $\mathbf{x}_y : [k] \rightarrow V$  with  $\mathbf{x}_y(i) = y_i$  for  $i \in \{1, \dots, k\}$  is an injective homomorphism  $F \hookrightarrow \mathcal{G}$  and  $\mathbf{x}_y(1) = y_1 = x$ . This contradicts our assumption about the node  $x$ . Therefore,  $p < k$ . By a similar argument, we know that  $q < k$ . Consequently,  $(z_1, \dots, z_q, y_1, \dots, y_p)$  is a  $(p+q)$ -path from  $z$  to  $y$ . This implies that  $d_{\mathcal{G}}(z, y) \leq p+q < 2(k-1)$ . Because the nodes  $y$  and  $z$  are arbitrary, this implies that  $\text{diam}(\mathcal{G}) < 2(k-1)$ , which contradicts the hypothesis. This completes the proof.  $\square$

We now state and prove our main theoretical result about our NDR algorithm (see Algorithm [NDR](#)).

**Theorem 7.10** (Guarantees of the NDR Algorithm (see Algorithm **NDR**) for Non-Bipartite Networks). *Let  $F = ([k], A_F)$  be a  $k$ -chain motif, and fix a network  $\mathcal{G} = (V, A)$  and a network dictionary  $W \in \mathbb{R}^{k^2 \times r}$ . We use Algorithm **NDR** with inputs  $\mathcal{G}$ ,  $F$ , and  $W$  and the parameter value  $T = \infty$ . Let  $\hat{\mathcal{G}}_t = (V, \hat{A}_t)$  denote the network that we reconstruct at iteration  $t$ , and suppose that  $\mathcal{G}$  satisfies assumption (a) of Theorem 7.4. Let*

$$\pi := \begin{cases} \pi_{F \rightarrow \mathcal{G}} & \text{if MCMC} \in \{\text{Glauber, pivot}\} \text{ and InjHom} = \text{F} \\ \pi_{F \leftrightarrow \mathcal{G}} & \text{if MCMC} \in \{\text{Glauber, pivot}\} \text{ and InjHom} = \text{T} \\ \hat{\pi}_{F \rightarrow \mathcal{G}} & \text{if MCMC} = \text{PivotApprox} \text{ and InjHom} = \text{F} \\ \hat{\pi}_{F \leftrightarrow \mathcal{G}} & \text{if MCMC} = \text{PivotApprox} \text{ and InjHom} = \text{T}. \end{cases}$$

The following statements hold:

(i) (Convergence of the network reconstruction) *The network  $\hat{\mathcal{G}}_t$  converges almost surely to some limiting network  $\hat{\mathcal{G}}_\infty = (V, \hat{A}_\infty)$  in the sense that*

$$\lim_{t \rightarrow \infty} \hat{A}_t(x, y) = \hat{A}_\infty(x, y) \in [0, \infty) \quad \text{almost surely for all } x, y \in V.$$

(ii) (Limiting reconstructed network) *Let  $\hat{A}_\infty$  denote the limiting matrix in (i). For each  $x, y \in V$ , we then have that*

$$\hat{A}_\infty(x, y) = \sum_{\mathbf{y} \in \Omega_{xy}} \left[ \sum_{a, b \in \{1, \dots, k\}} \hat{A}_{\mathbf{y}; W}(a, b) \mathbb{1}\left((x, y) \xleftrightarrow{\mathbf{y}} (a, b)\right) \right] \frac{\pi(\mathbf{y})}{\mathbb{E}_{\mathbf{x} \sim \pi} [N_{xy}(\mathbf{x})]}, \quad (32)$$

where we regard the right-hand side to be 0 when  $|\Omega_{xy}| = 0$ .

(iii) (Bounds for the Jaccard reconstruction error) *Suppose that the range of  $A$  is contained in  $\{0\} \cup [1, \infty)$  and assume that **denoising** = F. Let  $\hat{A}_\infty$  denote the limiting matrix in (i). We then have that*

$$\rho^{-1} \text{JD}_\pi(\mathcal{G}, \hat{\mathcal{G}}) \leq \text{JD}_\pi(\mathcal{G}, \hat{\mathcal{G}}) \leq \frac{\mathbb{E}_{\mathbf{x} \sim \pi} [\|A_{\mathbf{x}} - \hat{A}_{\mathbf{x}; W}\|_1]}{2(k-1)}, \quad (33)$$

where the constant  $\rho > 0$  is as in Proposition 7.8.

*Proof.* Let  $\mathbf{x}$  denote a random homomorphism  $F \rightarrow \mathcal{G}$  with distribution  $\pi$ , and let  $\mathbb{P}$  and  $\mathbb{E}$  denote the associated probability measure and expectation, respectively.

We first verify (i) and (ii) simultaneously. Let  $(\mathbf{x}_t)_{t \geq 0}$  denote the Markov chain that we generate during the reconstruction process (see Algorithm **NDR**). Note that each  $\mathbf{x}_t$  is an injective homomorphism  $F \hookrightarrow \mathcal{G}$  if **InjHom** = T and that it is a homomorphism  $F \rightarrow \mathcal{G}$  that may or may not be injective if **InjHom** = F. We fix  $x, y \in V$  and let

$$M_t = \sum_{s=1}^t \sum_{a, b \in \{1, \dots, k\}} \mathbb{1}\left((x, y) \xleftrightarrow{\mathbf{x}_s} (a, b)\right) = \sum_{s=1}^t N_{xy}(\mathbf{x}_s),$$

where we defined the indicator  $\mathbb{1}\left((x, y) \xleftrightarrow{\mathbf{x}} (a, b)\right)$  in (27). If  $M_t = 0$ , then  $\hat{A}_t(x, y) = 0$ . Suppose that  $M_t \geq 1$ . The key observation is that

$$\begin{aligned} \hat{A}_t(x, y) &= \frac{1}{M_t} \sum_{s=1}^t \sum_{a, b \in \{1, \dots, k\}} \hat{A}_{\mathbf{x}_s; W}(a, b) \mathbb{1}\left((x, y) \xleftrightarrow{\mathbf{x}_s} (a, b)\right) \\ &= \sum_{a, b \in \{1, \dots, k\}} \frac{1}{M_t} \sum_{s=1}^t \sum_{\mathbf{y} \in \Omega_{xy}} \hat{A}_{\mathbf{y}; W}(a, b) \mathbb{1}\left((x, y) \xleftrightarrow{\mathbf{y}} (a, b)\right) \end{aligned} \quad (34)$$

$$= \sum_{\mathbf{y} \in \Omega_{xy}} \sum_{a, b \in \{1, \dots, k\}} \hat{A}_{\mathbf{y}; W}(a, b) \mathbb{1} \left( (x, y) \overset{\mathbf{x}_s}{\leftrightarrow} (a, b) \right) \frac{t}{M_t} \frac{1}{t} \sum_{s=1}^t \mathbb{1}(\mathbf{x}_s = \mathbf{y}).$$

With assumption (a), the Markov chain  $(\mathbf{x}_t)_{t \geq 0}$  of homomorphisms  $F \rightarrow \mathcal{G}$  is irreducible and aperiodic with the unique stationary distribution  $\pi$  (see (1)). By the Markov-chain ergodic theorem (see, e.g., [62, Theorem 6.2.1 and Example 6.2.4] or [66, Theorem 17.1.7]), it follows that

$$\lim_{t \rightarrow \infty} \frac{t}{M_t} \frac{1}{t} \sum_{s=1}^t \mathbb{1}(\mathbf{x}_s = \mathbf{y}) = \frac{\mathbb{P}(\mathbf{x} = \mathbf{y})}{\mathbb{E}[N_{xy}(\mathbf{x})]}.$$

By the definition of the probability distribution  $\pi$ , we have that  $\pi(\mathbf{x}) > 0$  for all injective homomorphism  $\mathbf{x} : F \hookrightarrow \mathcal{G}$ . Therefore,  $\mathbb{E}_{\mathbf{x} \sim \pi}[N_{xy}(\mathbf{x})] > 0$  if and only if  $|\Omega_{xy}| \geq 1$ . This proves both (i) and (ii).

We now prove (iii). Conditions (a) and (b) of Proposition 7.8 are satisfied for  $\hat{G} = \hat{G}_\infty$  with the assumed choice of  $\pi$ . Therefore, the first inequality in (33) follows immediately from Proposition 7.8. To verify the second inequality, we prove a slightly more general result. Let  $\mathcal{G}' = (V, B)$  be a network with the same node set  $V$  as  $\mathcal{G} = (V, A)$ . Assume that  $B$  is symmetric and that its range is contained in  $\{0\} \cup [1, \infty)$ . For each  $a, b \in \{1, \dots, k\}$ , define the indicator function

$$\mathbb{1}_{ab} := \mathbb{1} \left( \begin{array}{l} \text{denoising} = \mathbf{F} \\ \text{or } A_F(a, b) = 0 \end{array} \right). \quad (35)$$

We will show that

$$\frac{\|B - \hat{A}_\infty\|_{1, \pi}}{\|B \vee \hat{A}_\infty\|_{1, \pi}} \leq \frac{1}{2(k-1)} \sum_{\mathbf{y} \in \Omega} \sum_{a, b \in \{1, \dots, k\}} \left| B_{\mathbf{y}}(a, b) \mathbb{1}_{ab} - \hat{A}_{\mathbf{y}; W}(a, b) \mathbb{1}_{ab} \right| \pi(\mathbf{y}). \quad (36)$$

If  $\text{denoising} = \mathbf{F}$ , the right-hand side of (36) reduces to  $\frac{1}{2(k-1)} \mathbb{E}_{\mathbf{x} \sim \pi}[\|B_{\mathbf{x}} - \hat{A}_{\mathbf{x}; W}\|_1]$ , so (iii) is a special case of (36).

To verify (36), we first claim that

$$\|B - \hat{A}_\infty\|_{1, \pi} \leq \sum_{\mathbf{y} \in \Omega} \sum_{a, b \in \{1, \dots, k\}} \left| B_{\mathbf{y}}(a, b) \mathbb{1}_{ab} - \hat{A}_{\mathbf{y}; W}(a, b) \mathbb{1}_{ab} \right| \pi(\mathbf{y}). \quad (37)$$

For each  $a, b \in \{1, \dots, k\}$  and  $x, y \in \{1, \dots, n\}$ , let  $\Omega_{ab \rightarrow pq}$  denote the set of homomorphisms  $\mathbf{x} : F \rightarrow \mathcal{G}$  such that  $\mathbb{1}((x, y) \overset{\mathbf{x}}{\leftrightarrow} (a, b)) = 1$ . By changing the order of the sums, we rewrite the formula in (32) as

$$\hat{A}_\infty(x, y) = \sum_{a, b \in \{1, \dots, k\}} \mathbb{1} \left( (x, y) \overset{\mathbf{x}_s}{\leftrightarrow} (a, b) \right) \sum_{\mathbf{y} \in \Omega_{ab \rightarrow pq}} \hat{A}_{\mathbf{y}; W}(a, b) \frac{\mathbb{P}(\mathbf{x} = \mathbf{y})}{\mathbb{E}[N_{xy}(\mathbf{x})]}.$$

Additionally, because the indicator function  $\mathbb{1}_{ab}$  does not depend on the homomorphism  $\mathbf{y}$ , observe that

$$\begin{aligned} \mathbb{E}[N_{xy}(\mathbf{x})] &= \mathbb{E} \left[ \sum_{a, b \in \{1, \dots, k\}} \mathbb{1}(\mathbf{x}(a) = p, \mathbf{x}(b) = q) \mathbb{1} \left( \begin{array}{l} \text{InjHom} = \mathbf{F} \\ \text{or } \mathbf{x} \text{ is injective} \end{array} \right) \mathbb{1}_{ab} \right] \\ &= \sum_{a, b \in \{1, \dots, k\}} \mathbb{1}_{ab} \sum_{\mathbf{y} \in \Omega_{ab \rightarrow pq}} \mathbb{P}(\mathbf{x} = \mathbf{y}). \end{aligned}$$

We now calculate

$$\begin{aligned}
& \sum_{x,y \in V} \left| B(x,y) - \hat{A}_\infty(x,y) \right| \mathbb{E} [N_{xy}(\mathbf{x})] \\
&= \sum_{x,y \in V} \left| B(x,y) \mathbb{E} [N_{xy}(\mathbf{x})] - \sum_{a,b \in \{1,\dots,k\}} \mathbb{1}_{ab} \sum_{\mathbf{y} \in \Omega_{ab \rightarrow pq}} \hat{A}_{\mathbf{y};W}(a,b) \mathbb{P}(\mathbf{x} = \mathbf{y}) \right| \\
&= \sum_{x,y \in V} \left| \sum_{a,b \in \{1,\dots,k\}} \mathbb{1}_{ab} \sum_{\mathbf{y} \in \Omega_{ab \rightarrow pq}} \left( B(x,y) - \hat{A}_{\mathbf{y};W}(a,b) \right) \mathbb{P}(\mathbf{x} = \mathbf{y}) \right| \\
&\leq \sum_{x,y \in V} \sum_{a,b \in \{1,\dots,k\}} \sum_{\mathbf{y} \in \Omega_{ab \rightarrow pq}} \left| B(\mathbf{y}(a), \mathbf{y}(b)) \mathbb{1}_{ab} - \hat{A}_{\mathbf{y};W}(a,b) \mathbb{1}_{ab} \right| \mathbb{P}(\mathbf{x} = \mathbf{y}) \\
&= \sum_{x,y \in V} \sum_{a,b \in \{1,\dots,k\}} \sum_{\mathbf{y} \in \Omega} \left| B(\mathbf{y}(a), \mathbf{y}(b)) \mathbb{1}_{ab} - \hat{A}_{\mathbf{y};W}(a,b) \mathbb{1}_{ab} \right| \\
&\quad \times \mathbb{P}(\mathbf{x} = \mathbf{y}) \mathbb{1}(\mathbf{y}(a) = p, \mathbf{y}(b) = q) \\
&= \sum_{\mathbf{y} \in \Omega} \mathbb{P}(\mathbf{x} = \mathbf{y}) \sum_{a,b \in \{1,\dots,k\}} \left| B_{\mathbf{y}}(a,b) \mathbb{1}_{ab} - \hat{A}_{\mathbf{y};W}(a,b) \mathbb{1}_{ab} \right| \sum_{x,y \in V} \mathbb{1}(\mathbf{y}(a) = p, \mathbf{y}(b) = q) \\
&= \sum_{\mathbf{y} \in \Omega} \sum_{a,b \in \{1,\dots,k\}} \left| B_{\mathbf{y}}(a,b) \mathbb{1}_{ab} - \hat{A}_{\mathbf{y};W}(a,b) \mathbb{1}_{ab} \right| \pi(\mathbf{y}),
\end{aligned}$$

where we recall that the indicator  $\mathbb{1}_{ab}$  is defined in (35). This verifies the claim (37).

It now suffices to show that

$$\|B \vee \hat{A}_\infty\|_{1,\pi} \geq 2\|A_F\|_1 = 2(k-1), \quad (38)$$

where the equality uses the fact that  $F$  is a  $k$ -chain motif. For each  $a, b \in \{1, \dots, k\}$  and a homomorphism  $\mathbf{x} : F \rightarrow \mathcal{G}$ , observe that

$$(A_F(a,b) + A_F(b,a)) \sum_{x,y \in V} B(x,y) \sum_{\mathbf{y} \in \Omega_{ab \rightarrow pq}} \mathbb{1}(\mathbf{x} = \mathbf{y}) \geq A_F(a,b) + A_F(b,a). \quad (39)$$

The inequality (39) uses the fact that  $\mathbf{x}$  is a homomorphism. Therefore,  $A_F(a,b) + A_F(b,a) > 0$  and  $\{\mathbf{x}(a), \mathbf{x}(b)\} = \{x, y\}$  implies that  $B(x,y) + B(y,x) > 0$ . Because we assume that  $B$  is symmetric and that the range of  $B$  is contained in  $\{0\} \cup [1, \infty)$ , it follows that  $B(x,y) \geq 1$  and verifies the inequality (39).

Recall the notation  $\Omega_{ab \rightarrow pq}$  below the inequality (37). Observe that

$$\begin{aligned}
\|B \vee \hat{A}_\infty\|_{1,\pi} &= \sum_{x,y \in V} \left| B(x,y) \vee \hat{A}_\infty(x,y) \right| \mathbb{E}_{\mathbf{x} \sim \pi} [N_{xy}(\mathbf{x})] \\
&= \mathbb{E}_{\mathbf{x} \sim \pi} \left[ \sum_{x,y \in V} \mathbb{1}((B(x,y) \vee \hat{A}_\infty(x,y)) > 0) N_{xy}(\mathbf{x}) \right] \\
&= \mathbb{E}_{\mathbf{x} \sim \pi} \left[ \sum_{x,y \in V} \mathbb{1}((B(x,y) \vee \hat{A}_\infty(x,y)) > 0) \sum_{a,b \in \{1,\dots,k\}} \sum_{\mathbf{y} \in \Omega_{ab \rightarrow pq}} \mathbb{1}(\mathbf{x} = \mathbf{y}) \right] \\
&\geq \mathbb{E}_{\mathbf{x} \sim \pi} \left[ \sum_{a,b \in \{1,\dots,k\}} \sum_{x,y \in V} B(x,y) \sum_{\mathbf{y} \in \Omega_{ab \rightarrow pq}} \mathbb{1}(\mathbf{x} = \mathbf{y}) \right]
\end{aligned}$$

$$\begin{aligned}
&\geq \mathbb{E}_{\mathbf{x} \sim \pi} \left[ \sum_{a,b \in \{1, \dots, k\}} (A_F(a, b) + A_F(b, a)) \sum_{x, y \in V} B(x, y) \sum_{\mathbf{y} \in \Omega_{ab \rightarrow pq}} \mathbb{1}(\mathbf{x} = \mathbf{y}) \right] \\
&= \mathbb{E}_{\mathbf{x} \sim \pi} \left[ \sum_{a,b \in \{1, \dots, k\}} (A_F(a, b) + A_F(b, a)) \right] = 2 \|A_F\|_1.
\end{aligned}$$

For the last inequality, we have used the fact that  $(A_F(a, b) + A_F(b, a)) \in \{0, 1\}$ . This proves that (38), as desired.  $\square$

**Remark 7.11.** Suppose that the original network  $\mathcal{G} = (V, A)$  is binary. The Jaccard reconstruction error bound in Theorem 7.10(iii) concerns a direct comparison between the weighted reconstructed network  $\hat{\mathcal{G}} = (V, \hat{A})$  and the original binary network  $\mathcal{G} = (V, A)$ . In Figure 5 in the main manuscript, we instead used binary reconstructed networks  $\hat{\mathcal{G}}(\theta) := (V, \mathbb{1}(\hat{A} > \theta))$  that we obtain by thresholding the edge weights  $\hat{A}(x, y)$  at some threshold  $\theta \in (0, 1)$ . By modifying the argument in the proof of Theorem 7.10(iii), we can obtain a similar bound for the Jaccard reconstruction error for the thresholded reconstructed network  $\hat{\mathcal{G}}(\theta) := (V, \mathbb{1}(\hat{A} > \theta))$ . We now sketch the argument.

Let  $\theta' := \min(1 - \theta, \theta)$ . For  $a \in \{0, 1\}$  and  $\hat{a} \in [0, 1]$ , we obtain the inequalities

$$\theta' |a - \mathbb{1}(\hat{a} > \theta)| \leq |(a - \hat{a}) \mathbb{1}(|a - \hat{a}| > \theta')| \leq |a - \hat{a}|.$$

Because  $A : V^2 \rightarrow \{0, 1\}$  and  $\hat{A} : V^2 \rightarrow [0, 1]$ , it follows that

$$\theta' \|A - \mathbb{1}(\hat{A} > \theta)\|_{1, \pi} \leq \|(A - \hat{A}) \mathbb{1}(|A - \hat{A}| > \theta')\|_{1, \pi} \leq \|A - \hat{A}\|_{1, \pi}.$$

By modifying the argument in the proof of Theorem 7.10(iii), one can show that

$$\theta' \text{JD}_\pi(\mathcal{G}, \hat{\mathcal{G}}(\theta)) \leq \frac{\|(A - \hat{A}) \mathbb{1}(|A - \hat{A}| > \theta')\|_1}{\|A\|_{1, \pi}} \stackrel{(*)}{\leq} \frac{\|A - \hat{A}\|_1}{\|A\|_{1, \pi}} \leq \frac{\mathbb{E}_{\mathbf{x} \sim \pi} [\|A_{\mathbf{x}} - \hat{A}_{\mathbf{x}; W}\|_1]}{2(k-1)}. \quad (40)$$

By using Proposition 7.8, one can also deduce that

$$\text{JD}(\mathcal{G}, \hat{\mathcal{G}}(\theta)) \leq (\rho/\theta') \frac{\mathbb{E}_{\mathbf{x} \sim \pi} [\|A_{\mathbf{x}} - \hat{A}_{\mathbf{x}; W}\|_1]}{2(k-1)}. \quad (41)$$

The inequalities in (41) give a bound for the unweighted Jaccard distance between the original binary network  $\mathcal{G}$  and the thresholded binary reconstructed network  $\hat{\mathcal{G}}(\theta)$ . However, the bounds in (41) seem to be crude because of the possibly large constant  $\rho/\theta'$  (which is at least 2.5 for  $\theta = 0.4$ ), the gap between the left- and the right-hand side of the inequality in (41) could be large. For instance, in Figure 7c, we see that if  $\mathcal{G}$  is UCLA and  $W$  is the network dictionary of  $r = 9$  latent motifs of UCLA itself, the right-hand side of (41) is at least  $2.5 * 0.2 = 0.5$  for  $\theta = 0.4$ . However, from Figure 5c, we see the empirical value of the left-hand side of (41) is about 0.05. To obtain some insight into this discrepancy, observe that the second inequality in (40) (which we mark with  $(*)$ ) becomes very crude if many entries of  $A$  and  $\hat{A}$  do not differ by more than  $\theta$ , which appears to be the case in our numerical computations.

**Remark 7.12.** Suppose that `denoising` = F in Theorem 7.10(iii). Recall that the columns of  $W$  encode  $r$  latent motifs  $\mathcal{L}_1, \dots, \mathcal{L}_r \in \mathbb{R}_{\geq 0}^{k \times k}$  (see Section B.4). According to (33), we have a perfect reconstruction  $\mathcal{G} = \hat{\mathcal{G}}_\infty$  if the right-hand side of (33) is 0. This is the case if  $\sup_{\mathbf{x}: F \rightarrow \mathcal{G}} \ell(\text{vec}(A_{\mathbf{x}}), W) = 0$ , which implies that  $W$  can perfectly approximate all mesoscale patches  $A_{\mathbf{x}}$  of  $\mathcal{G}$ . However, the right-hand side of (33) can still be small if the worst-case approximation error  $\sup_{\mathbf{x}: F \rightarrow \mathcal{G}} \ell(\text{vec}(A_{\mathbf{x}}), W)$  is large but the expected approximation error

$\mathbb{E}_{\mathbf{x} \sim \pi} [\ell(\text{vec}(A_{\mathbf{x}}), W)]$  is small (i.e., when  $W$  is effective at approximating most of the mesoscale patches).

How can we find a network dictionary  $W$  that minimizes the right-hand side of (33)? Although it is difficult to find a globally optimal network dictionary  $W$  that minimizes the non-convex objective function on the right-hand side of (33), Theorems 7.4 and 7.7 guarantee that our NDL algorithm (see Algorithm NDL) always finds a locally optimal network dictionary. From these theorems, we know that the NDL algorithm with  $N = 1$  computes a network dictionary  $W$  that is approximately a local optimum of the expected loss function

$$f(W) = \mathbb{E}_{\mathbf{x} \sim \pi} [\ell(\text{vec}(A_{\mathbf{x}}), W)] , \quad (42)$$

where  $\pi = \hat{\pi}_{F \hookrightarrow \mathcal{G}}$  if  $\text{MCMC} = \text{PivotApprox}$  and  $\pi = \pi_{F \hookrightarrow \mathcal{G}}$  if  $\text{MCMC} \in \{\text{Glauber}, \text{pivot}\}$ . The function  $f$  in (42) is similar to the one in the upper bound in (33). In our experiments, we found that our NDL algorithm produces network dictionaries that are efficient at minimizing the reconstruction error. See Figure 5 and the left-hand sides of (33) and (41).

Another implication of Theorem 7.10(iii) is also relevant to network denoising (see Figure 9). Suppose that we have an uncorrupted network  $\mathcal{G}' = (V, B)$  and a corrupted network  $\mathcal{G} = (V, A)$ . Additionally, suppose that we have trained the network dictionary  $W$  for the uncorrupted network  $\mathcal{G}'$ , but that we use it to reconstruct the corrupted network  $\mathcal{G}$ . Even if  $\hat{A}_{\mathbf{x};W}$  is a nonnegative linear approximation of the  $k \times k$  matrix  $A_{\mathbf{x}}$  of a mesoscale patch of the corrupted network  $\mathcal{G}$ , it may be close to the corresponding mesoscale patch  $B_{\mathbf{x}}$  of the uncorrupted network  $\mathcal{G}'$  because we use the network dictionary  $W$  that we learned from the uncorrupted network  $\mathcal{G}'$ . Theorem 7.10(iii) guarantees that the network  $\hat{\mathcal{G}}_{\infty}$  that we reconstruct for the corrupted network  $\mathcal{G}$  using the uncorrupted-network dictionary  $W$  is close to the uncorrupted network  $\mathcal{G}'$ .

**Remark 7.13.** The update step (see line 17) for global reconstruction in Algorithm NDR indicates that we loop over all node pairs  $(a, b)$  in a  $k$ -chain motif and that we update the weight of edge  $\{\mathbf{x}_t(a), \mathbf{x}_t(b)\}$  in the reconstructed network using the homomorphism  $\mathbf{x} : F \rightarrow \mathcal{G}$ . There may be multiple node pairs  $(a, b)$  in  $F$  that contribute to the edge  $\{x, y\}$  in the reconstructed network because  $\mathbf{x}_t(a) = p$  and  $\mathbf{x}_t(b) = q$  can occur for multiple choices of  $(a, b)$ . The output of this update step does not depend on the ordering of  $a, b \in \{1, \dots, k\}$ , as one can see from the expressions in (34).

One can also consider the following alternative update step for global reconstruction. In this alternative, we first choose two nodes,  $x$  and  $y$ , of the reconstructed network in the image  $\{\mathbf{x}_t(j) \mid j \in \{1, \dots, k\}\}$  of the homomorphism  $\mathbf{x}_t$  and average over all pairs  $(a, b) \in [k]^2$  such that  $(x, y)$  is visited by  $(a, b)$  through  $\mathbf{x}_t$ ; we then update the weight of  $(x, y)$  in the reconstructed network with this mean contribution from  $\mathbf{x}_t$ . Specifically, for each  $a, b \in \{1, \dots, k\}$ , let  $\mathbb{1}((x, y) \xleftrightarrow{\mathbf{x}_t} (a, b))$  denote the indicator in (27) and let  $N_{xy}(\mathbf{x}_t) \geq 0$  denote the number of visits of  $\mathbf{x}_t$  to  $(x, y)$  (see (28)). We can then replace line 17 in Algorithm NDR with the following line:

*Alternative update for global reconstruction:*

**For**  $x, y \in V$  such that  $N_{xy}(\mathbf{x}_t) > 0$ :

$$\tilde{A}_{\mathbf{x}_t;W}(x, y) \leftarrow \frac{\sum_{1 \leq a, b \leq k} \hat{A}_{\mathbf{x}_t;W}(a, b) \mathbb{1}((x, y) \xleftrightarrow{\mathbf{x}_t} (a, b))}{\sum_{1 \leq a, b \leq k} \mathbb{1}((x, y) \xleftrightarrow{\mathbf{x}_t} (a, b))} , \quad j \leftarrow A_{\text{count}}(x, y) + 1$$

$$A_{\text{recons}}(x, y) \leftarrow (1 - j^{-1})A_{\text{recons}}(x, y) + j^{-1}\tilde{A}_{\mathbf{x}_t;W}(x, y) .$$

For the alternative NDR algorithm that we just described, we can establish a convergence result that is similar to Theorem 7.7 using a similar argument as the one in our proof of Theorem 7.10. Specifically, (i) holds for the alternative NDR algorithm, so there exists a limiting reconstructed

network. In the proof of **(ii)**, the formula for the limiting reconstructed network is now

$$\hat{A}_\infty(x, y) = \sum_{\mathbf{y} \in \Omega_{xy}} \tilde{A}_{\mathbf{y}; W}(x, y) \mathbb{P}_{\mathbf{x} \sim \pi}(\mathbf{x} = \mathbf{y} \mid \mathbf{x} \in \Omega_{xy}) \quad \text{for all } x, y \in V,$$

where  $\Omega_{xy}$  is the set of all homomorphisms that visit  $(x, y)$  (see (29)). In particular, if  $\mathcal{G}$  is an undirected and unweighted graph, then

$$\hat{A}_\infty(x, y) = \frac{1}{|\Omega_{xy}|} \sum_{\mathbf{y} \in \Omega_{xy}} \tilde{A}_{\mathbf{y}; W}(x, y) \quad \text{for all } x, y \in V.$$

In the proofs of **(iii)** and **(iv)**, the same error bounds hold with  $\mathbb{E}_{\mathbf{x} \sim \pi}[N_{xy}(\mathbf{x})]$  replaced by  $\mathbb{P}_{\mathbf{x} \sim \pi}(\mathbf{x} \in \Omega_{xy})$ . We omit the details of the proofs of the above statements for this alternative NDR algorithm.

We now discuss the convergence results of Algorithm **NDR** for a bipartite network  $\mathcal{G}$ . Recall the notation and discussions about bipartite networks above Theorem 7.7. Additionally, for bipartite networks, recall that there exist disjoint subsets  $\Omega_1$  and  $\Omega_2$  of the set  $\Omega$  of all homomorphisms  $F \rightarrow \mathcal{G}$  such that (1)  $\Omega = \Omega_1 \cup \Omega_2$  and (2) the Markov chain  $(\mathbf{x})_{t \geq 0}$  restricted to each  $\Omega_i$  (with  $i \in \{1, 2\}$ ) is irreducible but is not irreducible on the set  $\Omega$ .

**Theorem 7.14** (Convergence of our NDR Algorithm (see Algorithm **NDR**) for Bipartite Networks). *Let  $F = ([k], A_F)$  be a  $k$ -chain motif, and let  $\mathcal{G} = (V, A)$  be a network that satisfies assumption (a') in Theorem 7.7. Let  $\hat{\mathcal{G}}_t = (V, \hat{A}_t)$  denote the network that we reconstruct using Algorithm **NDR** at iteration  $t$  with a fixed network dictionary  $W \in \mathbb{R}^{k^2 \times r}$ . Fix  $i \in \{1, 2\}$  and an initial (not necessarily injective) homomorphism  $\mathbf{x}_0 \in \Omega_i$ . Let  $\pi = \hat{\pi}_{F \rightarrow \mathcal{G}}$  if  $\text{MCMC} = \text{PivotApprox}$  and  $\pi = \pi_{F \rightarrow \mathcal{G}}$  for  $\text{MCMC} \in \{\text{Glauber}, \text{pivot}\}$ . The following properties hold:*

**(i)** (Convergence of the network reconstruction) *The network  $\hat{\mathcal{G}}_t$  converges almost surely to some limiting network  $\hat{\mathcal{G}}_\infty = (V, \hat{A}_\infty)$  in the sense that*

$$\lim_{t \rightarrow \infty} \hat{A}_t(x, y) = \hat{A}_\infty(x, y) \quad \text{almost surely for all } x, y \in V.$$

**(ii)–(iii)** *The same statements as in statements **(ii)–(iii)** of Theorem 7.10 hold with the expectation  $\mathbb{E}_{\mathbf{x} \sim \pi}$  replaced by the conditional expectation  $\mathbb{E}_{\mathbf{x} \sim \pi}[\cdot \mid \mathbf{x} \in \Omega_i]$ .*

**(iv)** *The results in **(i)–(iii)** do not depend on  $i \in \{1, 2\}$  if  $k$  is even.*

*Proof.* The proofs of statements **(i)–(iii)** are identical to those for Theorem 7.10. Statement **(iv)** follows from a similar argument as in the proof of Theorem 7.7**(ii)** by constructing coupled Markov chains  $(\mathbf{x}_t)_{t \geq 0}$  and  $(\mathbf{x}'_t)_{t \geq 0}$  such that  $\mathbf{x}'_t = \bar{\mathbf{x}}_t$  for all  $t \geq 0$ .  $\square$

**Remark 7.15.** In Theorem 7.14**(ii)**, let  $\hat{\mathcal{G}}_\infty^{(i)} = (V, \hat{A}_\infty^{(i)})$ , with  $i \in \{1, 2\}$ , denote the limiting reconstructed network for  $\mathcal{G}$  conditional on initializing the Markov chain in the subset  $\Omega_i$ . When  $k$  is even, Theorem 7.14**(iv)** implies that  $\hat{\mathcal{G}}_\infty^{(1)} = \hat{\mathcal{G}}_\infty^{(2)}$ . When  $k$  is odd, we run the NDR algorithm (see Algorithm **NDR**) twice with the Markov chain initialized once in  $\Omega_1$  and once in  $\Omega_2$ . We then define the network  $\hat{\mathcal{G}}_\infty = (V, (\hat{A}_\infty^{(1)} + \hat{A}_\infty^{(2)})/2)$  whose weight matrix is the mean of those of the two limiting reconstructed networks  $\hat{\mathcal{G}}_\infty^{(i)}$  for  $i \in \{1, 2\}$ . We obtain a similar error bound as in Theorem 7.14**(iii)** for the mean limiting reconstructed network  $\hat{\mathcal{G}}_\infty$ . In practice, one can obtain a sequence of reconstructed networks that converges to  $\hat{\mathcal{G}}_\infty$  by reinitializing the Markov chain every  $\tau$  iterations of the reconstruction procedure for any fixed  $\tau$ .

## 8. AUXILIARY ALGORITHMS

We now present auxiliary algorithms that we use to solve various subproblems of Algorithms **NDL** and **NDR**. Let  $\Pi_S$  denote the projection operator onto a subset  $S$  of a space. For each matrix  $A$ , let  $[A]_{\bullet i}$  (respectively,  $[A]_{i\bullet}$ ) denote the  $i^{\text{th}}$  column (respectively,  $i^{\text{th}}$  row) of  $A$ .

**Algorithm A1.** Coding

- 
- 1: **Input:** Data matrix  $X \in \mathbb{R}^{d \times b}$ , dictionary matrix  $W \in \mathbb{R}^{d \times r}$
  - 2: **Parameters:**  $T \in \mathbb{N}$  (the number of iterations)  $\lambda > 0$  (the coefficient of an  $L_1$ -regularizer)  
 $\mathcal{C}^{\text{code}} \subseteq \mathbb{R}^{r \times b}$  (a convex constraint set of codes)

3: **For**  $t = 1, \dots, T$ :

4:     **Do:**

$$H \leftarrow \Pi_{\mathcal{C}^{\text{code}}} \left( H - \frac{1}{\text{tr}(W^T W)} (W^T W H - W^T X + \lambda J) \right),$$

where  $J \subseteq \mathbb{R}^{d \times b}$  is the matrix with all 1 entries

5: **Output:**  $H \in \mathcal{C}^{\text{code}} \subseteq \mathbb{R}^{r \times b}$

---

**Algorithm A2.** Dictionary-Matrix Update

- 
- 1: **Input:** Previous dictionary matrix  $W_{t-1} \in \mathbb{R}^{k^2 \times r}$ , previous aggregate matrices  $(P_t, Q_t) \in \mathbb{R}^{r \times r} \times \mathbb{R}^{r \times N}$

2: **Parameters:**  $\mathcal{C}^{\text{dict}} \subseteq \mathbb{R}^{k^2 \times r}$  (compactness and convexity constraint for dictionary matrices)  
 $T \in \mathbb{N}$  (the number of iterations)

3: **For**  $t = 1, \dots, T$ :

4:      $W \leftarrow W_{t-1}$

5:     **For**  $j = 1, 2, \dots, N$ :

$$W(:, j) \leftarrow \Pi_{\mathcal{C}^{\text{dict}}} \left( W(:, j) - \frac{1}{A_t(j, j) + 1} (W P_t(:, j) - Q_t^T(:, j)) \right)$$

6: **Output:**  $W_t = W \in \mathcal{C}^{\text{dict}} \subseteq \mathbb{R}_{\geq 0}^{k^2 \times r}$

---

**Algorithm A3.** Rejection Sampling of Homomorphisms

- 
- 1: **Input:** Network  $\mathcal{G} = (V, A)$ , a  $k$ -chain motif  $F = ([k], A_F)$

(▷ This algorithm works for all motifs, but we specialize it to  $k$ -chain motifs.)

2: **Requirement:** There exists at least one homomorphism  $F \rightarrow \mathcal{G}$

3: **Repeat:** Sample  $\mathbf{x} = [\mathbf{x}(1), \mathbf{x}(2), \dots, \mathbf{x}(k)] \in V^{[k]}$  so that the quantities  $\mathbf{x}(i)$  are independent and identically distributed

4:     **If**  $\prod_{i, j \in \{1, \dots, k\}} A(\mathbf{x}(i), \mathbf{x}(j))^{A_F(i, j)} > 0$

5:         **Return**  $\mathbf{x} : F \rightarrow \mathcal{G}$  and **Terminate**

6: **Output:** Homomorphism  $\mathbf{x} : F \rightarrow \mathcal{G}$

---



---

**Algorithm A4.** Vectorization

---

1: **Input:** Matrix  $X \in \mathbb{R}^{k_1 \times k_2}$ 2: **Output:** Matrix  $\text{vec}(X) := Y \in \mathbb{R}^{k_1 k_2 \times 1}$ , where

$$Y(k_2(j-1) + i, 1) = X(i, j) \quad \text{for all } i \in \{1, \dots, k_1\} \text{ and } j \in \{1, \dots, k_2\}$$

---

---

**Algorithm A5.** Reshaping

---

1: **Input:** Matrix  $X \in \mathbb{R}^{k_1 k_2 \times 1}$ , a pair  $(k_1, k_2)$  of integers2: **Output:** Matrix  $\text{reshape}(X) := Y \in \mathbb{R}^{k_1 \times k_2}$ , where

$$Y(i, j) = X(k_2(j-1) + i, 1) \quad \text{for all } i \in \{1, \dots, k_1\} \text{ and } j \in \{1, \dots, k_2\}$$

---

## 9. ADDITIONAL FIGURES



FIGURE 13. The accuracy, precision, and recall scores for the network-denoising experiments in Figure 9 in the main manuscript. For convenience, we recall the definitions of these quantities, which one uses for binary classification. One summarizes the result of a binary classification using combinations of four quantities: TP (true positives), which is the number of positive examples that are classified as positive; TN (true negatives), which is the number of negative examples that are classified as negative; FP (false positives), which is the number of positive examples that are classified as negative; and FN (false negatives), which is the number of negative examples that are classified as positive. The total number of examples is the sum of these four quantities. Accuracy is  $\frac{TP+TN}{TP+TN+FP+FN}$ , precision is  $\frac{TP}{TP+FP}$ , and recall is  $\frac{TP}{TP+FN}$ .

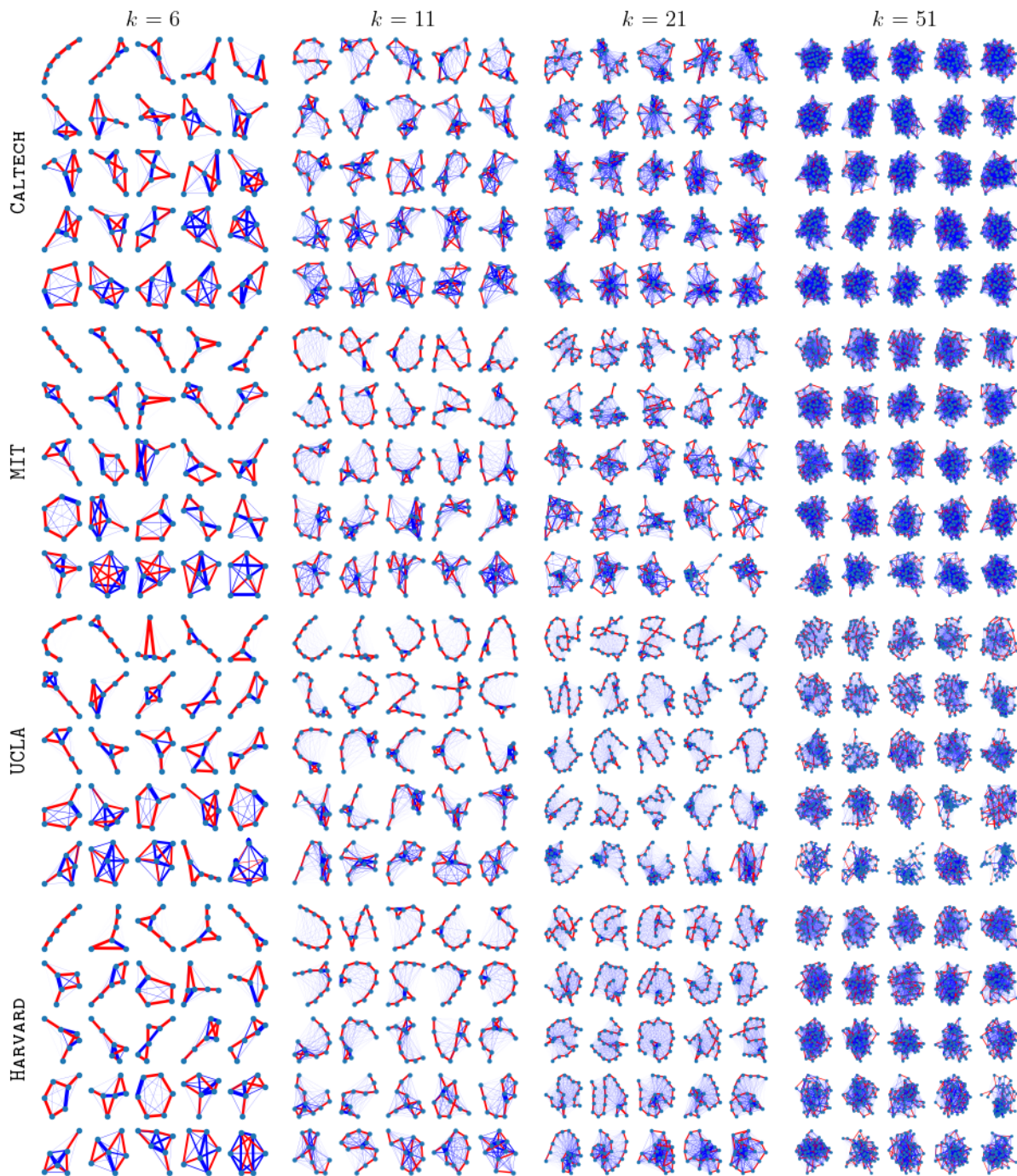


FIGURE 14. The  $r = 25$  latent motifs at scales  $k = 6$ ,  $k = 11$ ,  $k = 21$ , and  $k = 51$  that we learn from the networks CALTECH, MIT, UCLA, and HARVARD. See Section F for the details of these experiments.

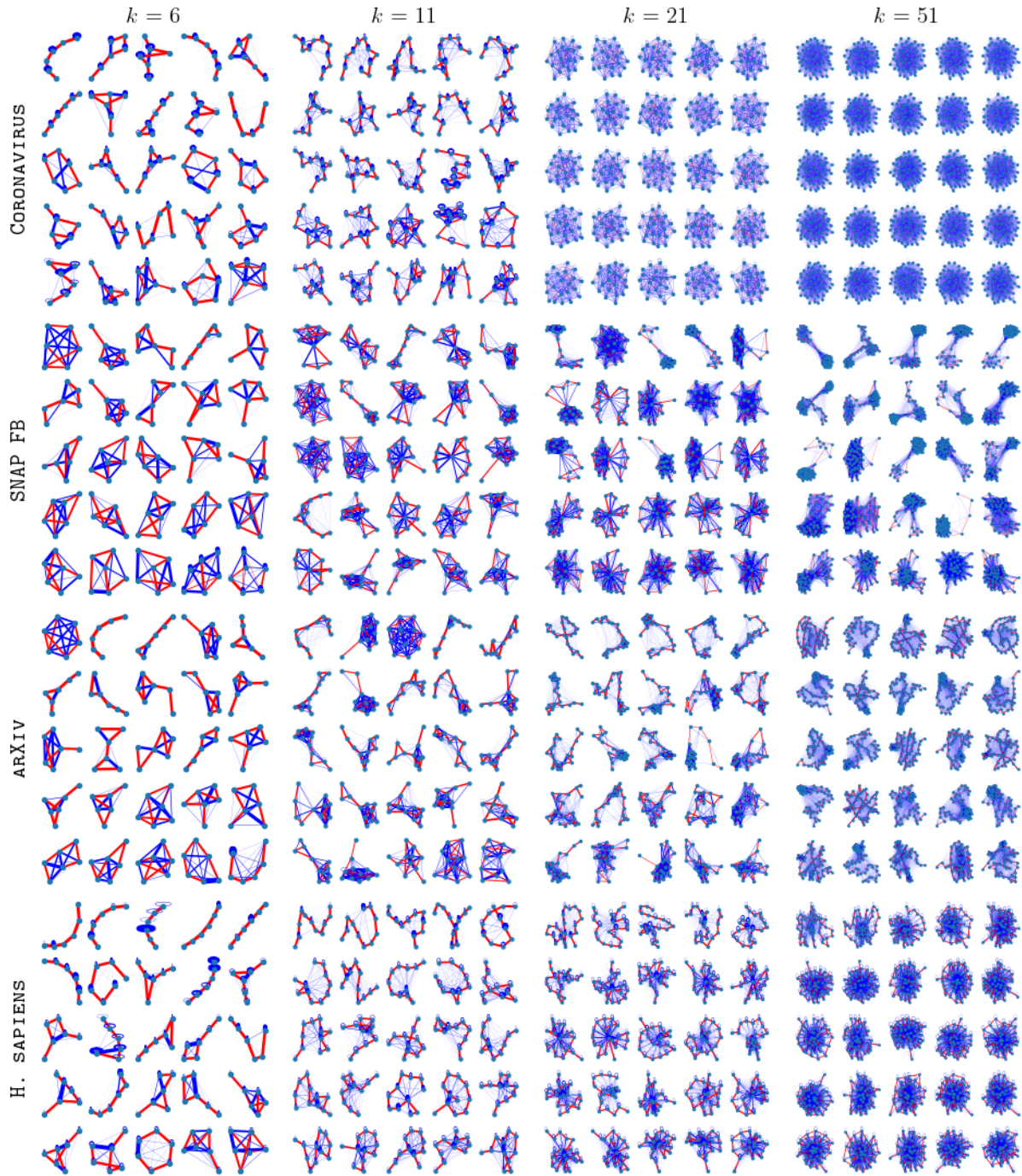


FIGURE 15. The  $r = 25$  latent motifs at scales  $k = 6$ ,  $k = 11$ ,  $k = 21$ , and  $k = 51$  that we learn from the networks CORONAVIRUS PPI, SNAP FACEBOOK, ARXIV ASTRO-PH, and HOMO SAPIENS PPI. See Section F for the details of these experiments.

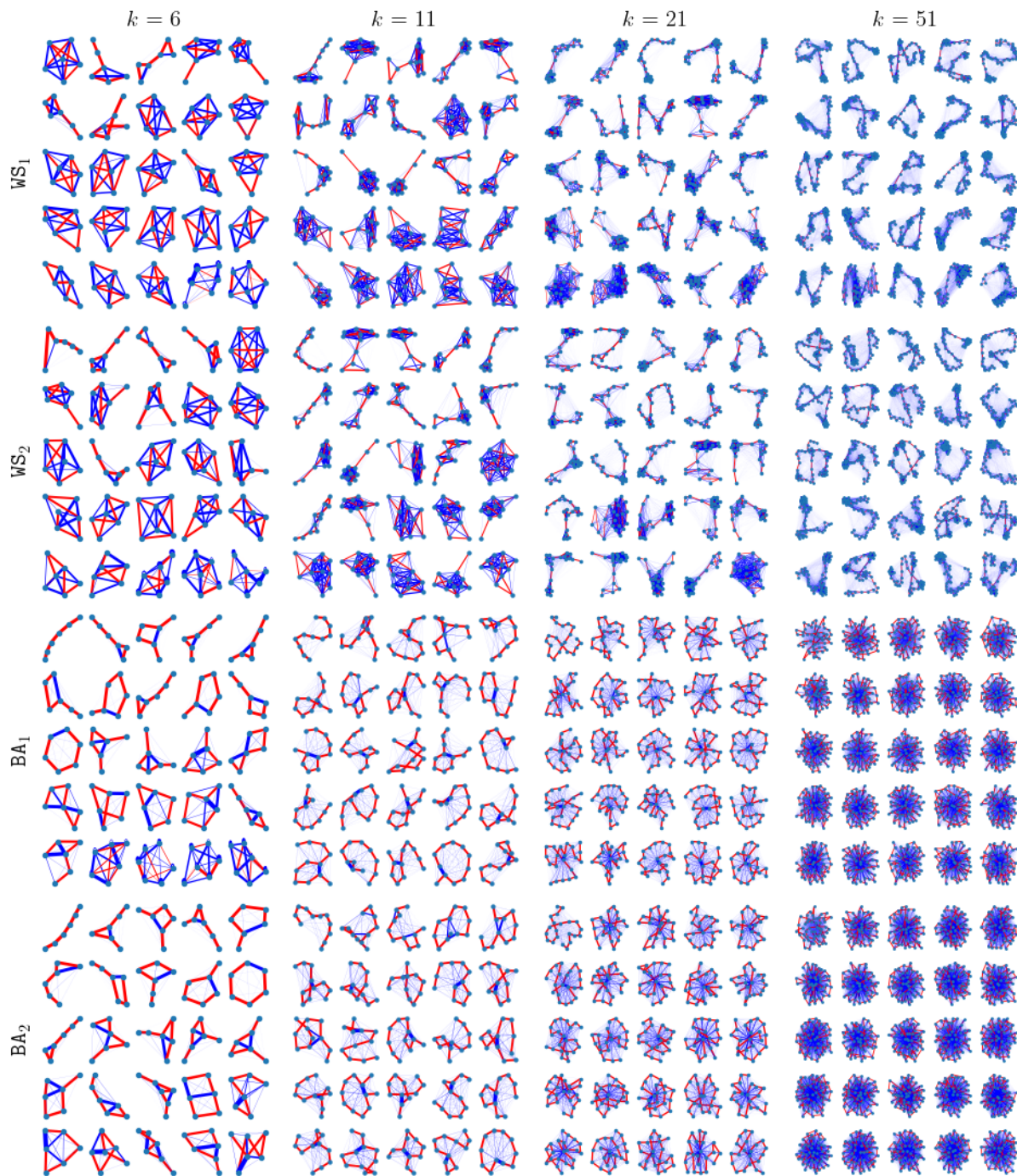


FIGURE 16. The  $r = 25$  latent motifs at scales  $k = 6$ ,  $k = 11$ ,  $k = 21$ , and  $k = 51$  that we learn from the networks  $WS_1$ ,  $WS_2$ ,  $BA_1$ , and  $BA_2$ . See Section F for details of the experiments.

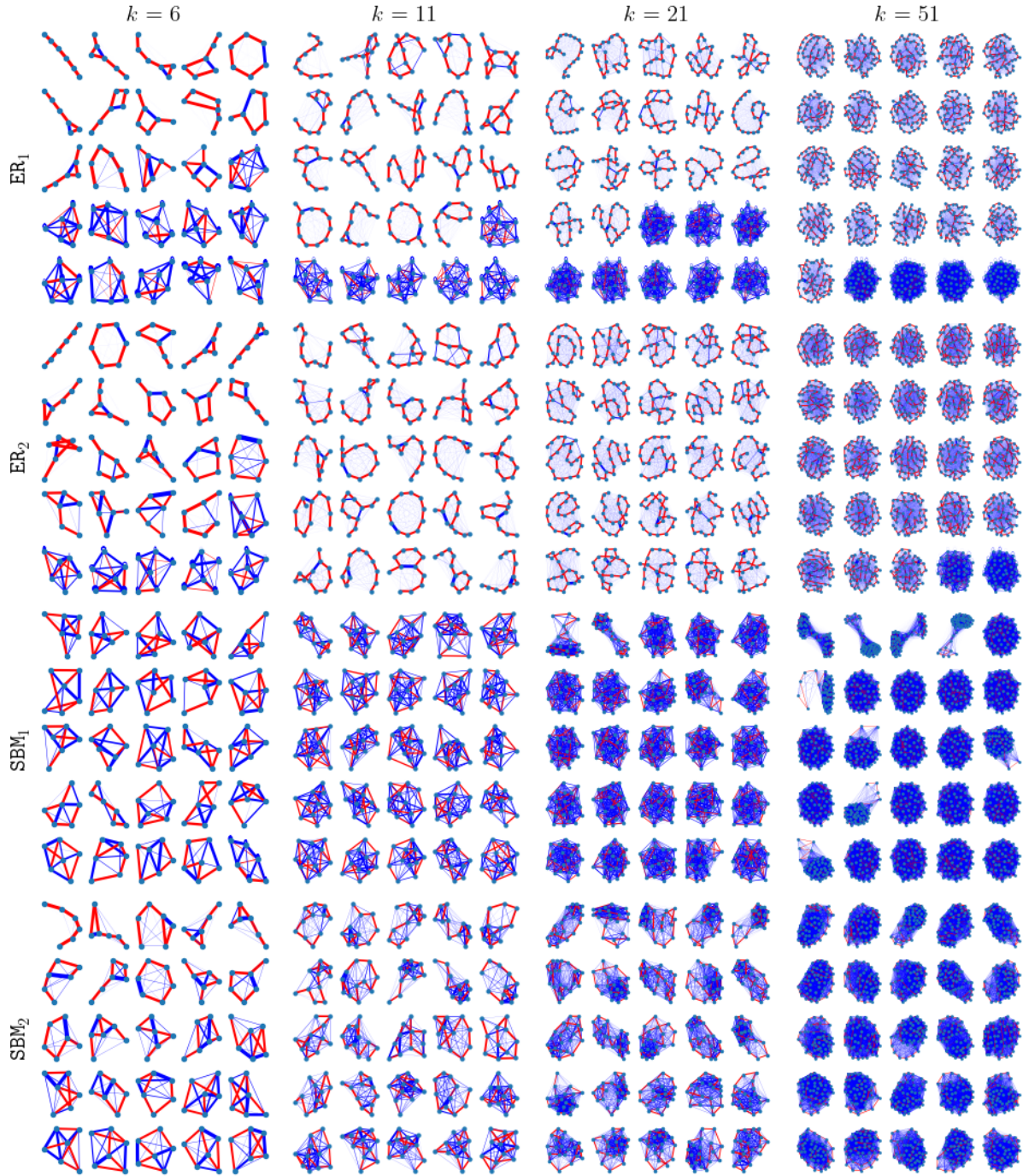


FIGURE 17. The  $r = 25$  latent motifs at scales  $k = 6$ ,  $k = 11$ ,  $k = 21$ , and  $k = 51$  that we learn from the networks  $ER_1$ ,  $ER_2$ ,  $SBM_1$ , and  $SBM_2$ . See Section F for details of the experiments.

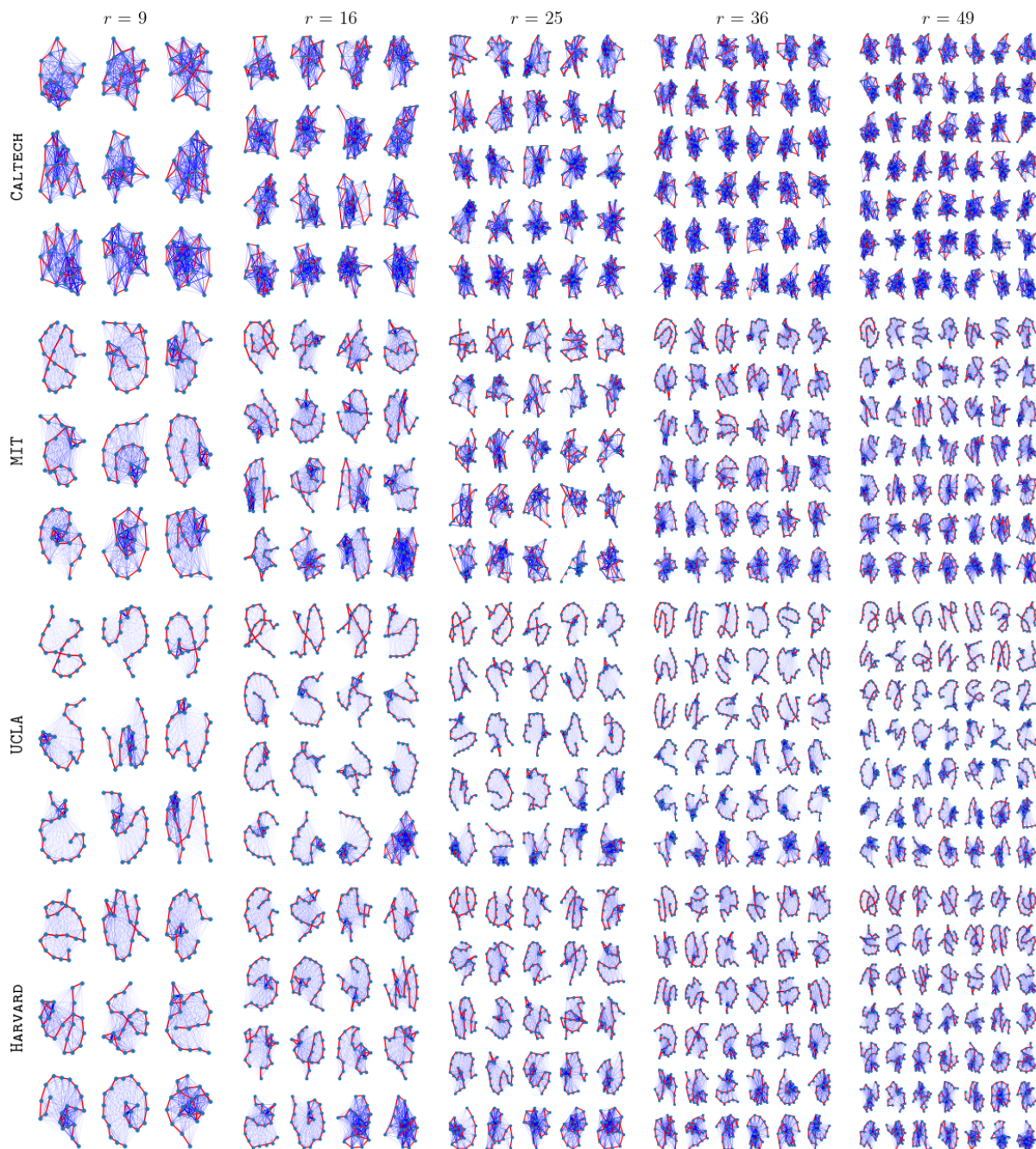


FIGURE 18. The 25 latent motifs for  $r \in \{9, 16, 25, 36, 49\}$  at scale  $k = 21$  that we learn from the networks CALTECH, MIT, and UCLA. The  $r = 25$  column is identical to the  $k = 21$  column in Figure 14. See Section F for details of the experiments.

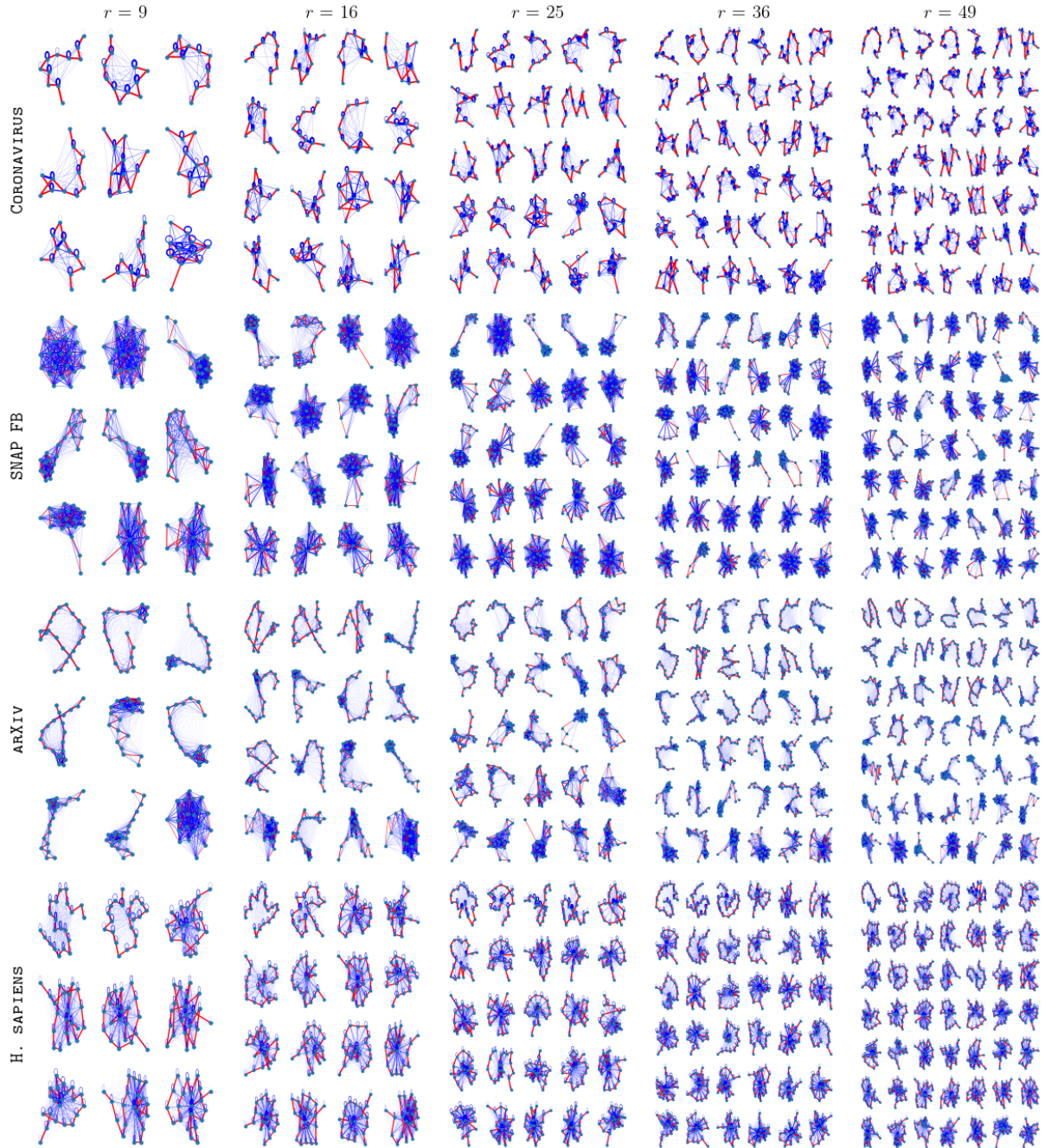


FIGURE 19. The latent motifs for  $r \in \{9, 16, 25, 36, 49\}$  that we learn from the networks SNAP FACEBOOK, ARXIV ASTRO-PH, and HOMO SAPIENS PPI at scale  $k = 21$  and from CORONAVIRUS PPI at scale  $k = 11$ . The  $r = 25$  column is identical to the  $k = 21$  column in Figure 15. See Section F for details of the experiments.



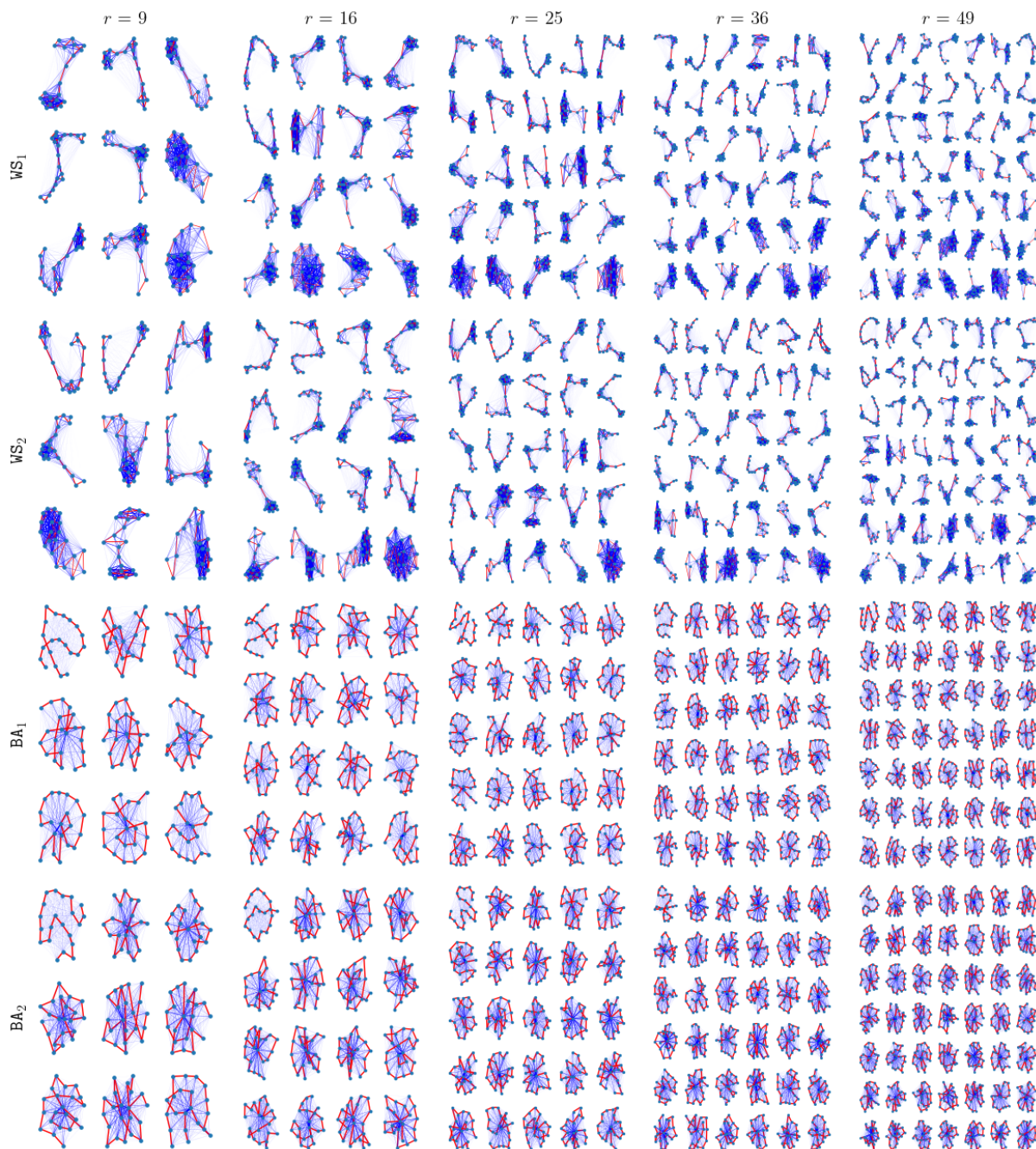


FIGURE 20. The latent motifs for  $r \in \{9, 16, 25, 36, 49\}$  at scale  $k = 21$  that we learn from the networks  $WS_1$ ,  $WS_2$ ,  $BA_1$ , and  $BA_2$ . The  $r = 25$  column is identical to the  $k = 21$  column in Figure 16. See Section F for details of our experiments.

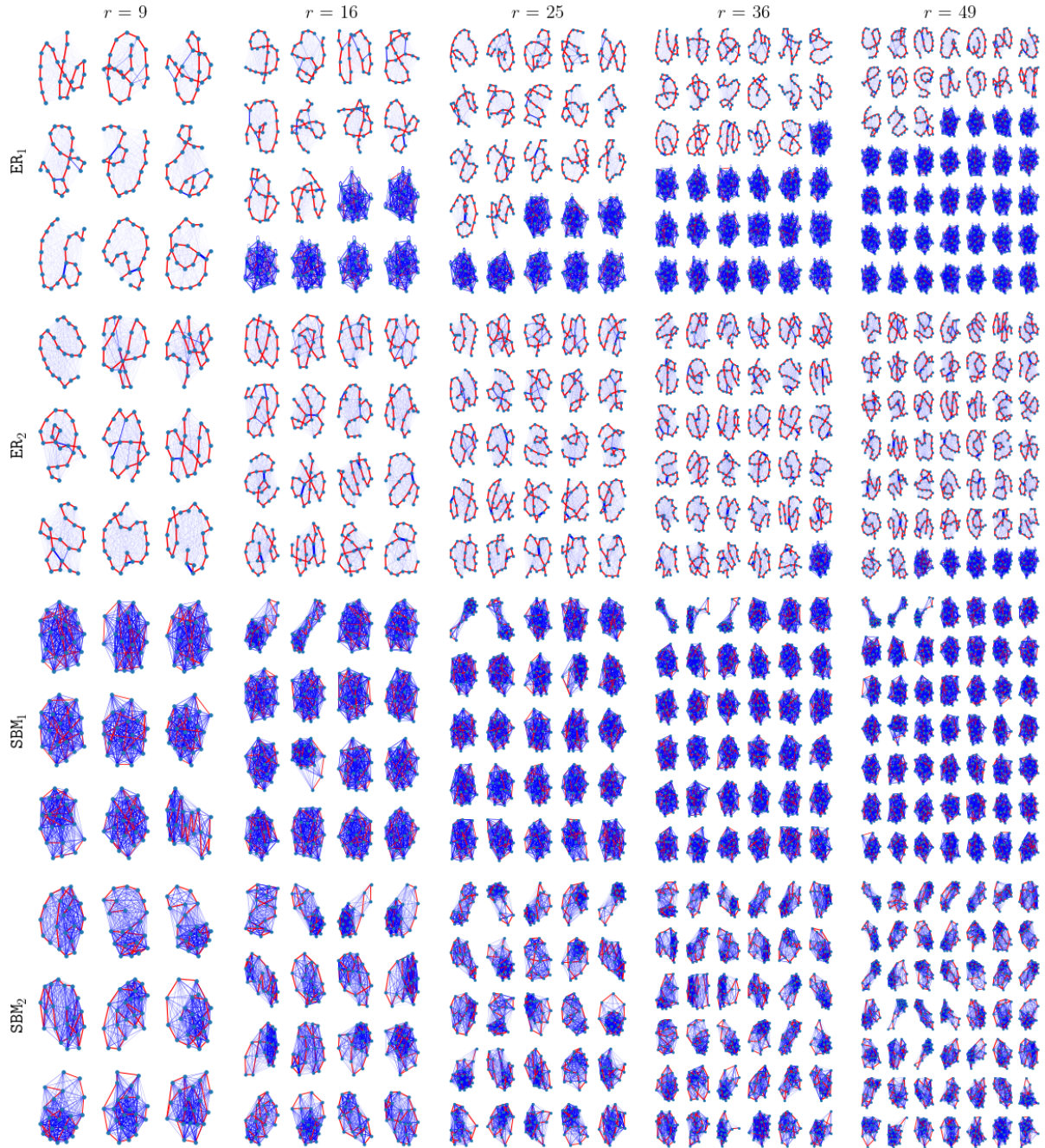


FIGURE 21. The latent motifs for  $r \in \{9, 16, 25, 36, 49\}$  at scale  $k = 21$  that we learn from the networks  $ER_1$ ,  $ER_2$ ,  $SBM_1$ , and  $SBM_2$ . The  $r = 25$  column is identical to the  $k = 21$  column in Figure 16. See Section F for details of our experiments.

## REFERENCES

- [55] Robert Tibshirani. “Regression shrinkage and selection via the lasso”. *Journal of the Royal Statistical Society: Series B (Methodological)* 58.1 (1996), pp. 267–288.
- [56] Bradley Efron, Trevor Hastie, Iain Johnstone, and Robert Tibshirani. “Least angle regression”. *The Annals of Statistics* 32.2 (2004), pp. 407–499.
- [57] Paul Glasserman. *Monte Carlo methods in financial engineering*. Vol. 53. Springer, 2004.
- [58] Nadav Kashtan, Shalev Itzkovitz, Ron Milo, and Uri Alon. “Efficient sampling algorithm for estimating subgraph concentrations and detecting network motifs”. *Bioinformatics* 20.11 (2004), pp. 1746–1758.
- [59] Jure Leskovec and Christos Faloutsos. “Sampling from large graphs”. *Proceedings of the 12th ACM SIGKDD International Conference on Knowledge Discovery and Data Mining*. 2006, pp. 631–636.
- [60] Sebastian Wernicke. “Efficient detection of network motifs”. *IEEE/ACM Transactions on Computational Biology and Bioinformatics* 3.4 (2006), pp. 347–359.
- [61] Honglak Lee, Alexis Battle, Rajat Raina, and Andrew Y. Ng. “Efficient sparse coding algorithms”. *Advances in Neural Information Processing Systems*. 2007, pp. 801–808.
- [62] Richard T. Durrett. *Probability: Theory and Examples*. Fourth Edition. Cambridge Series in Statistical and Probabilistic Mathematics. Cambridge, UK: Cambridge University Press, 2010, p. 428.
- [63] Lei Tang and Huan Liu. “Leveraging social media networks for classification”. *Data Mining and Knowledge Discovery* 23.3 (2011), pp. 447–478.
- [64] Roger A. Horn and Charles R. Johnson. *Matrix Analysis*. Second Edition. Cambridge, UK: Cambridge University Press, 2012.
- [65] László Lovász. *Large Networks and Graph Limits*. Vol. 60. Colloquium Publications. Providence, RI, USA: American Mathematical Society, 2012, p. 475.
- [66] Sean P Meyn and Richard L Tweedie. *Markov Chains and Stochastic Stability*. Heidelberg, Germany: Springer-Verlag, 2012.
- [67] Julien Mairal. “Stochastic majorization-minimization algorithms for large-scale optimization”. *Advances in Neural Information Processing Systems*. 2013, pp. 2283–2291.
- [68] Tomas Mikolov, Ilya Sutskever, Kai Chen, Greg S Corrado, and Jeff Dean. “Distributed Representations of Words and Phrases and their Compositionality”. *Advances in Neural Information Processing Systems*. Ed. by C.J. Burges, L. Bottou, M. Welling, Z. Ghahramani, and K.Q. Weinberger. Vol. 26. Curran Associates, Inc., 2013.
- [69] David A Levin and Yuval Peres. *Markov Chains and Mixing Times*. Providence, RI, USA: American Mathematical Society, 2017.
- [70] Marco Bressan. “Efficient and near-optimal algorithms for sampling connected subgraphs”. *Proceedings of the 53rd Annual ACM SIGACT Symposium on Theory of Computing*. STOC 2021. Virtual, Italy: Association for Computing Machinery, 2021, pp. 1132–1143.